Deletion of *Clmp* in Mice Reveals Essential Roles for CLMP in Growth, Survival, Gastrointestinal and Urinary Tract Functions

Inaugural-Dissertation
to obtain the academic degree
Doctor rerum naturalium (Dr. rer. nat.)

submitted to the
Department of Biology, Chemistry and Pharmacy
of Freie Universität Berlin

by

Hanna Langhorst

from Minden (Westf.)

2015

This thesis was prepared between November 2010 and October 2015 at the Max Delbrück Centre for Molecular Medicine in the Helmholtz Association under the supervision of Professor Dr Fritz G. Rathjen.

1. Reviewer: **Professor Dr Fritz G. Rathjen**
Department of Developmental Neurobiology,
Max Delbrück Centre for Molecular Medicine, Berlin-Buch

2. Reviewer: **Professor Dr Kai M. Schmidt-Ott**
Department of Molecular and Translational Kidney Research
Max Delbrück Centre for Molecular Medicine, Berlin-Buch
and Medical Department, Division of Nephrology
Charité Universitätsmedizin Berlin

Disputation: 16th February, 2016

To the ones I love

Es gibt viel zu verlieren, Du kannst nur gewinnen
Genug ist zu wenig – oder es wird so, wie es war
Stillstand ist der Tod, geh voran, bleibt alles anders
Der erste Stein fehlt in der Mauer
Der Durchbruch ist nah

Excerpt of Herbert Grönemeyer's "Bleibt alles anders"

CONTENTS

ABBREVIATIONS

°C	degree Celsius
aa	amino acid
AC	affinity chromatography
ACAM	adipocyte adhesion molecule
acc. no.	accession number
Ad	adenovirus
amp	ampicillin
AP	alkaline phosphatase
APS	ammonium persulfate
α-SMA	α-smooth muscle actin
BAC	bacterial artificial chromosome
BEAS-2B	human bronchial cell line
BCIP	5-bromo-4-chloro-3-indolyl phosphate *p*-toluidine salt
BMP 4	bone morphogenetic protein 4
bp	base pairs
Bq	Becquerel
BSA	bovine serum albumin
BT-IgSF	brain- and testis-specific IgSF member
BV	bed volume
CACO-2	human colorectal adenocarcinoma cell line
CAM	cell adhesion molecule
CAR	coxsackievirus-adenovirus receptor
cDNA	complementary DNA
CHAPS	3-[(3-cholamidopropyl)dimethylammonio]-1-propanesulfonate
CHO	Chinese hamster ovary
Ci	Curie
CIP	calf intestinal phosphatase
CLMP	CAR-like membrane protein
CNBr	cyanogen bromide
CNS	central nervous system
Cre	causes recombination
CSBS	congenital short-bowel syndrome
ctrl	control
CTX	cortical thymocyte marker in *Xenopus*
CTXL	cortical thymocyte marker in *Xenopus*-like
CVB	coxsackievirus of group B
DAPI	4',6-diamidino-2-phenylindole
dCTP	deoxycytidine triphosphate
dH_2O	distilled water
DIG	digoxigenin

DIV	days *in vitro*
DLGH 1	discs-large homologue 1
DMEM	Dulbecco's modified Eagle medium
DMF	dimethylformamide
DMSO	dimethyl sulfoxide
DNA	deoxyribonucleic acid
dNTPs	deoxyribonucleoside triphosphates
E	embryonic day
ε	extinction coefficient
E. coli	*Escherichia coli*
ECM	extracellular matrix
EDTA	ethylenediaminetetraacetic acid
EGF	epidermal growth factor
ES	embryonic stem
ESAM	endothelial cell-selective adhesion molecule
EST	expressed sequence tag
EtBr	ethidium bromide
EtOH	ethanol
EUCOMM	European Conditional Mouse Mutagenesis Programme
FBS	fetal bovine serum
FLNA	filamin A
Flp	flippase
FRT	flippase recognition target
G	goat
G418	geneticin
gDNA	genomic DNA
GPI	glycosylphosphatidylinositol
GST	glutathione S-transferase
h	human
H&E	haematoxylin and eosin
HCN 3	hyperpolarisation-activated cyclic nucleotide-gated channel 3
het	heterozygous
HRP	horseradish peroxidase
ICC	interstitial cells of Cajal
ICC-DMP	interstitial cells of Cajal in the deep muscular plexus
ICC-LC	interstitial cells of Cajal-like cells
Ig	immunoglobulin
IgCAM	cell adhesion molecule of the immunoglobulin superfamily
IgSF	immunoglobulin superfamily
IHPS	infantile hypertrophic pyloric stenosis
JAM	junctional adhesion molecule
JNK	c-Jun N-terminal kinase
kb	kilobase pairs
kDa	kilodalton
KLF4	Kruppel-like factor 4

KO	knockout
LAGeSo	Landesamt für Gesundheitliches und Soziales
LB	lysogeny broth
LIF	leukemia inhibitory factor
LNX	ligand-of-Numb protein-X
loxP	locus of crossover in P1
m	mouse
M	mouse
MAGI-1B	membrane-associated guanylate kinase, WW and PDZ domain containing 1B
MCS	multiple cloning site
MDC	Max Delbrück Centre for Molecular Medicine, Berlin
MDCK	Madin-Darby canine kidney
MEF	mouse embryonic fibroblast
mRNA	messenger ribonucleic acid
MUPP-1	multi-PDZ domain protein-1
NBT	nitro blue tetrazolium chloride
NCBI	National Center for Biotechnology Information
Neo	neomycin
NGAL	neutrophil gelatinase-associated lipocalin
n. s.	not significant
nt	nucleotide
OCT	optimal cutting temperature
OD	optical density
OLETF	Otsuka Long-Evans Tokushima fatty
OMIM	Online Mendelian Inheritance in Man
O/N	overnight
P	postnatal day
PBS	phosphate buffered saline
PCIA	phenol-chloroform-isoamyl alcohol
PCR	polymerase chain reaction
PDZ	structural domain shared by post synaptic density protein 95, discs large homologue 1, and zonula occludens-1 protein
PFA	paraformaldehyde
PGK	phosphoglycerate kinase 1
PI3K	phosphoinositide 3-kinase
PICK-1	protein interacting with C kinase 1
PKA	protein kinase A
PMSF	phenylmethylsulfonyl fluoride
PNGase F	peptide-*N*-glycosidase F
PNK	T4 polynucleotide kinase
PSD-95	postsynaptic density protein 95
PTCH	patched 1
PyRAT	Python Based Relational Animal Tracking
R	rat
RALDH 2	retinaldehyde dehydrogenase 2

Rb	rabbit
RNA	ribonucleic acid
ROI	region of interest
RT	room temperature
SDS	sodium dodecyl sulphate
SDS-PAGE	sodium dodecyl sulphate polyacrylamide gel electrophoresis
SEM	standard error of the mean
SHH	sonic hedgehog
SIX 1	SIX homeobox protein 1
SOX 9	SRY-box 9
SRY	sex-determining region Y
SSC	saline-sodium citrate
T4	enterobacteria phage T4
T84	human colonic adenocarcinoma cell line
T98G	human glioblastoma cell line
TAE	Tris-acetic acid-EDTA
TBS	Tris-buffered saline
TBX 18	T-box 18
TCF	Transgenic Core Facility at the MDC
TEMED	tetramethylethylenediamine
TK	thymidine kinase
TM4	murine testicular Sertoli cell line
TNFα	tumour necrosis factor α
TSHZ 3	teashirt 3
TTP	tristetraprolin
UPJ	ureteropelvic junction
UPK	uroplakin
UT	urinary tract
UVJ	ureterovesical junction
v/v	volume per volume
WT	wildtype
w/v	weight per volume
ZO-1	zonula occludens-1
^{32}P	phosphorous-32

ABSTRACT

Among the CTX family of IgCAMs, the coxsackievirus-adenovirus receptor (CAR) is a prototype of a subgroup that shares a protein structure consisting of extracellular Ig-like V-type and C2-type domains, a transmembrane segment and a cytoplasmic tail. Beside CAR itself, the CAR subgroup is composed of the related proteins CLMP (CAR-like membrane protein), BT-IgSF (brain- and testis-specific IgSF member), and ESAM (endothelial cell-selective adhesion molecule). Currently there is only limited information available about the functions of CLMP, BT-IgSF and ESAM. CLMP has been identified as closest to homologue to CAR and similarities between both molecules have been reported including the ability to induce homophilic cell adhesion, the localisation to epithelial tight junctions and high expression in brain, heart and adipose tissues. Furthermore, CLMP has been implicated in the pathogenesis of congenital short bowel syndrome (CSBS) in human patients.

In order to clarify the biological function of CLMP further, a constitutive *Clmp* knockout mouse model was generated and phenotypic analyses of homozygous CLMP-deficient mice revealed multiple recessive abnormalities in growth, survival, the gastrointestinal tract and the urinary system. *Clmp* mutant animals displayed a high rate of mortality during neonatal and early postnatal stages which was accompanied by a delay in body growth. Although the underlying mechanisms leading to compromised survival and growth have not been determined yet, it might be likely that gastrointestinal malfunctions are involved. Analogous to the reduction of small intestine length in CSBS patients, the bowel length of surviving adult *Clmp* mutant mice was analysed, but in contrast to CSBS patients, *Clmp* knockout mice did not display a shortening of the small bowel. Instead, gut disorganisation and duodenal dilation were observed.

In addition, homozygous *Clmp* mutant mice developed a high degree of bilateral hydronephrosis with onset at late embryonic stages. Hydronephrotic kidneys, characterised by accumulation of urine in renal pelvis and calyces and accompanied by renal parenchymal atrophy, were not caused by physical obstruction of the urinary tract. Instead, it could be shown that ureteral peristalsis, which is essential for propagation of urine from kidneys to urinary bladder, is impaired by the loss of CLMP. Calcium imaging experiments on ureteral explants revealed an absence of organised Ca^{2+} transients in *Clmp* mutants. Since attempts to identify CLMP-expressing cell types in the urinary tract were not successful, the reasons for the functional obstruction of the ureters of *Clmp* mutant mice remain to be determined.

Further research should concentrate on clarifying the expression pattern of CLMP in the gastrointestinal and urinary tracts and on cell biological and molecular biological functions of CLMP.

KURZFASSUNG

Der Coxsackievirus-Adenovirus-Rezeptor (CAR) stellt einen Prototyp einer Untergruppe der CTX-Familie von Zelladhäsionsmolekülen der Immunglobulinsuperfamilie (IgSF) dar. Die sogenannte CAR-Untergruppe besteht neben CAR aus dem CAR-ähnlichen Membranprotein (CLMP), dem gehirn- und testisspezifischen IgSF-Mitglied (BT-IgSF) sowie dem endothelzell-selektiven Adhäsionsmolekül (ESAM) und ist gekennzeichnet durch eine gemeinsame Proteinstruktur. Diese zeichnet sich durch eine extrazellulläre Region mit einer Immunglobulin-ähnlichen Domäne des V-Typs und einer des C2-Typs, eine Transmembrandomäne und eine zytoplasmatische Region aus. Bislang ist das Wissen um die Funktionen von CLMP, BT-IgSF und ESAM noch stark begrenzt. Allerdings wurde CLMP, welches die höchste Homologie zu CAR besitzt, bereits mit CAR-ähnlichen Eigenschaften wie der Induktion homophiler Zelladhäsion, der Lokalisation an epithelialen *tight junction*-Zellverbindungen sowie hoher Expression in Gehirn, Herz und Fettgewebe beschrieben. Desweiteren wurde CLMP in Zusammenhang mit der Pathogenese des angeborenen Kurzdarmsyndroms (CSBS) gebracht.

Um tiefere Erkenntnisse über die biologische Funktion von CLMP zu gewinnen, wurde ein Mausmodell mit einem konstitutiven *Knockout* von *Clmp* generiert. Phänotypische Analysen zeigten verschiedene Auswirkungen einer *Clmp*-Deletion in Bezug auf Wachstum, Überleben sowie Gastrointestinal- und Harntrakte. *Clmp*-Mutanten besaßen ein verzögertes Wachstum und eine hohe Mortalität in neonatalen und frühen postnatalen Stadien. Während keine CSBS-charakteristische Verkürzung des Dünndarms in CLMP-defizienten Mäusen nachgewiesen werden konnte, wies der Darm hingegen eine Desorganisation und eine duodenale Dilatation auf.

Zudem führte die Abwesenheit von CLMP zur Ausbildung einer ausgeprägten bilateralen Hydronephrose, die durch Urinrückstau im Nierenbecken und in Nierenkelchen sowie durch Atrophie des renalen Parenchyms gekennzeichnet war und bereits im späten Embryonalstadium begann. Es konnte gezeigt werden, dass die Entstehung der Hydronephrose nicht durch eine physische Obstruktion verursacht wird, und die Hydronephrose stattdessen das Ergebnis einer defekten Harnleiterperistaltik ist, welche essentiell für den Transport von Urin von den Nieren zur Harnblase ist. Weiterhin konnte mit *Calcium Imaging*-Experimenten ein Ausbleiben von organisierten Ca^{2+}-Transienten in *ex vivo*-kultivierten Ureteren festgestellt werden. Da die Identifikation CLMP-exprimierender Zelltypen im Harntrakt nicht gelang, bleiben die der fehlerhaften Peristaltik zugrundeliegenden Ursachen mit Abschluss dieser Studie ungeklärt.

Weitere Forschungsarbeiten sollten sich darauf konzentrieren, das Expressionsmuster von CLMP in Gastrointestinal- und Harntrakten sowie die zellbiologischen und molekular-biologischen Funktionen von CLMP zu ergründen.

1 INTRODUCTION

1.1 Cell adhesion molecules (CAMs) of the immunoglobulin superfamily (IgSF)

Cell adhesion is fundamental for tissue morphogenesis. Cell surface molecules termed cell adhesion molecules (CAMs) mediate coherence between cells and/or the extracellular matrix (ECM) and thus importantly contribute to the establishment and maintenance of tissues. Four families of cell adhesion molecules have been described: cadherins, integrins, selectins, and CAMs of the immunoglobulin superfamily (IgSF), also known as IgCAMs (Brümmendorf & Rathjen, 1995; Chothia & Jones, 1997; Elangbam *et al.*, 1997; Brümmendorf *et al.*, 1998). Cadherins, integrins and selectins are Ca^{2+}-dependent type I transmembrane CAMs and implicated in a variety of biological functions as for instance in the formation of cell layers and tissue structure (cadherins: Patel *et al.*, 2003) and in the immune system (integrins: Luo *et al.*, 2007; selectins: McEver, 2015). In contrast, IgCAMs function Ca^{2+}-independently and are cell surface glycoproteins with either a single-pass transmembrane domain or a glycosyl-phosphatidylinositol (GPI) anchor (Williams & Barclay, 1988; Elangbam *et al.*, 1997; Barclay, 2003). The IgSF represents the largest gene family in the human genome with so far 561 identified members, constituting about 2.7 % of human genes (www.genenames.org; Srinivasan & Roeske, 2005; Clamp *et al.*, 2007; Gray *et al.*, 2013), with the majority expressing adhesive proteins. The term immunoglobulin superfamily was founded in the 1980s when proteins were discovered to display domains similar to the constant and variable immunoglobulin folds (Richardson, 1981; Williams & Barclay, 1988; Bork *et al.*, 1994). These identified Ig-like domains share the structure of two antiparallel β-sheets forming a β-sandwich with Greek key β-barrel topology, and are the characteristics of IgSF members (Richardson, 1981; Williams & Barclay, 1988; Halaby & Mornon, 1998). Based on their numbers of strands and strand location, the Ig-like domains are classified into four different subtypes: the variable-like V-set, the constant-like C1-set and C2-set, and the intermediate I-set (Bork *et al.*, 1994; Harpaz & Chothia, 1994). The extracellular Ig-like domains are stable to proteolysis and mediate the adhesive functions of IgCAMs (Williams & Barclay, 1988). Intercellular and cell-ECM interactions are mediated via the Ig-like domains in a homophilic and/or heterophilic manner and are crucial for the execution of multiple biological processes which mainly reside in immune response and in the development of the nervous system. Therefore, defects in IgCAM-mediated functions are linked to a diversity of diseases, for instance in the immune system (Van Buul *et al.*, 2007; Xu & Jin, 2010) and the nervous system (Rougon & Hobert, 2003; Shapiro *et al.*, 2007).

1.2 CAR subgroup of IgSF cell adhesion molecules (IgCAMs)

Since the late 1990s, several IgCAMs have been discovered and assigned to the new CTX protein family, whose name refers to the founding member of this family, the cortical thymocyte marker in *Xenopus* (CTX) (Chrétien *et al.*, 1998). Beside CTX and its human and murine CTXL orthologues, the following type I transmembrane proteins have been included into the CTX family: the cell surface A33 antigen (also known as GPA 33) (Heath *et al.*, 1997), the junctional adhesion molecules JAM-A, JAM-B, JAM-C, JAM-L, and JAM-4 (Martìn-Padura *et al.*, 1998; Cunningham *et al.*, 2000; Liu *et al.*, 2000; Palmeri *et al.*, 2000; Arrate *et al.*, 2001; Aurrand-Lions *et al.*, 2001; Hirabayashi *et al.*, 2003; Moog-Lutz, 2003), the coxsackievirus-adenovirus receptor (CAR) (Bergelson *et al.*, 1997; Carson *et al.*, 1997; Tomko *et al.*, 1997), the CAR-like membrane protein (CLMP, also known as ACAM) (Raschperger *et al.*, 2004; Eguchi *et al.*, 2005), the brain- and testis-specific IgSF member (BT-IgSF, also known as IgSF 11) (Suzu *et al.*, 2002; Katoh & Katoh, 2003) and the endothelial cell-selective adhesion molecule (ESAM) (Hirata *et al.*, 2001; Nasdala *et al.*, 2002). Among the CTX family, CAR, CLMP, BT-IgSF and ESAM constitute a distinct subgroup, which is named after its most intensively studied member, CAR, and is characterised by a common domain structure and a high amino acid sequence similarity of at least 45 %. These four members of the CAR subgroup share a similar ectodomain architecture consisting of a membrane-distal V-type Ig-like domain, a short junction (with similarity to the immunoglobulin J segment), and a proximal C2-type Ig-like domain with an extra disulphide bond. Furthermore they all display a single membrane-spanning helix and a cytoplasmic tail with a PDZ domain binding motif (FIGURE 1; Bergelson *et al.*, 1997; Carson *et al.*, 1997; Tomko *et al.*, 1997; Hirata *et al.*, 2001; Nasdala *et al.*, 2002; Suzu *et al.*, 2002; Katoh & Katoh, 2003; Raschperger *et al.*, 2004; Schreiber *et al.*, 2014).

In addition to the shared structural organisation, all members of the CAR subgroup have been reported to mediate cell adhesive functions (CAR: Honda *et al.*, 2000; CLMP: Raschperger *et al.*, 2004; Eguchi *et al.*, 2005; BT-IgSF: Harada *et al.*, 2005; ESAM: Hirata *et al.*, 2001). However, the precise biological functions of CAR subgroup members remain to be fully resolved. Among the CAR subgroup of IgCAMs, CAR is the first identified and the predominantly investigated member, whereas the rather recently discovered members BT-IgSF, ESAM and especially CLMP have not been focus of extensive research. Since CLMP shares the highest similarity to CAR (49 % on amino acid level in the mouse) and its biological role has only poorly been elucidated yet, the aim of this thesis was to unravel the function of CLMP (sections 1.4 and 2).

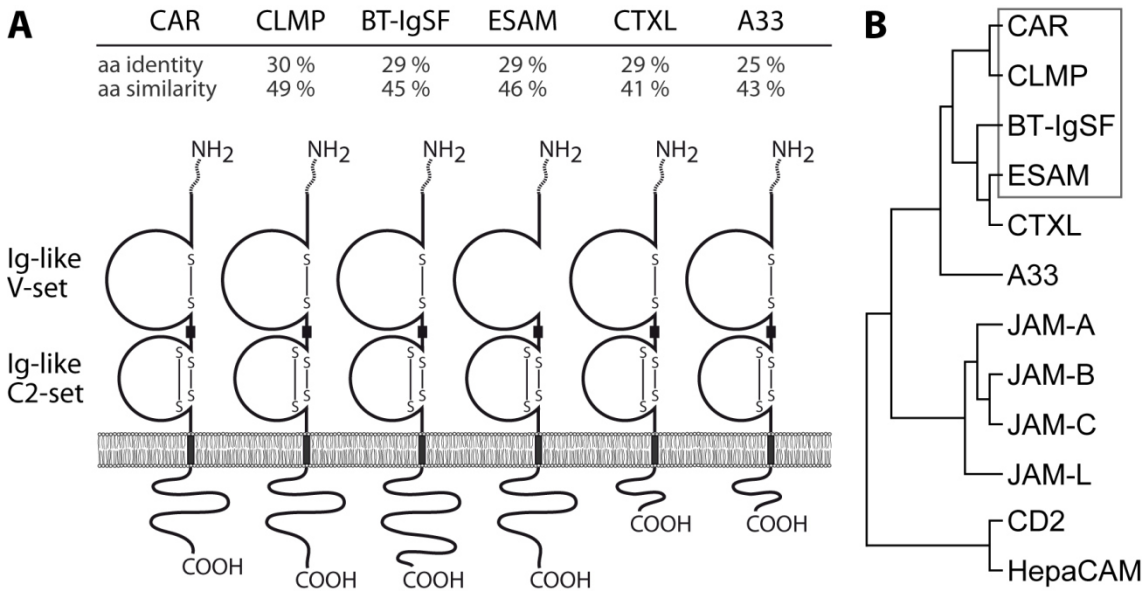

FIGURE 1. Shared protein structure and phylogenetic relationship of IgCAMs of the CTX family.

(A) Characteristic protein structure of selected CTX family members composed of an N-terminal signal peptide (shaded), an Ig-like V-set domain, a short junction sequence (black box), an Ig-like C2-set with an additional cysteine-cysteine disulphide bond, a single transmembrane region and a cytoplasmic tail of various lengths. Identities and similarities to murine CAR on amino acid level are indicated as percentages for each CTX family members in mouse. (B) Dendogram showing phylogenetic relations of all murine CTX family members in comparison to the more distantly related IgSF reference proteins CD2 and HepaCAM. CAR, CLMP, BT-IgSF and ESAM constitute the CAR subfamily.

1.3 The coxsackievirus-adenovirus receptor (CAR)

In 1997 three laboratories independently identified the shared receptor for group B coxsackieviruses (CVB) and groups A, C, D, E and F adenoviruses (Ad): Bergelson *et al.*, Carson *et al.* and Tomko *et al.* isolated the 46 kDa infection-mediating cell surface protein, which was named coxsackievirus-adenovirus receptor (CAR; Bergelson *et al.*, 1997; Carson *et al.*, 1997; Tomko *et al.*, 1997). The human CAR protein is encoded by eight exons of the *CXADR* gene on chromosome 21q21.1 (Hattori *et al.*, 2000; Excoffon *et al.*, 2010) and orthologues of CAR have been identified in multiple mammalian species like mouse (Tomko *et al.*, 1997; Bergelson *et al.*, 1998), rat, dog, pig (Fechner *et al.*, 1999) and cow (Thoelen *et al.*, 2001), as well as in zebrafish (Petrella *et al.*, 2002) and chicken (Patzke *et al.*, 2010). Human and mouse CAR are highly conserved (Wang & Bergelson, 1999; Cohen *et al.*, 2001; Asher *et al.*, 2005). The murine *Cxadr* gene is localised to chromosome 16 and, similarly to human *CXADR*, consists of at least eight exons (Chen *et al.*, 2003). Both human and murine genes generate comparable primary transcripts of equal size, which are similarly processed (Tomko *et al.*, 1997) and give rise to the full-length protein chain of 365 amino acids. However, truncated isoforms with different cytoplasmic tails are generated by alternative splicing of exons 7 and 8 (Bergelson *et al.*, 1997; Tomko *et al.*, 1997).

Based on its role as viral receptor, much research has been performed dealing with CAR as receptor for adenoviral vehicles in gene therapies and suggested CAR expression to be

conversely correlated with tumour growth (Kanerva & Hemminki, 2004; Schreiber *et al.*, 2014). Apart from the implication of CAR in cancer tissues, several constitutive and conditional *Cxadr* knockout mouse lines were generated in order to investigate the physiological function of CAR. Strikingly, the global absence of CAR in the mouse resulted in embryonic lethality occurring between embryonic days (E) 11.5 and 12.5 due to malformations in the heart (Asher *et al.*, 2005; Dorner *et al.*, 2005; Chen *et al.*, 2006). Studies using mouse models with conditional ablation of *Cxadr* furthermore showed that CAR is required for proper electrical conduction in mature hearts (Lim *et al.*, 2008; Lisewski *et al.*, 2008; Pazirandeh *et al.*, 2011). Consistent with its role in cardiac function, CAR is strongly expressed in the developing heart and becomes restricted to the cardiomyocyte-connecting intercalated discs during maturation (Ito *et al.*, 2000; Fechner *et al.*, 2003; Shaw *et al.*, 2004). A similar developmentally regulated expression with a high abundance of CAR during embryonic and early postnatal stages has been found in the nervous system (Honda *et al.*, 2000; Tomko *et al.*, 2000; Hotta *et al.*, 2003). In addition, CAR expression has been described in a variety of tissues, including thyme, lung, liver, intestine, kidney, urinary bladder, pancreas, testis, white adipose tissue and lymphatic system, with a predominant localisation to epithelial tight junctions (Tomko *et al.*, 1997, 2000; Bergelson *et al.*, 1998; Cohen *et al.*, 2001; Nagai *et al.*, 2003; Coyne *et al.*, 2004; Excoffon *et al.*, 2004; Mirza *et al.*, 2006; Raschperger *et al.*, 2006, 2008; Gye *et al.*, 2011; Sultana *et al.*, 2014; Serrano *et al.*, 2015). Targeted disruption of *Cxadr* in these tissues at embryonic stages therefore may result in serious developmental defects like subcutaneous oedema, haemorrhage and foetal murine lethality (Mirza *et al.*, 2012) or in impaired differentiation of renal glomerular podocytes and tubular epithelial cells in zebrafish (Raschperger *et al.*, 2008), whereas inactivation of *Cxadr* in adult mice has been shown to lead to intestinal dilation, exocrine pancreas atrophy and abnormal thymopoiesis (Pazirandeh *et al.*, 2011).

Taken together, CAR is a ubiquitously expressed IgCAM that possesses essential roles in multiple biological functions. However, its underlying signalling pathways have not been resolved yet, although several interaction partners have yet been identified [for instance the epithelial tight junction proteins JAM-A (Mirza *et al.*, 2006), JAM-L (Zen *et al.*, 2005; Verdino *et al.*, 2010; Witherden *et al.*, 2010), zonula occludens-1 (ZO-1; Cohen *et al.*, 2001), occludin (Raschperger *et al.*, 2006), multi-PDZ domain protein-1 (MUPP-1; Coyne *et al.*, 2004), membrane-associated guanylate kinase, WW and PDZ domain containing 1B (MAGI-1B) and protein interacting with C kinase 1 (PICK-1; Excoffon et al., 2004), ligand-of-Numb protein-X (LNX; Sollerbrant *et al.*, 2003), LNX 2 (Mirza *et al.*, 2005), postsynaptic density protein 95 (PSD-95; Excoffon *et al.*, 2004) and ECM proteins fibulin, fibronectin, laminin, agrin, tenascin-R (Patzke *et al.*, 2010)].

1.4 The CAR-like membrane protein (CLMP)

1.4.1 Identification and structural information

In 2004, bioinformatics screening of expressed sequence tag (EST) and genomic databases led to the identification of cDNAs of human and murine origin that had high sequence similarity to the conserved regions within the Ig-like C2 domain and the junctional segment of previously known IgCAM members. Sequence alignments of the newly identified human and murine cDNAs revealed a type I transmembrane protein structure characteristic to the CTX family of IgCAMs, consisting of the extracellular Ig-like V-set and Ig-like C2-set with an extra pair of cysteines, a junction separating the two Ig-like domains, a single membrane-spanning transmembrane helix, and a cytoplasmic tail with a PDZ domain binding motif. Phylogenetic analyses assessed the close relationship of the new IgCAM to CAR, therefore it was termed CAR-like membrane protein (CLMP; FIGURE 1; Raschperger *et al.*, 2004).

Although the CLMP protein was first described as novel member of the CTX family of IgCAMs and characterised in 2004, its rat *Clmp* transcript, initially designated as *OL-16*, had been discovered earlier in 2000 in a screen for upregulated genes in visceral adipose tissue of Otsuka Long-Evans Tokushima fatty (OLETF) rats, a model of type 2 diabetes (Hida *et al.*, 2000). Rat *Clmp* mRNA was specifically detected in visceral adipose tissue of OLETF rats but not in other types of adipose tissue (Hida *et al.*, 2000). In a later study of 2005, the same laboratory reported the cDNA cloning of the full coding sequence of OL-16, termed it adipocyte adhesion molecule (ACAM) and confirmed the structural features of CTX IgCAMs (Eguchi *et al.*, 2005).

The human CLMP protein is encoded by the *CLMP* gene, which consists of seven exons on chromosome 11q24.1. The murine *Clmp* gene has a similar genomic organisation to its human orthologue and is composed of seven exons on chromosome 9A5.1 (Raschperger *et al.*, 2004). *In vitro* studies using the murine testicular Sertoli TM4 cell line have already determined the promoter site of the murine *Clmp* gene and the responsive elements that are required for basal *Clmp* expression in these cells, namely binding motifs for the transcription factors GATA-1, GATA-6, Kruppel-like factor 4 (KLF 4), and sex-determining region Y (SRY; Sze *et al.*, 2008*a*). In addition, *Clmp* transcript in TM4 cells has been found to be post-transcriptionally negatively regulated by the tumour necrosis factor α (TNFα) via the RNA-binding protein tristetraprolin (TTP) and the c-Jun N-terminal kinase (JNK) signalling pathway (Sze *et al.*, 2008*b*).

Human and mouse CLMP proteins are highly related with 93 % identity on amino acid level. Unfortunately, to date there is no information available about the crystallographic structures of neither human CLMP nor its mouse orthologue. Global Needleman-Wunsch alignments of murine amino acid sequences of all CTX family members confirm CLMP as closest homologue to CAR with an overall identity of 30 % and a similarity of 49 % for the mature protein. With 35 % identity and 51 % similarity on amino acid level, the Ig-like V-sets of CAR and CLMP are highly homologous, whereas the Ig-like C2-type domains yield 26 % identity and 51 % similarity, respectively. The transmembrane domains of both murine homologues are highly

related with an identity of 36 % and 50 % similarity. The cytoplasmic tail of CLMP, which is 11 amino acids longer than the tail of CAR, displays an identity of 27 % and a similarity of 41 %, respectively.

1.4.2 Expression on transcript and protein levels

To date, the expression of CLMP has not been fully investigated. The majority of experiments has been performed on cell lines in culture using antibodies in immunocytochemistry or Western blots, and only few analyses have been carried out to detect CLMP in tissue sections. Furthermore, transcript expression of murine *Clmp* and its human orthologue have been analysed in several tissues by Northern blot (Raschperger *et al.*, 2004) and quantitative real-time polymerase chain reaction (PCR; Eguchi *et al.*, 2005). Analysis of transcript expression has, however, yielded controversy results between the studies, and there appear to be differences in the expression pattern of *Clmp* orthologues among the species (Raschperger *et al.*, 2004; Eguchi *et al.*, 2005). Interestingly, both laboratories purchased total RNA and multiple tissue Northern blots from the same manufacturer. The developmental stages of dissected tissues, however, have not been specified, suggesting that the analysed transcripts might have derived from adult tissues.

In both studies of Raschperger *et al.* and Eguchi *et al.*, consistent results were obtained in murine heart and brain with a high expression of murine *Clmp* mRNA, whereas in human heart and brain, only low levels of *CLMP* could be observed (Raschperger *et al.*, 2004; Eguchi *et al.*, 2005). However, levels of transcript expression in other tissues differed among the techniques used in both studies. In murine kidney, lung, liver, spleen and testis no *Clmp* transcripts have been detected by quantitative real-time PCR (Eguchi *et al.*, 2005), while Northern blot analysis revealed weak or medium expression in these tissues (Raschperger *et al.*, 2004). In human tissues including liver and kidney, quantitative real-time PCR showed no *CLMP* transcripts (Eguchi *et al.*, 2005), but Northern blots discovered weak to medium expressions, respectively (Raschperger *et al.*, 2004). Furthermore, only medium *CLMP* mRNA expression was observed in human placenta by quantitative real-time PCR (Eguchi *et al.*, 2005), whereas analysis by Northern blot obtained high expression of *CLMP*, which represented, together with the very intense expression in human small intestine, by far the strongest detected signal among all tested human tissues (Raschperger *et al.*, 2004).

In addition, expression analysis in adipose tissues revealed a specific *Clmp* expression in white, but not brown adipose tissue. The high transcript expression was shared in human, mouse and rat. Interestingly, in Northern blots of several OLETF rat tissues including heart, brain, kidney, lung, liver, spleen, muscle, and intestine, the only signal of *Clmp* expression could be obtained in white adipose tissue (Hida *et al.*, 2000; Eguchi *et al.*, 2005). Moreover, expression of *Clmp* mRNA in rat white adipose tissue has been observed to increase during the maturation of adipocytes (Eguchi *et al.*, 2005).

Research of endogenous CLMP protein expression has been very fragmentary. Different polyclonal rabbit antibodies were used to analyse CLMP expression. One study utilised a

purchased antibody against human CLMP (Van der Werf *et al.*, 2012), whereas the other studies generated polyclonal rabbit antibodies against peptides of human or rat CLMP in their laboratories (Raschperger *et al.*, 2004; Eguchi *et al.*, 2005; Sze *et al.*, 2008*a*). Antibody specificity has been tested by signal detection in transfected cells and/or loss of signal by incubation of cells or tissue sections with the immunising antigen peptides or by omission of the primary antibody (Raschperger *et al.*, 2004; Eguchi *et al.*, 2005; Sze *et al.*, 2008*a*; Van der Werf *et al.*, 2012). However, no specificity tests have been carried out using CLMP-deficient tissues. Interestingly, some antibodies used in the studies have even been reported to result in nuclear staining [e. g. the antibody "CP-1" raised against the very cytoplasmic end of human CLMP (Raschperger *et al.*, 2004); the purchased antibody "HPA002385" raised against the cytoplasmic tail of human CLMP, see website of manufacturer Sigma-Aldrich (Van der Werf *et al.*, 2012)], which is somehow odd based on the aspect that CLMP is a transmembrane protein.

Only few immunohistochemical stainings were performed on mouse sections of lung, skeletal muscle, colon and trachea showing stainings at contact sites of epithelial cell types (Raschperger *et al.*, 2004). Additionally, CLMP has been found to localise to the blood-testis-barrier in sections of seminiferous tubules of mouse testes (Sze *et al.*, 2008*a*). Moreover, one study investigated CLMP expression in human foetal sections at several developmental stages (Van der Werf *et al.*, 2012). At seven and eight weeks of development, CLMP was highly expressed throughout the central and peripheral nervous systems and derivatives of the endodermal layer including intestine, lung, oesophagus and trachea. During later midterm development, CLMP became ubiquitously expressed with abundant localisation in intestinal crypts and the lowest expression in muscular and interstitial layers. Furthermore, CLMP was concentrated in the liver lobules, and fewer amounts were observed in the bile ducts. In the urinary system, strong signals were detected in the renal cortex, intermediate immunoreactivity was found in renal collecting ducts and only weak expression was observed in the ureteral smooth muscle (Van der Werf *et al.*, 2012).

In addition to tissue sections, endogenous CLMP expression has been detected in epithelial cell lines including the murine testicular Sertoli TM4 cells, human intestinal T84 cells, human bronchial BEAS-2B cells, and human colorectal adenocarcinoma CACO-2 cells (Raschperger *et al.*, 2004; Sze *et al.*, 2008*a*; Van der Werf *et al.*, 2012) as well as in human glioblastoma T98G cells (Raschperger *et al.*, 2004).

Taken together, expression of CLMP protein and its transcript has been investigated in several studies. While transcript expression suggests a specific expression of *Clmp* concentrated in brain, heart and adipose tissue, immunological studies indicate a rather ubiquitous expression of CLMP protein with a focus on epithelial cell types (Raschperger *et al.*, 2004; Eguchi *et al.*, 2005; Sze *et al.*, 2008*a*; Van der Werf *et al.*, 2012). However, more research is required to determine CLMP expression during murine development and its subcellular localisation in order to shed light on the biological function of CLMP.

1.4.3 Biological functions and implications in diseases

In order to elucidate the function of CLMP, mainly *in vitro* experiments have been carried out. Since CLMP is the closest homologue of CAR, its ability to mediate cell adhesion was investigated. Chinese hamster ovary (CHO) cells were transfected with full-length human CLMP or its rat orthologue and in fact, the transfections induced cell aggregation which was comparable to that of CAR. However, aggregation intensity was not as strong as observed by transfections with the adhesion molecule cadherin 1 (also known as E-cadherin; Raschperger *et al.*, 2004; Eguchi *et al.*, 2005; Van der Werf *et al.*, 2013*a*). Besides, CAR has been predominately observed at epithelial tight junctions and CLMP has been found to be expressed in epithelial cell types. Immunofluorescent and immunohistochemical analysis of the epithelial cell lines MDCK, TM4, T84 BEAS-2B, and CACO-2 revealed a co-localisation of endogenous or overexpressed CLMP with the tight junction molecules ZO-1 and occludin, suggesting that CLMP might be a tight junction molecule (Raschperger *et al.*, 2004; Sze *et al.*, 2008*a*; Van der Werf *et al.*, 2012). Consistent with a cell adhesive function and a tight junction localisation, transfection of MDCK epithelial monolayers with cDNA encoding full-length CLMP resulted in a significant increase of transepithelial electrical resistance (Raschperger *et al.*, 2004). The transfection of CHO cells with a mutated variant of human CLMP, which is unable to integrate into the plasma membrane but instead localises in the cytoplasm, leads to mislocalisation of ZO-1 with an increased aggregation of ZO-1 in the cytoplasm (Van der Werf *et al.*, 2012). Whether and how precisely CLMP might be involved in tight junction development and function remains to be determined.

In addition to epithelial cells, *Clmp* mRNA is abundantly and specifically expressed in white, but not in other types of adipose tissues. In white adipose tissue of OLETF rats, which represent an animal model for type 2 diabetes and obesity, *Clmp* expression was upregulated in comparison to normal rats, and moreover it was found to correlate with adipocyte maturation (section 1.4.2). When obesity was stimulated in OLETF rats by administration of the hormone pioglitazone, the white adipose tissue of these animals expressed even higher amounts of *Clmp* transcript and CLMP protein as compared to non-treated OLETF rats, suggesting that CLMP might function in the conversion of premature to mature adipocytes (Eguchi *et al.*, 2005). Thus, these findings indicate that CLMP might play a role in obesity, however the exact mechanisms still need to be investigated.

Similarly to the increased expression of *Clmp* mRNA after hormonal induction of gain in white adipose tissue, *Clmp* transcript expression has been reported to be stimulated during the peri-ovulatory period in rats. Peri-ovulatory processes in rat ovaries and ovarian cell cultures were induced by treatment with human chorionic gonadotrophin and shortly afterwards a rise in *Clmp* transcript and protein abundance was detected, which was controlled by signalling pathways dependent on protein kinase A (PKA), phosphoinositide 3-kinase (PI3K), p38 kinase and epidermal growth factor (EGF) receptor (Li *et al.*, 2014). Since cell adhesion is crucial for ovulation during the transition of the pre-ovulatory follicle to the corpus luteum and CLMP

expression is increased in this period, it might be hypothesised that CLMP might function in the associated processes.

Beside the indications that CLMP might be important in cell adhesion, obesity and ovulation, one study implicated CLMP in an enteric disease. Congenital short-bowel syndrome (CSBS) is a rare hereditary gastrointestinal disorder which manifests by a reduction in the length of the small intestine and is accompanied by intestinal malrotation (Hamilton *et al.*, 1969; Van der Werf *et al.*, 2015). The underlying genetic defects have remained to be elucidated for a long time, but recently mutations in genes encoding either CLMP or filamin A (FLNA) have been identified in subgroups of CSBS patients. While *FLNA* mutations are X-linked and therefore have only been found in male patients, *CLMP* mutations have been identified in both genders and with no abnormalities in the *FLNA* gene, suggesting that both genes independently contribute to the disease (Van der Werf *et al.*, 2012, 2013*b*). Different mutations in the *CLMP* gene have been detected in five CSBS patients by a genome-wide scan and homozygosity mapping. The defects in *CLMP* included frameshift, missense, and splice donor site mutations in coding regions and an intronic deletion, which were not present in chromosomes of control individuals. *In silico* and *in vitro* experiments showed that these mutations most likely result in a loss of function of CLMP (Van der Werf *et al.*, 2012). To determine whether a loss of function *in vivo* is indeed associated with a short bowel, the researchers generated morpholino knockdown zebrafish models. In zebrafish, two putative *clmp* transcripts have been identified and analysis by *in situ* hybridisation revealed that one transcript variant was specifically expressed in the zebrafish intestine. Knockdown of this enteric *clmp* variant by splice-blocking or translation-blocking morpholinos resulted in a significant developmental delay. When compared to wild type controls, the morphants exhibited a significantly shorter body length associated with a significant reduction of intestinal length, which, however, was proportional to the overall decreased body length. Interestingly, histological analyses revealed the absence of enteric goblet cells in morphants (Van der Werf *et al.*, 2012). Goblet cells are glandular epithelial cells and a typical attribute of the zebrafish midintestine, which is comparable to the human small intestine (Ng *et al.*, 2005). Thus, the authors supposed that loss goblet cells as markers for midintestinal epithelial tissue might indicate a lack of small intestine in zebrafish *clmp* morphants (Van der Werf *et al.*, 2012). Based on the reported co-localisation of CLMP with epithelial tight junction markers like ZO-1, which is involved in cell proliferation (Matter & Balda, 2007), it was hypothesised that loss-of-function *CLMP* mutations in CSBS patients might be important for proliferative processes of enteric epithelia during intestinal human development (Van der Werf *et al.*, 2012). Further *in vitro* analyses using T84 colonic adenocarcinoma cells transfected with cDNA encoding a missense mutant of CLMP, which had been reported in one of the CSBS patients, could not show any implication of CLMP in key processes of intestinal epithelial development including migration, proliferation, viability and transepithelial electrical resistance (Van der Werf *et al.*, 2013*a*). Thus, the precise function of CLMP in CSBS pathogenesis remains to be elucidated.

2 AIMS OF THE STUDY

The IgCAMs CAR and CLMP do not only share a high amino acid homology of 30 % and the same protein architecture, CLMP has also been reported to display several properties similar to CAR, including induction of cell adhesion in transfected cells (CLMP: Raschperger *et al.*, 2004; Eguchi *et al.*, 2005; Van der Werf *et al.*, 2012; CAR: Honda *et al.*, 2000), high expression in brain, heart (CLMP: Raschperger *et al.*, 2004; Eguchi *et al.*, 2005; CAR: Tomko *et al.*, 1997; Honda *et al.*, 2000; Ito *et al.*, 2000; Fechner *et al.*, 2003; Hotta *et al.*, 2003; Shaw *et al.*, 2004) and white adipose tissue (CLMP: Hida *et al.*, 2000; Eguchi *et al.*, 2005; CAR: Serrano *et al.*, 2015), and localisation to epithelial tight junctions (CLMP: Raschperger *et al.*, 2004; Eguchi *et al.*, 2005; Sze *et al.*, 2008*a*; Van der Werf *et al.*, 2012; CAR: Cohen *et al.*, 2001; Nagai *et al.*, 2003; Coyne *et al.*, 2004; Raschperger *et al.*, 2006; Gye *et al.*, 2011). Still, CLMP might act differently from CAR since for instance several mutations in the *CLMP* gene have been identified in the disease CSBS (Van der Werf *et al.*, 2012) which have not been described for the *CXADR* gene yet. However, the precise biological function of CLMP has not yet been determined. In order to elucidate the functional role of CLMP, this subject was approached by pursuing the following objectives:

1) For investigating the role of CLMP in the living organism, it is a valuable tool to determine the consequences of a global absence of CLMP in the organism. Therefore, the aim was to generate a constitutive knockout mouse model, which lacks CLMP protein in every cell and at all developmental stages, by genetic targeting of the start codon-containing exon of the *Clmp* gene. Phenotypic analyses of the *Clmp* knockout animals in comparison to wild type and heterozygous littermates were carried out to draw conclusions about the biological function of CLMP.

2) The expression pattern of CLMP has not been extensively studied yet, especially not during development. Information on temporal and spatial expression, however, is essential for investigations of the *Clmp* knockout phenotype. In order to address this question, the aim was to investigate the expression pattern of CLMP during mouse development. For this purpose, antibodies raised against the ectodomain and the cytoplasmic tail of CLMP were generated, purified and tested for specificity. Specific antibodies were utilised for expression analysis of CLMP protein. Techniques for *Clmp* transcript detection were applied to complement expression analysis.

3 MATERIALS

3.1 Chemicals

Name	Company
Acetic acid, glacial, 100 %	Merck
Acetic anhydride	Sigma-Aldrich
Acrylamide/bisyacrylamide, 30 % solution, 37.5:1 ratio	Bio-Rad
Agar-agar	Roth
Agarose	Roth
Ammonium chloride (NH_4Cl)	Merck
Ammonium persulphate (APS)	GE Healthcare
Ammonium sulphate ($(NH_4)_2SO_4$)	Merck
Aluminium sulphate ($Al_2(SO_4)_3$)	Sigma-Aldrich
Aprotinin	Roth
Bacto Tryptone	BD Biosciences
Bacto Yeast Extract	BD Biosciences
Blocking Reagent	Roche Applied Science
Bovine serum albumin (BSA), fraction V	Biomol
5-Bromo-4-chloro-3-indolyl phosphate *p*-toluidine salt (BCIP)	Roth
Chloramphenicol	Sigma-Aldrich
3-[(3-Cholamidopropyl)dimethylammonio]-1-propanesulfonate (CHAPS)	Merck
CNBr-activated sepharose 4B	GE Healthcare
Coomassie G-250	Serva
Copper(II) chloride ($CuCl_2$)	Merck
dCTP[α-^{32}P], 3000 Ci/mmol, 10 mCi/ml	PerkinElmer
Denhardt's solution, 50x	Life Technologies
4',6-Diamidino-2-phenylindole (DAPI)	Dianova
Diethylamine	Sigma-Aldrich
DIG-labelled control RNA	Roche Applied Science
DIG RNA labelling mix, 10x conc.	Roche Applied Science
N,N-Dimethylformamide (DMF)	Sigma-Aldrich
Dimethyl sulfoxide (DMSO) - sterile	Merck
dNTP mix, 10 mM each	Invitrogen
Entellan	Merck
Eosin Y, 89 % dye	Sigma-Aldrich
Ethanol, 100% p.a.	Merck
Ethidium bromide	AppliChem
Ethylenediaminetetraacetic acid (EDTA)	Merck
Ethylene glycol, ≥ 99 %	Roth
Formaldehyde, 37% stabilised	Merck
Formamide, deionised, RNase-free	Roth
Freund's adjuvant, complete	Sigma-Aldrich
Freund's adjuvant, incomplete	Sigma-Aldrich
Gelatin	Merck
Glutathione-sepharose 4B	GE Healthcare
Glycerol	Merck

Name *(continued)*	**Company** *(continued)*
Glycine	Merck
Goat serum, heat-inactivated	Linaris
Haematoxylin	Sigma-Aldrich
Hydrochloric acid (HCl), 32 %	Merck
IgG 1, native, human	Calbiochem
Immu-Mount	Thermo Scientific
Ink, royal blue 4001	Pelikan
Isoflurane (Forene)	Abbott
Isopropanol	Merck
N-Lauroylsarcosine, 30 % aqueous solution	Sigma-Aldrich
Leupeptin	Sigma-Aldrich
Levamisole	Sigma-Aldrich
Lipocalin 2 (NGAL), recombinant mouse protein	R&D Systems
Lipofectamine 2000	Invitrogen
Magnesium chloride ($MgCl_2$)	Merck
Magnesium sulphate ($MgSO_4$)	Merck
Maleic acid	Sigma-Aldrich
2-Mercaptoethanol (β-mercaptoethanol)	Sigma-Aldrich
Methanol (MeOH)	Merck
Milk powder	Roth
Nitro blue tetrazolium chloride (NBT)	Roth
$Oligo(dT)_{18}$ primer	Thermo Scientific
Paraformaldehyde (PFA)	Merck
PBS (without Ca^{2+}, Mg^{2+})	Biochrom
Pentane	Merck
Pepstatin-A	Sigma-Aldrich
Phenol-chloroform-isoamyl alcohol (25:24:1 mixture)	Sigma-Aldrich
Phenylmethylsulfonyl fluoride (PMSF)	Enzo Life Sciences
Phosphoric acid (H_3PO_4), 85 %	Merck
Ponceau S	Merck
Potassium carbonate (K_2CO_3)	Merck
Potassium permanganate ($KMnO_4$)	Merck
Proteinase K, 20 mg/ml, RNase-free	Peqlab
Proteinase K, 20 mg/ml	Roche
Protein A-sepharose CL-4B	GE Healthcare
RNaseOUT	Life Technologies
Roti-Histokitt	Roth
SDS, ≥ 99 %	Roth
SDS, 20 % (w/v) solution	Bio-Rad
Silver nitrate ($AgNO_3$)	Merck
Sodium acetate (NaAc)	Merck
Sodium chloride (NaCl)	Merck
Sodium citrate	Merck
Sodium hydrogen carbonate ($NaHCO_3$)	Merck
Sodium hydroxide (NaOH)	Merck
Sodium iodate ($NaIO_3$)	Sigma-Aldrich
Sperm DNA, from herring, 10 mg/ml, RNase-free	Life Technologies
Sucrose	Merck
Technovit 3040	Kulzer
Technovit 7100	Kulzer

Name *(continued)*	**Company** *(continued)*
N,*N*,*N*',*N*'-Tetramethylethane-1,2-diamine (TEMED)	Bio-Rad
Thionin acetate salt, 85 % dye	Sigma
Tissue-Tek O.C.T. compound	Sakura
Transferrin (apo-)	Sigma-Aldrich
Trichloroacetic acid	Merck
Triethanolamine, ≥ 99 %	Sigma-Aldrich
Tris(hydroxymethyl)aminomethane	Merck
tRNA from yeast, 10 mg/ml, RNase-free	Sigma
Tween-20	Sigma-Aldrich
Zinc chloride ($ZnCl_2$)	Merck

3.2 Polymerases

Name	**Company**
Phusion DNA polymerase	New England Biolabs
SP6 RNA polymerase	Roche Applied Science
T7 RNA polymerase	Roche Applied Science
Taq DNA polymerase	New England Biolabs
Q5 DNA polymerase	New England Biolabs

3.3 Restriction enzymes

Name	**Company**
*Bgl*II - Fast Digest	Thermo Scientific
*Eco*RI	New England Biolabs
*Eco*RV	New England Biolabs
*I-Ceu*I	New England Biolabs
*Nco*I - High Fidelity	New England Biolabs
*Xba*I	New England Biolabs

3.4 Other enzymes

Name	**Company**
Calf Intestinal Phosphatase (CIP)	Roche Applied Science
PNGase F	New England Biolabs
PreScission Protease	GE Healthcare
RNase A, 100 mg/ml	Qiagen
SuperScript II Reverse Transcriptase	Life Technologies
T4 DNA Ligase	Life Technologies
T4 Polynucleotide Kinase (PNK)	Life Technologies

3.5 Molecular weight markers

Name	**Company**
GeneRuler 1kb Plus DNA Ladder	Life Technologies
Lambda DNA/*Hin*dIII Marker 2	Life Technologies
SDS-PAGE Molecular Weight Standard, High Range	Bio-Rad
SDS-PAGE Molecular Weight Standard, Low Range	Bio-Rad

3.6 Oligonucleotides

Sequencing of pVBTK-CLMP targeting vector			
Primer name	**Sequence**	**Binding sites in attached file**	**Strand**
Clmp 5'arm F1	5'-CCAAGTTATGTCCTTGGCTCTG-3'	upstream of sequenced region	+
Clmp 5'arm F2	5'-CCCCTACACTTGTTTTTGGTG-3'	460-480	+
Clmp 5'arm F3	5'-GTGTTCTGCAGCTCAGGATG-3'	998-1017	+
Clmp 5'arm F4	5'-CGACGTTAAACAAATTCCAG-3'	1496-1515	+
Clmp 5'arm F4-5	5'-TCTCTCCATTGGATTTGATGG-3'	1803-1823	+
Clmp 5'arm F5	5'-CCAGGACATTGGACTTGTGG-3'	1985-2004	+
Clmp 5'arm F6	5'-ATTTGCCTATGGTGCCACAC-3'	2483-2502	+
Clmp 5'arm FOR	5'-TCCTAAGAAGGGACGACGAG-3'	2242-2261	+
Clmp insert 5' F	5'-AATTCAGTCGACTGGATCCG-3'	2762-2781	+
Clmp insert 3' F	5'-AAGAGCCCTTCTGGGTGGT-3'	4726-4744	+
Clmp Neo FOR RC	5'-ATTGTCTGTTGTGCCCAGTC-3'	4027-4046	+
Clmp Neo RC FOR1	5'-TCAGCAATATCACGGGTAGC-3'	3424-3443	+
Clmp Neo RC REV1	5'-GCTCCTGCCGAGAAAGTATC-3'	3772-3791	-
Clmp 3'arm F1	5'-AATTAGATGGAGGCTGGAACC-3'	5201-5221	+
Clmp 3'arm F1-2	5'-CTAGATGGCACCTTTGTCAGC-3'	5456-5476	+
Clmp 3'arm F2	5'-CAACAAAGCCACAAGCTCAC-3'	5704-5723	+
Clmp 3'arm F2-3	5'-CTGAGGCAGAGATCAGAGGA-3'	5879-5898	+
Clmp 3'arm F3	5'-TCTCCAGCCCTTGTTTCTTC-3'	6146-6165	+
Clmp 3'arm F3-4	5'-CAGAGACAGGCATCAAAAAGG-3'	6416-6436	+
Clmp 3'arm F4	5'-AGCCAGCAACAAAACAAACC-3'	6719-6738	+
Clmp 3'arm F4-5	5'-CCAGTGGGCTTCTTGCAT-3'	6887-6904	+
Clmp 3'arm F5	5'-ATCTTTCCTGGCTTTCTTGC-3'	7219-7238	+
Clmp 3'arm F5-6	5'-GCTTGTAAAAAGCCATTGTGC-3'	7518-7538	+
Clmp 3'arm F6	5'-AGCACAGGTCTTTCCCTCATC-3'	7748-7768	+
Clmp 3'arm F7	5'-ATGTGTTCCCTGCCCTTTC-3'	8266-8284	+
Clmp 3'arm F8	5'-GAGCAATTGGTGGCAGATG-3'	8749-8767	+
Clmp 3'arm F9	5'-TTTCACTGAGAGAGGATTCCG-3'	9276-9296	+
Clmp 3'arm R1-2	5'-CCTTCTCTCCTTGGGCTGTA-3'	5374-5393	-
Clmp 3'arm R5-6	5'-CAAGATCTTCTACCTGACCTGCT-3'	7386-7408	-
Clmp 3'arm R6-7	5'-ATCCCCTCCCCCAAGTTGT-3'	7946-7964	-
Clmp 3'arm REV	5'-AAATGAGGACCACCCAGAAG-3'	4733-4752	-
Clmp 3'arm REV2	5'-GTCCAGCCCAGGAATGTCAG-3'	4818-4837	-

Southern probe generation			
Probe; BAC clone	**Primer name**	**Sequence**	**Amplicon**
***Clmp* 5' probe**	Clmp_Sonde1_FOR	5'-GGCGAGGGGGAGCACTTTCA-3'	829 bp
BAC bMQ83N17	Clmp_Sonde1_REV	5'-GGAGGCGGCAGGCTTGGTATT-3'	
***Clmp* 3' probe**	Clmp_Sonde2_FOR	5'-GGAAGCCCAGAGAAATG-3'	605 bp
BAC bMQ83N17	Clmp_Sonde2_REV	5'-CAGGGAAAGGGGATGTGATAA-3'	

Mouse genotyping			
Mouse strain	**Primer name**	**Sequence**	**Amplicon**
Clmp strains,	Clmp WT1 FOR	5'-GAGAACCGTTTCGTGGAGAG-3'	459 bp
WT allele	Clmp WT1 REV	5'-TTCAGGAGGGGCAGAATATG-3'	
Clmp strains,	Clmp 5‘ arm FOR	5'-TCCTAAGAAGGGACGACGAG-3'	428 bp
KO allele	Clmp insert5’ REV	5'-AGCCAGTAAGCAGTGGGTTC-3'	
Cre-Deleter	Cre_New1	5'-GAACGCACTGATTTCGACCA-3'	200 bp
	Cre_New2	5'-AACCAGCGTTTTCGTTCTGC-3'	

cDNA amplification			
Gene; Acc. no.	**Primer name**	**Sequence**	**Amplicon**
***Actb* (β-actin)**	β-actin FOR	5'-CGTGGGCCGCCCTAG-3'	238 bp
NM_007393.3	β-actin REV	5'-CTTAGGGTTCAGGGGGGC-3'	
Clmp	Clmp_cDNA_CDS_F	5'-ATCTCACCATGGCCTCCTC-3'	499 bp
NM_133733.4	Clmp_cDNA_CDS_R	5'-GTGCTGAGTGTGGTTTCTGC-3'	
Clmp	Clmp_cDNA_F1072	5'-CAGGAGCAGTGACAGGCATA-3'	165 bp
NM_133733.4	Clmp_cDNA_R1236	5'-AGGAGCTAGGCTTCACAAGG-3'	
Clmp	Clmp_cDNA_F369	5'-GGGATGTCCCTCTTCTTCCT-3'	111 bp
NM_133733.4 transcript-specific	Clmp_cDNA_R479	5'-ATGGTGACAGGGCAAGGTAA-3'	
Clmp	Clmp_X1_F25	5'-AAGCTTCAGCTCCTTCCAAA-3'	162 bp
XM_006510602.1 transcript-specific	Clmp_cDNA_R479	5'-ATGGTGACAGGGCAAGGTAA-3'	
Clmp	Clmp_X2_F33	5'-GCTAAACCCAGCAGGAGATG-3'	122 bp
XM_006510603.1 transcript-specific	Clmp_cDNA_R479	5'-ATGGTGACAGGGCAAGGTAA-3'	
***In situ* hybridisation probe generation**			
Probe; Acc. no.	**Primer name**	**Sequence**	**Amplicon**
***Clmp* antisense**	Clmp_ABA_FOR	5'-GCTCATTTTCCTCCTGATATGG-3'	770 bp
NM_133733.4	Clmp_ABA_R_SP6	5'-gcgatttaggtgacactatagCTTCTTGACTGT GGTGACTTGC-3' (SP6 promoter)	
***Clmp* sense**	Clmp_ABA_F_SP6	5'-gcgatttaggtgacactatagGCTCATTTTCCTC CTGATATGG-3' (SP6 promoter)	770 bp
NM_133733.4	Clmp_ABA_REV	5'-CTTCTTGACTGTGGTGACTTGC-3'	

3.7 Bacterial strains

Name	Company
E. coli DH5α	Life Technologies
E. coli DH10B	Life Technologies
E. coli DH10B, BAC clone bMQ83n17	Source BioScience

3.8 Antibodies

Primary antibodies			
Target	**Host**	**Dilution**	**Company**
Actin, α-smooth muscle	mouse	IF: 5 µg/ml	Sigma-Aldrich
CLMP	rabbit 6504	WB: 0.5 µg/ml	Rathjen laboratory
Cytokeratin 8	rat	IF: 1:500	Developmental Studies Hybridoma Bank (DSHB)
E-cadherin	mouse	WB: 1:1,000	BD Transduction Laboratories
Lipocalin 2 (NGAL)	goat	WB: 1:1.000	R&D Systems
RALDH 2	rabbit	IF: 1:500	Abcam

Secondary antibodies				
Target	**Conjugate**	**Host**	**Dilution**	**Company**
Digoxigenin (DIG)	AP	sheep	DB: 1:5,000 ISH: 1:1,000	Roche Applied Science
Goat IgG	HRP	rabbit	WB: 1:20,000	Jackson ImmunoResearch
Mouse IgG	Cy 3	goat	IF: 1:500	Jackson ImmunoResearch
Mouse IgG	Alexa 647	goat	IF: 1:500	Jackson ImmunoResearch

Secondary antibodies *(continued)*				
Target	**Conjugate**	**Host**	**Dilution**	**Company**
Rabbit IgG	Cy 3	goat	IF: 1:500	Jackson ImmunoResearch
Rabbit IgG	HRP	goat	WB: 1:20,000	Jackson ImmunoResearch
Rat IgG	Alexa 488	goat	IF 1:500	Jackson ImmunoResearch

3.9 Solutions and buffers

Name	Composition
AC acid elution buffer	0.1 M acetic acid, 150 mM NaCl
AC basic elution buffer	0.1 M diethylamine pH 11.5; adjust pH with NaOH
AC coupling buffer	0.1 M $NaHCO_3$
Agarose gel	1-2 % (w/v) agarose in 1x TAE buffer; dissolve by boiling, cool down to 60 °C, add 0.01 % (v/v) ethidium bromide, mix and pour into gel tray
AP detection buffer	100 mM Tris-Cl pH 9.7, 5 mM $MgCl_2$, 0.01 mM $ZnCl_2$
BCIP stock solution	50 mg/ml in DMF; store at -20 °C
Church hybridisation buffer	0.5 M NaH_2PO_4, 1 mM EDTA; adjust pH to 7.2 with NaOH, then add 1 % (w/v) BSA; after dissolving at 68 °C, add 7 % (w/v) SDS and dissolve at 68 °C; filter through 0.8 µm and store at -20 °C
Colloidal coomassie solution	0.1 % (w/v) coomassie G-250, 0.76 M $(NH_4)_2SO_4$, 1.7 % (v/v) H_3PO_4, 20 % (v/v) methanol
EDTA stock solution	500 mM EDTA; adjust pH to 8.0 with NaOH to dissolve EDTA
ES cell lysis buffer	10 mM Tris-Cl pH 7.5, 10 mM NaCl, 10 mM EDTA, 0.5 % (w/v) *N*-lauroylsarcosine
H&E acid ethanol	1 % (v/v) HCl in 70 % (v/v) ethanol
H&E eosin solution	0.5 % (w/v) eosin Y, 2 drops glacial acetic acid in 96 % (v/v) ethanol
H&E Gill's haematoxylin	0.6 % (w/v) haematoxylin, 0.06 % (w/v) $NaIO_3$, 5.28 % (w/v) $Al_2(SO_4)_3$, 6 % (v/v) glacial acetic acid in 25 % (v/v) ethylene glycol
IF blocking solution	0.1 % Triton X-100, 1 % goat serum in PBS
IF M.O.M. antibody solution	0.08 % (v/v) Vector M.O.M. Protein Concentrate in PBS
IF M.O.M. blocking solution	0.0175 % (v/v) Vector M.O.M. Blocking Reagent in PBS
IF washing solution	0.1 % Triton X-100 in PBS
ISH acetylation buffer	0.1 M triethanolamine, 0.053 % (v/v) HCl in DEPC-H_2O
ISH blocking solution	10 % (v/v) heat-inactivated goat serum, 1 % (w/v) Blocking Reagent in ISH MABT
ISH hybridisation buffer	5x DEPC-SSC, 50 % deionised formamide, 5x Denhardt's solution, 250 µg/ml yeast tRNA, 500 µg/ml herring sperm DNA
ISH MAB solution, 5x	500 mM maleic acid, 1.5 M NaCl, adjust pH to 7.5 by adding about 4 % (w/v) NaOH pellets
ISH MABT solution	0.1 % (v/v) Tween-20 in 1x ISH MAB solution
ISH NTMT solution	100 mM Tris-Cl pH 9.5, 100 mM NaCl, 50 mM $MgCl_2$, 0.1 % (v/v) Tween-20; prepare freshly
ISH RNase buffer	10 mM Tris-HCl pH 8.0, 1 mM EDTA, 500 mM NaCl
ISH washing buffer I	2x SSC, 50 % (v/v) formamide, 0.1 % (w/v) *N*-lauroylsarcosine
ISH washing buffer II	2x SSC, 0.1 % (w/v) *N*-lauroylsarcosine
ISH washing buffer III	0.2x SSC, 0.1 % (w/v) *N*-lauroylsarcosine
LB agar	1.5 % (w/v) agar in LB medium; autoclave and store at 4 °C
LB medium	1 % (w/v) Bacto Tryptone, 0.5 % (w/v) Bacto Yeast Extract, 1 % (w/v) NaCl; autoclave and store at 4 °C
NBT stock solution	50 mg/ml NBT in 70 % (v/v) DMF; store at -20 °C

Name *(Continued)*	**Composition** *(Continued)*
Nissl thionin solution, 0.2 % (w/v)	0.2 M glacial acetic acid, 36 mM NaOH; adjust pH 4.0, then add Nissl thionin stock solution to a final thionin concentration of 0.2 %
Nissl thionin stock solution, 1.3 % (w/v)	1.3 % (w/v) thionin acetate salt (85 % dye); stir and heat gently for 1 h; filter after dissolving
PBS stock solution, 10x	dissolve 1 package (#L182-50) in 5 l ddH_2O
PBST	0.5 % (v/v) Tween-20 in PBS
Protein sample buffer, non-reducing, 5x	62.5mM Tris-HCl pH 6.8, 25mM EDTA pH 6.8, 5 % (w/v) SDS, 0.025 % (w/v) bromophenol blue, 50 % (v/v) glycerol
Protein sample buffer, reducing, 5x	62.5mM Tris-HCl pH 6.8, 25mM EDTA pH 6.8, 5 % (w/v) SDS, 5 % (v/v) 2-mercaptoethanol, 0.025 % (w/v) bromophenol blue, 50 % (v/v) glycerol
Protein solubilisation buffer	1 % (w/v) CHAPS in PBS, supplemented with protease inhibitors: 100 µM aprotinin, 10 µM leupeptin, 10 µM pepstatin A, 100 µM PMSF
Protein sucrose buffer	0.34 M sucrose in PBS, supplemented with protease inhibitors: 100 µM aprotinin, 10 µM leupeptin, 10 µM pepstatin, 100 µM PMSF
SB denaturation buffer	0.5 M NaOH, 1 M NaCl
SB depurination buffer	250 mM HCl
SB neutralisation buffer	0.5 M Tris, 1 M NaCl; adjust pH to 7.5
SB washing buffer I	1x SSC, 1 % SDS
SB washing buffer II	1x SSC, 0.1 % SDS
SB washing buffer III	0.5x SSC, 0.1 % SDS
SB washing buffer IV	0.2x SSC, 0.1 % SDS
SB washing buffer IV	0.1x SSC, 0.1 % SDS
Scott's tap water substitute	81 mM $MgSO_4$, 24 mM $NaHCO_3$ in tap water
SDS-PAGE running buffer	0.19 M glycine, 25 mM Tris, 0.1 % (w/v) SDS
SDS-PAGE separating gel	0.375 M Tris-Cl pH 8.8, 0.1 % (w/v) SDS, varying concentrations (7.5 %/ 10 %/ 12 %, v/v) of acrylamide/ bisacrylamide solution (30 %, 19:1) , 0.05 % (w/v) APS, polymerisation initiated by 0.05 % (v/v) TEMED
SDS-PAGE stacking gel	0.123 M Tris-Cl pH 6.8, 0.1 % (w/v) SDS, 3.858 % acrylamide/ bisacrylamide solution (30 %, 19:1), 0.05 % (w/v) APS, polymerisation initiated by 0.01 % (v/v) TEMED
Silver stain developer I	10 % (w/v) K_2CO_3
Silver stain developer II	2 % (w/v) K_2CO_3, 0.01 % (v/v) formaldehyde
Silver stain ethanol solution	10 % (v/v) ethanol
Silver stain fixation solution	50 % (v/v) methanol, 12 % (v/v) trichloroacetic acid, 2 % (w/v) $CuCl_2$
Silver stain silver solution	0.2 % (w/v) $AgNO_3$
Silver stain washing solution	10 % (v/v) ethanol, 5 % (v/v) acetic acid
SSC, 20x	3 M NaCl, 0.3 M sodium citrate; adjust pH to 7.0, filter through 0.45 µm pore size
TAE stock solution, 50x	2 M Tris, 1 M acetic acid, 50 mM EDTA; use EDTA stock solution pH 8.0 to adjust pH
TBS stock solution, 10x	1.5 M NaCl, 0.5 M Tris; adjust pH to 7.4 with 32 % HCl
TBST	0.5 % (v/v) Tween-20 in TBS
TE buffer	10 mM Tris-Cl pH 8.0, 1 mM EDTA pH 8.0
Tissue lysis buffer	50 mM KCl, 2 mM $MgCl_2$, 10 mM Tris pH 8.0, 0.01 % (w/v) gelatin, 0.45 % (v/v) Triton X-100, 0.45 % (v/v) Tween-20

Name *(Continued)*	**Composition** *(Continued)*
WB blocking solution (BSA)	2 % (w/v) BSA, 0.5 % (v/v) Tween-20 in PBS
WB blocking solution (milk)	5 % milk (w/v) in TBS
WB chemiluminescent substrate	Super Signal West Dura, Extended Duration Substrate, Thermo Scientific (see Kits)
WB colourimetric substrate	165 µg/ml NBT, 82.5 µg/ml BCIP in AP detection buffer
WB ponceau solution	0.1 % (w/v) Ponceau S, 5 % (v/v) acetic acid
WB transfer buffer	20 % (v/v) methanol, 0.19 M glycine, 25 mM Tris

3.10 Cell culture solutions, media and antibiotics

Solutions	**Company**
DMEM + GlutaMAX + 4.5 g/l glucose + pyruvate	Gibco
Fetal bovine serum (FBS)	Gibco
Geneticin (G418), dissolved as 100 mg/ml in sterile dH_2O	Life Technologies
Leukemia inhibitory factor (LIF), COS cell supernatant	C. Birchmeier lab, MDC
2-Mercaptoethanol, 50 mM	Gibco
MEM non-essential amino acids (NEAA), 100x	Gibco
Mitomycin C, dissolved as 1 mg/ml in 5 % (v/v) sterile DMSO in sterile PBS	Sigma-Aldrich
Opti-MEM	Gibco
Penicillin 10000 U/ml - Streptomycin 10000 µg/ml	Gibco
Trypsin 0.05 % / EDTA 0.02 % in PBS w/o Ca^{2+} and Mg^{2+}	PAN Biotech
DMEM	Gibco
Ham's F12 + GlutaMAX	Gibco
Media	**Composition**
COS-7 cell culture medium	DMEM + GlutaMAX + 4.5 g/l glucose + pyruvate supplemented with 10 % (v/v) FBS, 100 µg/ml penicillin, 100 U/ml streptomycin
ES cell culture medium	DMEM + GlutaMAX + 4.5 g/l glucose + pyruvate, supplemented with 15 % (v/v) FBS, 1 % (v/v) NEAA, 100 µg/ml penicillin, 100 U/ml streptomycin, 100 µM 2-mercaptoethanol, 350 µl LIF per 500 ml medium; during selection processes, 400 µg/ml G418 was added to the medium
ES cell freezing medium	65 % (v/v) ES cell culture medium, 25 % (v/v) FBS, 10 % (v/v) DMSO
MEF cell culture medium	DMEM + GlutaMAX + 4.5 g/l glucose + pyruvate, supplemented with 10 % (v/v) FBS, 1 % (v/v) NEAA, 100 µg/ml penicillin, 100 U/ml streptomycin, 90 µM 2-mercaptoethanol
MEF cell freezing medium	65 % (v/v) MEF cell culture medium, 25 % (v/v) FBS, 10 % (v/v) DMSO
Ureter *ex vivo* culture medium	1:1 DMEM/Ham's F12 + GlutaMAX, supplemented with 5 µg/ml transferrin, 100 µg/ml penicillin, 100 U/ml streptomycin

3.11 Kits

Name	**Company**
DIG Wash and Block Buffer Set	Roche Applied Science
Genomic DNA Buffer Set	Qiagen
Genomic-tip 500/G	Qiagen
Illustra MicroSpin G-50 Columns	GE Healthcare
Invisorb DNA Fragment CleanUp	Invitek
Plasmid Midi Kit	Qiagen

Name *(Continued)*	**Company** *(Continued)*
Plasmid Mini Kit	Qiagen
Prime-IT RmT Random Primer Labeling Kit	Agilent Technologies
RNase-free DNase Set	Roche Applied Science
RNeasy Mini Kit	Qiagen
SuperSignal West Dura Extended Duration Substrate	Thermo Scientific
Vector M.O.M. Immunodetection Kit	Vector Laboratories

3.12 Consumables

Name	**Company**
Amicon PM30 Ultrafiltration Discs, 30 kDa NMWL	Merck Millipore
Amicon Ultra-15 Centrifugal Filter Units, 10 kDa NMWL	Merck Millipore
Blotting paper, 400 g/m^2	Macherey-Nagel
Cell culture 0.4 µm PET filter membrane hanging inserts	BD Falcon
Cellophane foil	GE Healthcare
Cover slips	Menzel
Dialysis tubes (MW cut-off 12-16 kDa)	Biomol
Falcon tubes, RNase-free (15 ml, 50 ml)	Greiner
Gene pulser cuvettes, 0.4 cm electrode gap, sterile	Bio-Rad
Glass slides Superfrost	Menzel
Glass slides Superfrost Plus	Menzel
Microtubes, safe-lock (0.5 ml, 1.5 ml, 2 ml)	Eppendorf; Sarstedt
Microtubes, RNase-free (1.5 ml)	Brand
Microtubes, PCR ultra thin wall (0.2 ml)	Kisker Biotech
Multiwell plates (6-, 12-, 24-, 48-, 96-well)	Greiner
Nitrocellulose membrane, 0.45 µm	GE Healthcare
Nylon membrane, positively charged, Amersham Hybond-N+	GE Healthcare
Pipette tips	Biozym; Greiner; Sarstedt
Technovit Histoblocs	Kulzer
UVette photometer cuvette	Eppendorf

3.13 Equipment

Name	**Company**
Agarose gel documentation system GelDoc XR+	Bio-Rad
AxioCam HRc camera	Zeiss
Cell freezing container	Thermo Scientific
Centrifuge Megafuge 1.0 R	Heraeus
Centrifuge Sorvall RC 6+	Thermo Scientific
Centrifuge Sorvall RC M150GX	Thermo Scientific
Confocal microscope LSM 710	Zeiss
Cryostat CM1950	Leica
Electroporation device	Bio-Rad
Fluorescence microscope Biozero BZ-8100	Keyence
Hybridisation oven PerfectBlot	Peqlab
Incubator CB 150	Binder
Injection equipment Cell Tram Oil	Eppendorf
Micromanipulator	constructed at MDC
Micropipette puller Model P-97 Flaming/Brown	Sutter Instruments
Microtome	Mikrom

Name *(Continued)*	**Company** *(Continued)*
Peristaltic pump	Bio-Rad
Photometer BioPhotometer	Eppendorf
Phosphorimager Typhoon FLA 9500	GE Healthcare
Phosphorimager FLA 7000	Fuji
Stereomicroscopes (Stemi DRC, Stemi SV11)	Zeiss
SDS-PAGE equipment (horizontal chamber)	Bio-Rad
Slide dryer	Omnilab Jürgens
Thermocycler PeqSTAR 96X Universal Gradient	Peqlab
Thermomixer	Eppendorf
UV crosslinker	Thermo Scientific
Vacuum gel dryer Drygel Jr.	Hoefer Scientific Instruments
Western blot documentation system ChemiDoc XRS	Bio-Rad
Western tank blot equipment	Bio-Rad

3.14 Software

Name	**Version**	**Company**
BZ Analyzer		Keyence
BZ Viewer		Keyence
Lasergene	5.03	DNASTAR
Excel	2010 14.0.7151.5001	Microsoft
Image Lab	5.1	Bio-Rad
ImageJ	1.46r	NIH USA
Photoshop	CS4 11.0.2	Adobe
PyRAT	3.2-266	Scionics
Quantity One	4.6.5	Bio-Lab
Serial Cloner	2.6.1	SerialBasics
SigmaStat	3.5	Systat Software, Inc.
ZEN Black	2012	Zeiss
ZEN Blue	2012	Zeiss

4 METHODS

4.1 Standard molecular biological and microbiological techniques

The molecular biological and microbiological methods used in this thesis are mainly based on protocols from *"Molecular Cloning: A Laboratory Manual"* (Sambrook & Russell, 2001) or on manufacturers' instructions from kit manuals and were performed as described in the following sections.

4.1.1 Polymerase chain reaction (PCR)

The polymerase chain reaction (PCR) technique was carried out to amplify DNA fragments for several downstream applications, of which two major purposes were pursued: First, to synthesize a specific DNA fragment for usage in molecular cloning or hybridisation procedures. Second, to examine whether a specific DNA fragment is present in the template DNA, e.g. in genotyping or reverse transcription PCR applications.

PCR utilises the ability of DNA polymerase to synthesise a DNA sequence complementary to the template DNA by sample incubation in repeated temperature cycles. In the first step, the template DNA is denatured, followed by an annealing step, in which oligonucleotide primers hybridise to the single-stranded DNA, and a subsequent elongation step, in which the DNA strand is extended by DNA polymerase-mediated complementary incorporation of deoxyribonucleoside triphosphates (dNTPs).

The *Taq* DNA polymerase was mainly used for animal genotyping (section 4.3), while proofreading DNA polymerases with 3'->5' exonuclease activity like Phusion or Q5 were used in amplifications for molecular cloning or for probe generation. Phusion and Q5 DNA polymerases generate blunt-ended PCR products, which were used in blunt-ended cloning (section 4.1.6). Generally, PCR reaction buffers that were supplied with the DNA polymerase were used to ensure optimal reaction conditions for each polymerase. Template DNA amount, concentrations of oligonucleotide primers and dNTPs as well as thermocycling conditions were adjusted according to the manufacturer's instructions.

4.1.2 Enzymatic restriction of DNA

DNA was digested by restriction endonucleases for several applications, e.g. molecular cloning procedures, targeting vector linearisation for electroporation into embryonic stem cells, or genomic DNA (gDNA) fragmentation for Southern blot analysis. Appropriate enzymes were chosen to digest DNA at specific restriction sites and generate blunt ends. In the reaction mix, the unit amount of restriction enzyme was adjusted to the amount and type of DNA (genomic or plasmid DNA) and DNA was digested in the supplied reaction buffer according to the manufacturer's instructions at the recommended temperature for 2 h until O/N.

4.1.3 Agarose gel electrophoresis

Agarose gel electrophoresis served to separate DNA fragments according to their molecular weights in an electric field. The pore size determining agarose concentration in the gel was adjusted to the DNA fragment sizes in order to obtain best separation. Agarose was dissolved in 1x TAE buffer by heating, supplemented with ethidium bromide, poured and allowed to cool down. Prior to loading, DNA samples were supplemented with DNA loading dye. The molecular weight marker GeneRuler 1kb Plus DNA Ladder was loaded to estimate the size of DNA fragments in the gel. In case of DNA fragment quantification, 7 µl of Lambda DNA/*Hin*dIII Marker 2 were additionally loaded. The gels were usually run at around 100 V for 30 min-1h in 1x TAE buffer. Visualisation of DNA was performed under UV light in the GelDoc XR+ gel documentation system with Image Lab software.

4.1.4 Gel extraction of DNA fragments

In order to purify DNA fragments that had been generated by PCR amplification or by enzymatic restriction (section 4.1.2) and separated by agarose gel electrophoresis (section 4.1.3), the DNA fragments were cut from the gel and DNA was extracted by means of the Invisorb DNA Fragment CleanUp kit according to manufacturer's instructions. Briefly, the gel piece was solubilised in a supplied buffer at 50 °C and subsequently purified via a DNA binding silica spin filter. After washing, DNA was eluted with nuclease-free H_2O or supplied elution buffer.

4.1.5 DNA phenol-chloroform-isoamyl alcohol (PCIA) extraction & ethanol precipitation

To extract DNA from tissue digestion samples or after endonuclease restrictions, a 25:24:1 phenol-chloroform-isoamyl alcohol (PCIA) mixture was added to the sample in an equal volume and vortexed vigorously to mix the phases. After centrifugation at 12,000 x g for 2 min to separate the phases, the aqueous upper phase containing the DNA was carefully transferred to a new tube. The PCIA addition was repeated once more by adding PCIA in a 1:1 volume, followed by vortexing, spinning and transferring the upper phase to a new tube. Then, a 1:1 volume of chloroform was added to the solution, which was vortexed and spinned again at 12,000 x g for 2 min. After transferring the upper phase to a new tube, the DNA was precipitated using an ethanol-salt solution. First, 1/10 volumes of 3 M sodium acetate, pH 5.2, were added and mixed, followed by addition of 2 volumes cold 100 % ethanol. The sample was mixed and left O/N at -20 °C to precipitate the DNA. The DNA was pelleted by centrifugation at 12,000 x g for 30 min at 4 °C and the supernatant was carefully decanted. The DNA pellet was washed twice using cold 70 % ethanol and allowed to air dry. Finally, depending of the purpose the DNA was dissolved in either nuclease-free ddH_2O or TE buffer, pH 8.0.

4.1.6 Molecular blunt-end cloning

4.1.6.1 Phosphorylation and dephosphorylation of blunt 5' DNA termini

In order to enhance blunt cloning efficiency and avoid vector religation (self-ligation) without insert incorporation, the 5' blunt ends of PCR products were phosphorylated by T4 polynucleotide kinase (T4 PNK), while 5' phosphates of blunt-ended linearised vectors were removed by calf intestinal phosphatase (CIP). PCR fragments were gel-purified and incubated in ATP-containing 1x T4 DNA ligase buffer with 10 U of T4 PNK for 1 h at 37 °C followed by 20 min at 65 °C. Linearised, gel-purified vectors were dephosphorylated with 3 U CIP in supplied dephosphorylation buffer for 1 h at 37 °C and CIP was subsequently inactivated for 20 min at 80 °C. Phosphorylated inserts and dephosphorylated vectors were purified and DNA concentration was estimated by quantitative gel analysis.

4.1.6.2 Blunt-end DNA ligation

During a ligation reaction, linear double-stranded DNA fragments are fused covalently in order to create a recombinant circular plasmid. T4 DNA ligase is used to catalyse the formation of phosphodiester bonds between the 5' phosphoryl terminus of one DNA fragment and the 3' hydroxyl terminus of the other DNA fragment. For blunt-end ligation, the blunt-ended, CIP-treated linearised vector and the blunt-ended, T4 PNK-treated DNA insert were mixed in a molar ratio of 1:3. To determine the volume of insert DNA that is required for ligation with 1 µl of vector DNA, the following formula was used:

$$insert\ volume\ [\mu l]\ per\ 1\ \mu l\ vector = \frac{3 * vector\ concentration\ \left[\frac{ng}{\mu l}\right] * insert\ size\ [bp]}{1 *\ insert\ concentration\ \left[\frac{ng}{\mu l}\right] * vector\ size\ [bp]}$$

The calculated amounts of vector and insert DNA were mixed, and nuclease-free water was added to a final volume of 8 µl. The DNA mixture was denatured at 95 °C for 5 min and immediately chilled on ice for 1 min. Then, 5 U T4 DNA ligase were added to the sample and incubated in supplied T4 ligase buffer for 2 h at RT. The ligation mix was immediately used for bacterial transformation.

4.1.7 Bacterial plasmid DNA amplification

To amplify recombinant plasmids, the plasmid DNA was introduced into chemically competent bacteria by heat-shock transformation, followed by bacteria cultivation, bacteria lysis and plasmid extraction. Bacterial handling required working under sterile conditions in a laminar flow hood. All materials and solutions were autoclaved prior to use.

4.1.7.1 Bacterial culture

Bacterial *E. coli* strains DH5α or DH10B were either streaked on LB-agar plates or grown with shaking in LB medium at 37 °C. The LB agar plates and the LB medium were supplemented with appropriate antibiotics for cultivation and selection of transformed bacteria. Ampicillin was used at a concentration of 100 µg/ml, while chloramphenicol was used at 20 µg/ml.

4.1.7.2 Bacterial heat-shock transformation

A frozen aliquot containing 130 µl of chemically competent *E. coli* strain DH5α or DH10B was slowly thawed on ice. The ligation sample was added to the bacteria, gently mixed and incubated for 20 min on ice. Then, bacteria underwent a heat shock by exposure to 42 °C for 2.5 min, followed by immediate chilling on ice for 1 min. Pure LB medium (without antibiotic) was added up to a final volume of 500 µl, and bacteria were shaken for 1 h at 37 °C and 250 rpm in order to develop the plasmid-mediated antibiotic resistance. Afterwards, the bacteria were streaked onto LB-agar plates containing the appropriate antibiotics and grown O/N at 37 °C.

4.1.7.3 Inoculation of bacterial mini and midi cultures

Bacterial mini cultures were inoculated by picking single bacterial clones, transferring them into 3 ml of antibiotic-containing LB medium and culturing 8 h until O/N. Mini cultures were screened for successful transformation by isolation and restriction of plasmid DNA (sections 4.1.8 and 4.1.2), and positive clones were amplified in larger cultures. For this purpose, 50-100 ml midi cultures were inoculated with 200-400 µl of the positive mini culture and cultivated O/N.

4.1.8 Extraction of plasmid DNA from bacteria

Plasmid DNA was extracted from bacteria using the Qiagen Plasmid Mini and Plasmid Midi kits according to manufacturer's instructions. Briefly, bacteria were pelleted, lysed in presence of RNase A and plasmid DNA was purified via anion-exchange columns.

4.1.9 Extraction of bacterial artificial chromosome (BAC) DNA from bacteria

To isolate DNA from bacteria carrying a bacterial artificial chromosome (BAC), harvested cells were lysed and the lysate was neutralised according to the Qiagen Plasmid Mini kit handbook. Instead of further purifying BAC DNA by Qiagen plasmid purification columns, BAC DNA was purified by PCIA extraction and ethanol precipitation (section 4.1.5).

4.1.10 Bacterial glycerol stocks

For long-term storage of recombinant bacteria, bacterial cultures were diluted to 80 % (v/v) in sterile glycerol and stored at -70 °C.

4.1.11 RNA techniques

Special attention was required for the work with RNA due to degradation by ubiquitous RNases. To work under RNase-free conditions, all equipment and solutions were purchased or prepared RNase-free. Equipment was wrapped in aluminium foil and subjected to baking for 3 h at 180 °C to destroy RNases. To inhibit RNases in solutions, solutions were treated with 0.1 % (v/v) DEPC, left stirring O/N and autoclaved afterwards, except for amine group containing solutions, which were prepared using DEPC-treated dH_2O.

4.1.11.1 Isolation of total RNA from tissue

Immediately after mouse sacrifice, the tissue was rapidly but precisely dissected, transferred to a microtube and frozen in a mixture of dry ice and ethanol. 30 mg of tissue were used for RNA isolation using the RNeasy Mini Kit according to manufacturer's instructions. Briefly, the tissue was lysed and cell debris was removed. Thereafter, the RNA was purified by means of silica-based columns, eluted in dH_2O and stored at -80 °C.

4.1.11.2 Reverse transcription PCR (RT-PCR)

First strand complementary DNA (cDNA) was synthesised from total RNA using $Oligo(dT)_{18}$ primers and SuperScript II Reverse Transcriptase according to manufacturer's instructions. The RNase inhibitor RNaseOUT was included in the reaction sample to avoid RNA degradation. cDNA was either stored at -20 °C or immediately used as template in PCR analysis using exon-exon overlapping primers to prevent amplification of gDNA.

4.1.12 Determination of nucleic acid concentration

The concentration of nucleic acids was either determined by a spectrophotometer or estimated in a quantitative agarose gel. Photometrically, the absorbance at 260 nm wavelength was measured and used to calculate the DNA concentration via the formula

$$DNA\ concentration\ [\mu g/\mu l] = \frac{OD_{260} \times dilution\ factor \times 50\ \mu g/ml}{1000}$$

or to calculate the RNA concentration via the formula

$$RNA\ concentration\ [\mu g/\mu l] = \frac{OD_{260} \times dilution\ factor \times 40\ \mu g/ml}{1000}$$

Alternatively to the spectrophotometric measurements, the concentration of DNA bands was estimated in a quantitative agarose gel by comparing the band intensities to a molecular weight marker with bands of a known DNA amount.

4.2 Generation of *Clmp* knockout mouse strain

4.2.1 Targeting strategy

The targeting strategy aims at a traditional *Clmp* knockout by replacing the start codon-containing exon 1 of the *Clmp* gene by a *Neo* gene cassette. For this purpose, the pVBTK-CLMP targeting vector was designed and obtained from Vega BioLab. The structure of the targeting vector was as follows (from 5' to 3'): linearisation site – 5' homologous arm – *loxP* cassette – phosphoglycerate kinase 1 (PGK) terminator (reverse complement) – *Neo* gene cassette (reverse complement) – PGK promoter (reverse complement) – *loxP* cassette – 3' homologous arm. Downstream the 3' homologous arms, a thymidine kinase (TK) cassette was inserted consisting of a herpes simplex virus *TK* gene flanked by PGK promoter and terminator sequences (FIGURE 3).

4.2.2 Sequencing of targeting vector

The sequences of the pVBTK-CLMP targeting vector that are relevant for homologous recombination (ranging from the 5' homologous arm to the 3' homologous arm) were sequenced by MWG Genomics using forward and reverse primers (section 3.6). Sequence analysis was performed using Lasergene and Serial Cloner software and the full sequence can be found in the supplementary information (section 8).

4.2.3 Targeting vector preparations for electroporation into embryonic stem (ES) cells

The pVBTK-CLMP targeting vector was delivered as purified plasmid DNA. To obtain enough vector DNA for electroporation, the plasmid was transformed into *E. coli* DH10b cells and purified as described in sections 4.1.7 and 4.1.8. 120 µg of targeting vector DNA were linearised O/N at 37 °C using 240 U of restriction enzyme *I-Ceu*I. The digested targeting vector was purified by PCIA extraction, precipitated and resuspended in sterile TE buffer, pH 8 (section 4.1.5). A quantitative gel was used to estimate the DNA concentration (section 4.1.11).

4.2.4 Genetic targeting of ES cells

For generation of transgenic mice, the targeting vector was electroporated into embryonic stem (ES) cells in order to incorporate the targeting construct into the ES cell genome via homologous recombination. The ES cells required special culture conditions to maintain their pluripotency. ES cells were co-cultured on a feeder layer of mitomycin C-treated murine embryonic fibroblasts (MEF) and were constantly exposed to leukemia inhibitory factor (LIF) to prevent cell differentiation.

The ES cell line used to generate Clmp transgenic mice was the 129P2/OlaHsd strain-derived E14.1 line (Hooper *et al.*, 1987; Kühn *et al.*, 1991). The MEF cells carried a *Neo* resistance gene conferring resistance to the antibiotic geneticin, which was applied during ES selection processes. Both ES and MEF cells were kindly provided by the C. Birchmeier-Kohler lab, MDC.

4.2.4.1 Murine embryonic fibroblast (MEF) cell culture

The MEF cells were obtained as frozen primary cells from dissected diaphragms and were considered as passage 0. A vial of passage 0 MEF cells was rapidly thawed, diluted in MEF culture medium and centrifuged for 4 min at 150 x g. The cells were resuspended in fresh MEF culture medium and seeded onto a 15 cm dish in 20 ml MEF culture medium. The cells were incubated at 37 °C in a humidified atmosphere of 5 % CO_2 in air and the medium was changed every second day. Confluent MEF cells could be passaged up to three times by trypsinisation. For passaging, MEF cells were washed two times with PBS and incubated in 0.05 % trypsin/0.02 % EDTA in PBS (trypsin-EDTA) for 3 min at 37 °C. Trypsinised cells were diluted in MEF culture medium and pelleted at 150 x g for 4 min. After resuspension in MEF culture medium, MEF cells were splitted 1:4 onto new 15 cm culture dishes. In order to grow MEF cells as a feeder layer for ES cell culture, their cell divisions had to be previously inactivated. To block further proliferation, confluent MEF cells were treated with 0.1 mg/ml mitomycin C for

2 h at 37 °C, washed with PBS and either incubated in MEF culture medium for further culture or frozen at -80 °C for later use. For storage, cells were pelleted and trypsinised as described above and resuspended in pre-cooled MEF cell freezing medium containing the cryopreservative DMSO. The cell suspension was transferred to sterile cryovials and frozen at -80 °C in freezing containers filled with isopropanol to obtain a slow freezing rate.

4.2.4.2 Murine ES cell culture

ES cells were grown on a feeder layer of inactivated MEF cells in LIF-containing ES cell culture medium with 5 % CO_2 under humidified conditions. In contrast to the confluently growing MEF cells, ES cells grew as dense, spherical colonies on top of the MEF layer. The ES cell population of each colony derived from a single cell, making all cells of the colony genetically identical. Consequently, each colony was considered as an individual clone. The culture of ES cells required a medium change every day. Thawing, splitting and freezing procedures of ES cells were carried out analogous to the MEF cells, except for using ES cell culture medium instead of MEF cell culture medium.

4.2.4.3 Electroporation of pVBTK-CLMP into ES cells

For electroporation, ES cells of two 10 cm culture dishes were washed, trypsinised as described above and resuspended in 20 ml ES cell culture medium. After cell number determination of 10 µl cell suspension in a Neubauer chamber, the suspension was spinned at 150 x g for 4 min. The cell pellet was resuspended in an appropriate volume of PBS to gain a concentration 1.2 x 10^7 cells/800 µl. 800 µl of the suspension were then mixed with 30 µg linearised pVBTK-CLMP and transferred into a pre-cooled Gene Pulser electroporation cuvette with 0.4 cm gap. The electroporation was performed for 2 ms at 300 V and 1200 µF and cells were subsequently cooled on ice for 5 min. Afterwards, the electroporated cells were suspended in 9 ml ES cell culture medium and dispensed onto three 10 cm MEF dishes.

4.2.4.4 Selection of ES cell clones by geneticin

Two days after electroporation, the positive selection process of ES cell clones started by supplementing the ES cell culture medium with 400 µg/ml geneticin (G418). ES cells that had incorporated the *Neo* gene containing pVBTK-CLMP vector into their genome were conferred a G418 resistance, thus surviving this positive selection. On the contrary, cells that were negative for the targeting construct died over time.

The pVBTK-CLMP vector also contained a TK expression cassette downstream the 3' homologous arm for negative selection of ES cell clones. Cell clones that had incorporated the construct by non-homologous recombination at any site in the genome can be eliminated by exposition to ganciclovir. However, this counter selection process by ganciclovir application was not deemed necessary and was therefore not performed.

Ten days after electroporation, the G418 selection was completed. ES clones with a spherical shape and a well-defined border were picked with a pipette tip and transferred to a separate well of an empty 96-well plate. Here, clones were singularised in 50 µl trypsin-EDTA at 37 °C

for 4 min and resuspended in additional 80 µl of ES cell culture medium. The single cell clones were transferred to a MEF layered 96-well plate and grown for about 3 days with daily medium change. When the wells were densely grown, cells were washed with PBS, trypsinised with 30 µl trypsin-EDTA for 3 min at 37 °C, resuspended in ES cell culture medium and splitted 1:3 onto one MEF layered 96-well plate and two 96-well plates coated with 0.1 % gelatin. Between four and six days after splitting, the ES cells grown on the MEF 96-well plate were washed, trypsinised as described above and resuspended in 100 µl pre-cooled ES cell freezing medium. The plate was wrapped with paper towels, put in a styrofoam box and frozen at -80 °C. The ES cells on the gelatin-coated plates were overgrown for seven till ten days for later extraction of gDNA and subsequent primary Southern blot analysis.

ES cell clones that had been screened positive in primary Southern blot analysis were thawed and expanded from one 96-well via 48-wells, 24-wells, and 12-wells to finally one MEF 6-well and two gelatin-coated 6-wells (as described). During this long period of expansion, fractions of the ES cell clones were occasionally frozen to -80 °C and later transferred to liquid nitrogen as a precaution. The ES cell gDNA from gelatin-coated 6-wells was rescreened in a secondary Southern blot analysis prior to blastocyst injection (sections 4.2.5 and 4.2.6).

4.2.5 Southern blot analysis

The correct integration of the targeting construct into the ES cell and mouse genome by homologous recombination was verified by capillary Southern blotting and hybridisation with ^{32}P-labelled DNA probes.

4.2.5.1 Southern probe generation

Two external DNA probes were selected to hybridise to gDNA regions outside the targeting construct in order to detect whether the construct has been integrated into the gDNA by homologous recombination. A 5' probe was designed to bind to a region upstream of the 5' homologous arm of the targeting construct, while a 3' probe was designed to hybridise to a region downstream the 3' homologous arm.

In a first step, the Ensembl browser was screened to identify a bacterial artificial chromosome (BAC) clone that covered an appropriate sequence range of the *Clmp* gene in order to amplify the probes from BAC clone DNA. Since no BAC library with a 129P2/OlaHsd genetic background was available, a BAC library that had been generated from 129S7/SvEvBrd-*Hprt*$^{b\text{-}m2}$-derived AB2.2 ES cells (Adams *et al.*, 2005) was screened. The BAC clone bMQ83n17 contained a 122,930 bp sequence that spanned the genomic region from 40,645,194 to 40,768,124 on the forward strand of murine chromosome 9, covering almost the complete *Clmp* gene (40,685,962 to 40,785,319) including the probe binding sites. This BAC clone bMQ83n17 was purchased from Source BioScience as *E. coli* DH10B culture. The bacteria were cultured in LB medium supplemented with 20 µg/ml chloramphenicol and BAC DNA was purified as described in section 4.1.9. A 829 bp 5' probe and a 605 bp 3'probe were amplified by PCR using 10 ng BAC DNA template and 1 U of Phusion DNA polymerase (sections 4.1 and 3.6) to

guarantee proofreading and to generate blunt ends for cloning. The probes were purified by gel extraction (section 4.1.4) and phosphorylated (section 4.1.6.1), while the vector pBlueScript II SK (+) was linearised using blunt end generating *Eco*RV, gel-purified and subsequently dephosphorylated (section 4.1.6.1). The phosphorylated probe inserts and the dephosphorylated vector were purified via gel extraction and thereafter ligated by T4 DNA ligase for 2 h at RT (section 4.1.6.2). The ligation sample was transformed into chemically competent *E. coli* DH5α cells (section 4.1.7.2) and the cells were streaked on LB-ampicillin plates and cultured at 37 °C O/N. Bacterial mini cultures were inoculated and plasmids were purified (sections 4.1.7.3 and 4.1.8). Plasmid mini DNA was digested with *Eco*RI and *Xba*I to test insert orientation of the 5' probe and the 3' probe, respectively. Positive clones were used to inoculate midi cultures, and plasmid midi DNA was purified using the Qiagen Plasmid Midi Kit and sequenced. Finally, the plasmid DNA was restricted with *Ava*I to excise probe inserts and subsequently probes were gel-purified. Quantitative agarose gel electrophoresis was used to analyse probe concentration and to ensure successful purification.

4.2.5.2 Southern probe dCTP[α-^{32}P] labelling

For Southern hybridisation, probes were labelled with radioactive phosphorous-32 (^{32}P) in order to autoradiographically detect the desired DNA fragments on a nylon membrane. Due to the short half-life of ^{32}P, probes were freshly labelled immediately before hybridisation using the Prime-It RmT Random Primer Labeling Kit according to manufacturer's instructions. Briefly, 50 ng probe DNA were denatured at 95 °C for 10 min and then radiolabelled by incorporation of about 16.65 pmol dCTP[α-^{32}P] with a specific activity of 3000 Ci/mmol using 12 U of Magenta polymerase for 10 min at 37 °C. Afterwards, the labelling reaction was stopped by addition of EDTA-containing Stop Mix solution. Thereafter, unincorporated nucleotides were removed by gel filtration by centrifugation in Illustra MicroSpin G-50 spin columns at 200 x g for 2 min. The purified probe samples were mixed with 10 µg of sheared mouse gDNA to block unspecific probe binding. 1 ml Church hybridisation buffer was added to the probe and incubated at 65 °C for 30 min - 1 h. For hybridisation of probe to target DNA, the radiolabelled probe was pipetted to the prehybridised nylon membrane.

4.2.5.3 Preparation of genomic DNA for Southern blot analysis

To obtain gDNA of ES cells for the primary screen, ES cells grown in gelatin-coated 96-wells were digested in 50 µl ES cell lysis buffer supplemented with 200 µg/ml proteinase K in a humidified chamber on a shaker at 55 °C O/N. After digestion, the gDNA was precipitated by adding 1/10 volume of 3 M sodium acetate, pH 5.2, and 2.5 volumes of cold ethanol. The mixture was left at 4 °C O/N and the precipitated gDNA was spinned down. Afterwards, the lysis solution was carefully decanted by inverting the multiwell plate, and the gDNA pellet was washed three times with cold 70 % ethanol and finally air-dried. Per 96-well, about 7-11 µg gDNA were yielded for the primary screen.

For rescreens of ES cell clones that had been identified positive in primary screens, clones were thawed and expanded to a 6-well multiplate. ES cells in one 6-well were digested using 200 µg/ml proteinase K in 600 µl of ES cell lysis buffer O/N at 55 °C. A subsequent PCIA purification and ethanol precipitation (section 4.1.5) were performed to purify gDNA.

To verify homologous recombination of the target construct in the genetically modified animals, gDNA of adult wild type, heterozygous and knockout animals was purified from liver samples using the Qiagen Genomic-tip 500/G kit according to manufacturer's instructions.

After extraction, gDNA was digested with the restriction enzyme *Bgl*II for later detection of 8.9 kb wild type and 6.8 kb mutant fragments via the 5' probe, whereas gDNA for 3' probe detection was digested with *Nco*I to reveal 12.3 kb wild type and 6.9 kb mutant fragments. Restrictions with *Bgl*II or *Nco*I were performed O/N at 37 °C in appropriate buffers and with RNase A added to a final concentration of 50 µg/ml. For the primary screen, the entire gDNA (about 7-11 µg) of 96-well ES cell clones was digested with 10 U of restriction enzyme in a final volume of 45 µl. For rescreens of positive ES cell clones and for genetically modified animals, an amount of 20 µg gDNA was digested with 55 U of enzyme in a final volume of 60 µl.

4.2.5.4 Southern blotting

Digested gDNA was separated O/N in a 1 % agarose gel at low voltage of 26-28 V. Afterwards, the gel was stained with ethidium bromide to visualise gDNA, destained again and pretreated for neutral capillary Southern blot transfer. First, the gDNA was depurinised by an 8 min incubation of the gel in SB depurination buffer, then denatured two times for 15 min in SB denaturation buffer, and finally the gel was neutralised by incubation in SB neutralisation buffer two times for 1 h. The gel was then incubated in 20x SSC transfer solution and by means of two gel trays turned over so that the lower, smooth gel side faced the top. A positively charged Hybond N+ nylon membrane was equilibrated in 10x SSC, placed on top of the smooth gel side and covered by 10x SSC-soaked blotting paper. A couple of dry paper sheets and a glass plate were placed on top of the filter papers. The whole blotting sandwich was again turned over, pressed gently by putting a weight onto the sandwich top and left O/N. Using this capillary blotting procedure, gDNA fragments in the gel were transferred to the nylon membrane. After blotting, the membrane was briefly washed in 2x SSC and air-dried, followed by gDNA cross-linking using UV exposure of 70,000 µJ/cm^2. Until hybridisation, the membrane was stored at RT between two sheets of blotting paper.

4.2.5.5 Southern blot hybridisation

The membrane was transferred to roller bottles and prehybridised in an appropriate amount of Church hybridisation buffer in a hybridisation oven at 65 °C for 1 h. Then, the freshly radiolabelled probe was added to the membrane and hybridised at 65 °C O/N. After hybridisation, unspecifically bound probes were removed by a series of washing steps at 68 °C with increasing stringency. First, the membrane was washed for 10 min with 1x SSC containing SB washing buffer I, followed by two 20 min washing steps with SB washing buffer II, where

the SDS concentration was decreased. Then, the membrane was washed with SSC concentration reducing SB washing buffers III, IV and V for at least 15 min each. Once the radiation reached background levels, the membrane was placed between one acetate sheet and one sheet of blotting paper, wrapped in foil and autoradiographically developed by exposition to a photostimulable phosphor plate at RT O/N.

4.2.6 Blastocyst injection and chimaera production

To freshly prepare ES cells for blastocyst injection, frozen 6-well vials of positive ES cell clones were thawed and expanded for several ways to one MEF 6-well. Then, the cells were washed twice with PBS, trypsinised and resuspended in 2 ml ES cell culture medium. In order to divide ES cells from MEF cells, the suspension was transferred to one 12-well and incubated at 37 °C for 45 min. During this time, ES cells were gravitating to the ground while the MEF cells remained floating in the medium. Thereafter, the medium containing the MEF was carefully discarded and the ES cells were resuspended in 300 µl of ES cell culture medium. The ES cell suspension was quickly delivered to the MDC Transgenic Core Facility for immediate blastocyst injection.

Injections of positive ES cell clones into blastocysts and subsequent procedures to obtain chimaeric mice were carried out at the MDC Transgenic Core Facility by technical assistant Katja Becker. For the injection of *Clmp*-targeted E14.1 ES cells clones, C57BL/6-derived blastocysts were used. The ES cells were injected into the blastocoel of the blastocyst, which was subsequently implanted into uteri of C57BL/6 recipient foster mothers. The produced chimaeric animals were evaluated by coat colour chimaerism and with seven weeks of age ready for matings.

4.2.7 Germline transmission, *Cre*-mediated *Neo* excision and backcrossing to C57BL/6 genetic background

Chimaeric male animals were mated with C57BL/6 females and the offspring's germline transmission was evaluated by brown coat colour, followed by validation by PCR genotyping. Progeny that was germline-negative was sacrificed while germline-positive animals were selected for further breedings to establish the "*Clmp*-2043" (B6;129P2-*Clmp*^{tm1aFgr}) mouse strain. The correct integration of the targeting vector in these animals was verified by Southern blot analysis (section 4.2.5). While a fraction of animals of the *Clmp*-2043 strain were inbred and phenotypically analysed, some *Clmp*-2043 mice were mated with mice of the *Cre*-Deleter strain (Schwenk *et al.*, 1995) to excise the *Neo* cassette. Latter progeny was genotyped (section 4.3) for *Cre* recombinase and *Neo* absence, and positive animals (*Clmp*$^{+/-(\Delta Neo)}$; *Cre*$^{+}$) were determined generation N0 and used for backcrossing procedures. Furthermore, the strain designation of backcrossing animals was changed to "*Clmp*-KO" (B6.129P2-*Clmp*$^{tm1a.1Fgr}$).

Backcrossing was started by mating *Clmp*$^{+/-}$ N0 mice with C57BL/6 animals, giving rise to offspring of N1 backcrossing generation, of which heterozygous animals were again backcrossed to C57BL/6 mice. The successive backcrossing of heterozygous *Clmp*-KO animals

of a certain backcrossing generation with new C57BL/6 mice was continued up to generation N10 to obtain a C57BL/6 genetic background.

4.3 Animal genotyping

Animals were genotyped by PCR amplification of a certain gDNA fragment with specific primers. For this purpose, gDNA had to be extracted from animals tissues. Tissues like for instance ear punches or tail biopsies were digested in tissue lysis buffer supplemented with 200 µg/ml proteinase K at 55 °C for several hours. Then, proteinase K was inactivated by incubating the lysis sample at 85 °C for 45 min. The tissue lysate served as gDNA template in PCR genotyping as described in the following chapters. After the PCR, samples were analysed by agarose gel electrophoresis (section 4.1.3).

4.3.1 Genotyping of *Cre*-Deleter strain

The *Cre*-Deleter strain or animals that were mated with *Cre*-Deleter mice were genotyped in a 30 µl PCR reaction mix consisting of 1x ThermoPol Reaction Buffer (supplied with *Taq* DNA polymerase), 250 µM of each dNTP, 3.33 µM of Cre_New1 forward primer (5'-GAA CGC ACT GAT TTC GAC CA-3'), 3.33 µM of Cre_New2 reverse primer (5'-AAC CAG CGT TTT CGT TCT GC-3'), 1.5 U of *Taq* DNA polymerase and 1 µl of the gDNA lysate. The thermocycling conditions were as follows:

Initial denaturation		94 °C – 2 min:30 sec
34 cycles of	denaturation	96 °C – 30 sec
	annealing	58 °C – 30 sec
	extension	68 °C – 40 sec
Storage		4 °C – infinite

After PCR, electrophoresis in a 1.8 % agarose gel revealed a 200 bp band in *Cre*-positive animals.

4.3.2 Genotyping of *Clmp* strains

The gDNA of both *Clmp* strains – the original *Neo* cassette containing *Clmp*-2043 strain and the *Neo*-deleted, backcrossed *Clmp*-KO strain – was analysed for wild type and knockout alleles. For this purpose, two separate PCR reactions were performed to prevent problems caused by primer binding competition to DNA targets. The primers for the wild type reaction were as follows: forward primer "Clmp WT1 FOR", 5'-GAG AAC CGT TTC GTG GAG AG-3' and reverse primer "Clmp WT1 REV", 5'-TTC AGG AGG GGC AGA ATA TG-3'. For detection of the mutant allele in both *Clmp* strains the following primers were used: forward primer "Clmp 5‘ arm FOR", 5'-TCC TAA GAA GGG ACG ACG AG-3' and reverse primer "Clmp insert5’ REV", 5'-AGC CAG TAA GCA GTG GGT TC-3'. These primers bind to the 5´homologous arm and to a sequence upstream the *loxP* sites and the *Neo* cassette and could be therefore used for genotyping of both *Clmp* strains. The PCR reaction was set up in a 25 µl volume with final concentrations of 1x ThermoPol Reaction Buffer (supplied with *Taq* DNA

polymerase), 200 µM of each dNTP, 0.3 µM forward primer, 0.3 µM reverse primer, 0.625 U of *Taq* DNA polymerase and 2-3 µl of the gDNA lysate. The thermocycling profile was as follows:

Initial denaturation		95 °C – 30 sec
45 cycles of	denaturation	95 °C – 30 sec
	annealing	61 °C – 30 sec
	extension	68 °C – 40 sec
Final extension		68 °C – 5 min
Storage		4 °C – infinite

Electrophoresis of the PCR samples was carried out in a 1.5 % agarose gel. PCR reactions with gDNA from wild type animals resulted in a 459 bp band, whereas PCR reactions detected a 428 bp band in knockout alleles.

4.4 Mouse biology of *Clmp* knockout strain

4.4.1 Mouse maintenance and breeding

Laboratory mice were housed at the MDC Animal Facility with conditions in agreement with § 11 TierSchG of German Animal Welfare Act and approved by Berlin authorities (Landesamt für Gesundheitliches und Soziales (LAGeSo)). Since animals of the *Clmp* strains are considered as medically compromised, these animals were additionally maintained under licence G 0371/13 with special attention to sickness. Housing was supervised by Animal Facility staff and technical assistant Karola Bach carried out breedings, sacrifices, and mouse identification activities. All mouse procedures were tracked and coordinated using the PyRAT software. Mice were kept in individually ventilated cages (type II, long) with *ad libitum* access to food and water and were maintained under a 12 h light-dark cycle.

For breedings, one or two females were mated to one male mouse earliest at the seventh postnatal week of life. Preferably, stud males older than the females were chosen and littermate breedings were avoided. During the lactation period, pups were kept in the mother's cage and weaning was carried out after three postnatal weeks. Tail biopsies (licence O 0032/03) and ear punches for genotyping were usually taken at the day of weaning. If earlier information about the genotype was required, tail biopsies were also collected from newborn pups accompanied by pup foot tattoo labelling.

For timed pregnancies, short-time breedings were arranged and female mice were checked for vaginal plugs twice a day. Considering that plugs were noticed mainly in the mornings, the day of plug detection is referred to as embryonic day (E) E 0.5.

4.4.2 Methods of sacrifice

Juvenile and adult mice were briefly anaesthetised with isoflurane and sacrificed by cervical dislocation. Pups and embryos were sacrificed by decapitation. All sacrificed animals and embryos older than E 14 that underwent dissections were registered under the licence T0313/97 approved by Berlin authorities (LAGeSo).

4.4.3 Body weight and length analysis

Animal body weights were noted at post- and pre-weaning stages by technical assistant Karola Bach at the MDC Animal Facility. First, pre-weaning body weights of littermate pups were detected daily from the day of birth on until the day of weaning. In a next set of measurements, post-weaning body weights and corresponding body lengths were tracked in littermates once a week over a period of 11 weeks, covering the postnatal days P 35, P 42, P 49, P 56, P 63, P 70, P 77, P 84, P 91, P 98, and finally P 105. The software SigmaStat was used for statistical analysis.

4.4.4 Survival rate analysis

By means of the regular animal observation during the body weight measurements, a reliable survival determination could be performed in the subset of pre-weaning mice.

4.4.5 Organ wet weight analysis

Weights of several organs was determined in adult animals between P 97 and P 140. Animals were briefly anaesthetised with isoflurane and then sacrificed by cervical dislocation (section 4.4.2). Organs were dissected free of surrounding tissue and weighed. Organs included in weight analysis were brain, heart, lung, liver, spleen, kidneys and gastrointestinal tract composed of stomach and intestine. Statistical comparison of wild type, heterozygous and knockout animals was conducted using the software SigmaStat.

4.4.6 Determination of urinary parameters

Urine was obtained from sacrificed, dissected animals. By means of syringe and needle, urine was directly collected by punctuating the urinary bladder. Samples were stored at -70 °C and urinary parameters were determined by Labor 28, Mecklenburgische Straße 28, 14197 Berlin. Analysed urinary parameters included pH, electrolytes (Na^+, K^+, Mg^{2+}, Ca^{2+}, Cl^-, PO_4^{3-}) as well as glucose, urea, creatinine, and total protein levels. Statistics were analysed by the software SigmaStat.

4.5 Intrapelvic ink injections

To prove whether urine flow from kidneys to urinary bladder may be impaired by physical barriers, ink was injected into the renal pelvis and the ink propagation to urinary bladder via the ureter was observed.

Embryos at developmental stage E 18.5 were dissected free from uteri of timed-pregnant female mice. The embryos were decapitated and a tail biopsy for later genotyping was taken. Then the embryos were placed into separate petri dishes with PBS and were abdominally opened. The urinary tracts were exposed by removal of gastrointestinal organs and single embryos were transferred to and fixed in a new dish with fresh PBS. Pulled pipettes were filled with 12.5 % ink diluted in dH_2O. Pipette tips were inserted into the renal pelvis by means of a micromanipulator. Little pressure was applied to the pipette using a Cell Tram oil injector to inject ink into the pelvis and further to the ureter and finally the urinary bladder.

Ink injections were observed under a dissection stereomicroscope equipped with a 0.6x objective. Images and videos were acquired using the AxioCam camera and Zeiss ZEN Blue software.

4.6 *Ex vivo* culture of ureter explants

To analyse ureteral peristaltic behaviours, ureters were isolated from E 15.5 embryos and cultured *ex vivo*. All dissection and culture procedures were performed under sterile conditions. Time-lapse recordings of ureters were carried out after five days in culture and analysed by ImageJ, Microsoft Excel, and SigmaStat software.

4.6.1 Dissection procedure

Pregnant female mice were briefly anaesthetised by isoflurane and sacrificed by cervical dislocation. E 15.5 embryos were dissected from uteri, decapitated and immediately transferred to ice-cold sterile PBS. The abdomen was opened and the gastrointestinal organs were removed to expose the urinary tract. After detachment of the reproductive organs, the complete urinary tract consisting of kidneys, ureters, and urinary bladder was isolated from the abdominal cavity. To separate the ureters from kidneys and urinary bladder, in a first step the connecting tissue located between the kidneys and ureters was removed. Then, thin membranes covering both kidney and ureter were stripped. By carefully pulling kidneys and bladder apart, the ureters safely detached from these organs without disruption. This is due to the rather lose connections between kidney and ureters on the one hand, and on the other hand the ureter-bladder connections are not yet completely established at that developmental stage.

4.6.2 Culture conditions

Multiwell plates were prepared with 400 µl or 1.8 ml pre-warmed culture medium per 24-well and per 6-well, respectively. After isolation, ureters were transferred to a dish with medium for a brief wash. To avoid any disruption in the ureteral tissue, ureters were only moved by carefully pipetting the ureter in medium by means of a 1 ml pipette tip. After washing, ureters were transferred to the top of a 0.4 µm filter membrane of a multiwell hanging insert. The filter insert was then placed into the medium-supplied multiwells and excessive liquid was carefully removed from the filter top to allow culturing of ureters at the air-liquid interface. Cultivation was carried out in an incubator at 37 °C and in a 5 % CO_2:95 % O_2 air atmosphere. The medium was changed every two days. After four days in culture, ureters began to generate unidirectional, peristaltic contractions.

4.6.3 Time-lapse recordings

At DIV 5, time-lapse images of ureter specimen were acquired using a Zeiss LSM710 inverted confocal microscope at the MDC Microscope Core Facility. Multiwell plates with hanging filter inserts fitted entirely into the microscope stage holder, which was equipped with temperature and CO_2 controllers to maintain normal sterile culture conditions during imaging. Zeiss ZEN

Black software was used to direct microscope settings. Transmitted light images using the 561 nm laser were captured with a 5x or 10x objective every 270 ms (= frame acquisition time) over a period of 2250-4500 frames (= total frame number), which corresponds to an overall time of 10-20 min. The size of time-lapse images was reduced to 348x350 resolution to allow the high acquisition speed. Image zoom was set to 0.9 which resulted in a pixel size of 5.4 µm. After time-lapse recordings, single images for illustration were captured at a higher resolution of 500x500. Acquired image series and single images were saved as lsm files for further processing.

4.6.4 Analysis of peristaltic contraction frequency and speed

Acquired time-lapse image series were used for analysis of ureter length, number and speed of peristaltic contraction waves, and ureter diameter changes during contractions. For the investigation of wave number and speed, Dr Zoltan Cseresnyes from the MDC Microscope Core Facility provided assistance during the early stages with developing an automated analysis.

Time-lapse image series were imported in ImageJ software. First, the length of ureter specimen was measured. In a next step, number of speed of contraction waves was analysed. For this purpose, an optical characteristic during the contraction process was utilised, during which the currently locally ureteral contraction site extremely darkens. One region of interest (ROI) covering the proximal end and one ROI covering the distal end of the ureter were defined. By means of the *"Plot Z-axis profile"* tool, mean grey values of each ROI were calculated for every frame, then imported into Excel software and analysed by means of a self-made Excel macro. Per ROI, image frames were identified where the mean grey values increased above a threshold value of 2, thereby indicating a contraction. Due to the fact that the grey value rise lasts during the complete contraction and is not restricted to the first frame, this calculation yielded in a much larger number of frames than the actual number of contraction waves. In order to exclude these false-positive frames, several calculations were included to note only the first frame marking the start of contraction in each ROI. The number of identified frames could differ between ROI 1 and ROI 2 if a contraction wave started at the proximal ureteral end (ROI 1) but stopped in between and did not reach the distal end (ROI 2). In this case, only complete contraction waves were considered for further analysis of contraction number and speed.

To determine complete contraction waves, previously identified image frames were listed in separate columns for ROI 1 and ROI 2. The columns were compared to each other by calculating differences between frames of ROI 1 and ROI 2 in the same line. If frame differences fell below 0 or exceeded a value of 30, the respective frames of ROI 2 were moved one line downwards. Using this calculation, only frames of ROI 1 and ROI 2 marking the start and the end of one contraction wave were aligned to the same line.

Only completely aligned frames represented a complete contraction wave and were used to determine the number of contraction waves. Then the contraction frequency was calculated using the formula:

$$contraction\ frequency\ [n/min] = \frac{number\ of\ complete\ contraction\ waves}{270\ ms\ frame\ acquisition\ time \times total\ frame\ number}$$

Finally, the frame difference number between ROI 1 and ROI 2 indicated the number of frames, which the wave needed to propagate from ROI 1 to ROI 2. The contraction duration was determined by:

$$contraction\ duration\ [s] = \frac{mean\ frame\ number\ required\ for\ propagation \times 270\ ms\ frame\ acquisition\ time}{1000}$$

The contraction speed was finally calculated by:

$$contraction\ speed\ [\mu m/s] = \frac{mean\ distance\ between\ ROI\ 1\ and\ ROI\ 2\ [\mu m]}{contraction\ duration\ [s]}$$

Statistical analysis was done using the software SigmaStat as outlined in section 4.12.

4.6.5 Analysis of ureteral lumen diameter

Ureteral lumen diameters were determined during contractions at four different sites along the ureter (one proximal, two medial and one distal site). By means of the software ImageJ, lumen diameters were manually measured in a course of 120 frames. Diameter values prior to contractions were set to 100 % relaxation and subsequent diameters were calculated proportionately.

4.7 CLMP antibody generation and purification

For the detection of CLMP protein in murine tissue, antibodies raised against the extracellular and cytoplasmic regions of mouse CLMP were generated. For this purpose, rabbits were immunised and the rabbit antisera were subsequently purified by affinity chromatography.

4.7.1 Antigen generation

The intracellular CLMP domain was cloned and produced by Christopher Patzke, whereas the extracellular CLMP domain was cloned by Mechthild Henning and the corresponding protein was purified by Anne Banerjee.

Mouse antigen	Nucleotides (NM_133733.4)	Amino acids (NP_598494.2)
CLMP extracellular domain	372-1067	1-232
CLMP intracellular domain	1134-1490	255-373

Briefly, extracellular and cytoplasmic *Clmp* DNA sequences were amplified from full-length murine *Clmp* cDNA clone (IMAGE clone IRAVp968H1062D, Source BioScience). The cytoplasmic *Clmp* sequence was cloned into pGEX-6P-1 vector to obtain a GST-tagged antigen, while the extracellular *Clmp* sequence was cloned into the pIG2 vector containing the genomic human IgG1 Fc domain. The plasmids were sequenced by Eurofins Genomics sequencing service to confirm the cloning. The generated plasmids were designated pIG2-mCLMP$_{ex}$-hFc and pGEX-6P-1-GST-mCLMP$_{cyt}$. The proteins were generated by either bacterial transformation (GST-mCLMP$_{cyt}$) or transfection in COS-7 cells (mCLMP$_{ex}$-hFc). The mCLMP$_{ex}$-hFc antigen was purified by affinity chromatography using a protein A-sepharose matrix, whereas the

GST-mCLMP$_{cyt}$ fragment was purified by glutathione-sepharose. The GST tag of GST-mCLMP$_{cyt}$ was removed by treatment with PreScission protease and the mCLMP$_{cyt}$ fragment was purified via gel filtration. The antigens mCLMP$_{ex}$-hFc and mCLMP$_{cyt}$ were tested by SDS-PAGE and silver staining, dialysed against PBS, and concentrated via Amicon PM30 Ultrafiltration Discs. Aliquots containing 50 µg antigen were stored at -20 °C until immunisation.

4.7.2 Immunisation

Antibodies against the cytoplasmic region of CLMP were generated at company BioGenes GmbH, Berlin. The mCLMP$_{cyt}$ antigen produced in our group was sent to BioGenes GmbH for immunisation of two rabbits (Rb 6504, Rb 6505).

For generation of antibodies against the extracellular CLMP domain, two rabbits (Rb 101, Rb 102) obtained from Harlan were immunised with mCLMP$_{ex}$-hFc antigen solution for five times at two-week intervals at the MDC Animal Facility. For each immunisation, 50 µg of mCLMP$_{ex}$-hFc protein was mixed at a ratio of 1:1 with Freund's adjuvant as immunopotentiator in a total volume of 1 ml and injected subcutaneously into the neck region. For the first immunisation, Freund's complete adjuvant including inactive mycobacteria was used, whereas in the following immunisations the complete form was replaced by Freund's incomplete adjuvant. Rabbits were exsanguinated one week after the fifth immunisation, and rabbit antisera were prepared by blood coagulation at RT and removal of the cruor by subsequent centrifugation. Antisera were maintained at 4 °C until purification procedures.

4.7.3 Antibody purification

Antibodies were purified from rabbit antiserum by affinity chromatography. In a first step, all antibodies in the antiserum were isolated by protein A-based chromatography and subsequently purified by tag-bound affinity chromatography (i.e. sepharose coupled to either glutathione or IgG 1) in order to remove unspecific antibodies against the hFc tag or residuals amounts of GST. Antibodies purified by these steps were referred to as the IgG fraction. If required, the IgG fraction was further affinity purified by an antigen-bound matrix (= IgG-AP fraction). Affinity chromatographies were performed with frit-supplied 10 ml columns connected to a peristaltic pump. All steps were carried out at 4 °C.

4.7.3.1 Coupling of proteins to CNBr-activated sepharose

For immobilisation of proteins in a sepharose matrix, cyanogen bromide (CNBr)-activated sepharose 4B was used. This type of sepharose is able to react with primary and secondary amines and thereby couples proteins permanently to the matrix. The coupling reaction was performed according to manufacturer's instructions, except that 0.1 M $NaHCO_3$ was used as AC coupling buffer. Briefly, CNBr-activated sepharose was suspended in and washed in 1 mM HCl. The proteins to be immobilised had previously been dialysed against the AC coupling buffer and were added to the sepharose. The coupling reaction was carried out O/N with gentle stirring. Remaining active amines were blocked by adding 0.5 ml of 1 M ethanolamine to the coupling mixture and incubation for 2 h. Subsequently, the gel matrix was transferred to a

column and washed with 5 bed volumes (BV) of PBS. For pre-elution, 5 BV of AC basic elution buffer (0.1 M diethylamine, pH 11.5) was applied to the column, followed by a washing step of 5 BV of PBS.

4.7.3.2 Protein A-sepharose affinity chromatography

For preparation of a protein A-column, 1 g of protein A-sepharose CL-4B beads were swelled according to manufacturer's instructions yielding a bed volume of 4-5 ml and applied to a column. The column was pre-eluted with 3 BV of AC acid elution buffer (0.1 M acetic acid/150 mM NaCl) at a speed of 0.8 ml/min and washed with 100 ml PBS at 0.3 ml/min.

For isolation of antibodies, 10 ml of rabbit antiserum were applied to the column at a speed of 0.1 ml/min. The flow-through was collected as precaution in case of insufficient binding capacity of the protein A matrix and, if required, applied again to the column in a next round of chromatography. After binding, the column was washed with 100 ml PBS at 0.4 ml/min and the antibodies bound to the matrix were subsequently eluted with 3-4 BV of AC acid elution buffer. To neutralise the acid elution buffer pH, the flow-through was collected in a vial containing 0.3-0.4 BV (= 1/10 of elution buffer volume) 1 M Tris-Cl, pH 8.8. Finally, the column was washed with 100 ml PBS at 0.4 ml/min and was ready for the next round of serum application. Antibody eluates were dialysed against PBS immediately after elution (section 4.7.3.5).

4.7.3.3 Tag-coupled sepharose affinity chromatography

Undesired antibodies that were raised against protein tags fused to the antigens (residual GST after protease treatment or hFc) should be excluded from the protein A-purified antibodies. For antibodies immunised with $mCLMP_{cyt}$, bacterially expressed GST was coupled to the matrix, whereas for antibodies immunised with $mCLMP_{ex}$-hFc, myeloma-expressed human IgG 1 was immobilised to the column (section 4.7.3.1). The protein A-purified antibodies were then applied to the respective columns at 0.1 ml/min and the flow-through was collected as purified IgG fraction (in the following referred to as IgG fraction). The column was washed with 100 ml PBS at 0.4 ml/min, eluted with 3-4 BV of AC basic elution buffer at 0.8 ml/min, and washed again with 100 ml PBS at 0.4 ml/min. The eluates, which contained antibodies against GST or hFc, respectively, were discarded. In case of low binding capacity, the purified IgG fraction was repeatedly applied to the column until antibodies against GST or hFc were no longer detectable.

4.7.3.4 Antigen-coupled sepharose affinity chromatography

If required, specific antibodies raised against the CLMP antigen were further extracted from unspecific antibodies. The antigens $mCLMP_{cyt}$ and $mCLMP_{ex}$-hFc were coupled to the sepharose matrix and IgG fractions were applied to the respective columns with a speed of 0.1 ml/min. The flow-through was collected as precaution and, if necessary, repeatedly applied to the column in a next round of chromatography. Washing was performed at 0.4 ml/min with 100 ml PBS, followed by fractionated elution of the specific antibodies by 3-4 BV of AC basic elution

buffer at 0.8 ml/min. The eluate fractions consisted of 30 drops, which corresponded to a volume of approximately 1 ml. Immediately after elution, small 16 µl aliquots were taken from each fraction for later SDS-PAGE silver staining analysis (section 4.9.4), and the eluate fractions were directly frozen at -20 °C. After silver staining analysis, antibody-containing fractions were combined and processed to dialysis (section 4.7.3.5). A final washing step of the column with 100 ml PBS at 0.4 ml/min completed the chromatography procedure.

4.7.3.5 Dialysis and concentration of antibody eluates

Antibody eluates were transferred to a dialysis tube with a molecular mass cut-off of 12-16 kDa and dialysed against PBS three times for 4 h each with stirring. After dialysis, the protein concentration was measured by OD_{280}/ε, where ε is the extinction coefficient of 1.4 for rabbit antibodies. If required, antibody solutions were concentrated using the Amicon Ultra-15 Centrifugal Filter Unit. Antibodies were either aliquoted and frozen to -20 °C or kept at 4 °C for short-term storage.

4.8 Culture and transfection of COS-7 cells

In order to test whether generated antibodies recognise CLMP in mammalian cells, a construct encoding full-length murine CLMP (pcDNA6/*myc*-His-mCLMP$_{fl}$) was transfected into COS-7 cells. Culture and transfection of COS-7 cells were carried out by technician Anne Banerjee. Briefly, COS-7 cells were cultivated according to standard procedures in COS-7 cell culture medium and splitted one day prior to transfection. Cells were transfected with 2 µg of pcDNA6/*myc*-His-mCLMP$_{fl}$ using Lipofectamine 2000 and Opti-MEM medium according to manufacturer's instructions. After transfection, COS-7 cells were either seeded onto chamber slides for immunofluorescent analyses or to dishes for protein extraction.

4.9 Protein biochemistry

4.9.1 Protein extraction from murine tissues

For protein extractions, it was important to carry out all steps on ice or at 4 °C. Tissues were dissected in cold PBS and immediately used for protein extraction or stored short-time at -20 °C for later usage.

4.9.1.1 Whole-cell protein extraction

To obtain whole-cell protein lysates, tissues were homogenised by a glass homogeniser in an appropriate amount of protein solubilisation buffer supplemented with protease inhibitors. A centrifugation step at 800 x g for 10 min precipitated cellular debris and nuclei. The OD_{280} of the supernatant was measured in a photometer and further divided by an estimated extinction coefficient ε of about 1.25 to obtain an approximate protein concentration.

4.9.1.2 Subcellular protein extraction

To obtain separate extractions of cytosol and membrane proteins, tissues lysates underwent subcellular fractionation. In contrast to the whole-cell extraction, dissected tissues were lysed in a glass homogeniser in protein sucrose solution supplemented with protease inhibitors. The lysate was spinned at 800 x g for 10 min to remove cellular debris and nuclei. The supernatant was transferred to a new tube and subjected to ultracentrifugation at 100,000 x g for 15 min. The resulting supernatant contained the cytosolic protein fraction, whereas the pellet contained the membrane fraction. To further purify the membrane fraction, the pellet was quickly stripped with 0.1 M diethylamine, pH 11.5, and spinned down by ultracentrifugation at 100,000 x g for 15 min. The supernatant was discarded and the pH was neutralised by adding PBS to the stripped membrane pellet, followed by an ultracentrifugation step at 100,000 x g for 15 min. In order to solubilise transmembrane proteins from the membrane, the pellet was treated with protein solubilisation buffer supplemented with protease inhibitors. A final ultracentrifugation step at 100,000 x g for 15 min separated the solubilised transmembrane proteins from the membrane pellet. The rough protein concentration of the supernatant was estimated by dividing OD_{280} by an averaged extinction coefficient ε of about 1.25.

4.9.1.3 Deglycosylation assay

In order to deglycolyse proteins, samples were treated with peptide-*N*-glycosidase F (PNGase F). The endoglycosidase PNGase F cleaves *N*-linked glycans from glycoproteins and was thus suitable to deglycolyse CLMP protein which has been reported be *N*-glycosylated (Gundry *et al.*, 2009).

Whole-cell or subcellular protein samples were treated with PNGase F according to manufacturer's instructions. Briefly, a 10 µg protein sample was denatured and then incubated with 500 U of PNGase F for 4 h at 37 °C. After a subsequent heat-inactivation step at 75 °C for 10 min, samples were further processed for loading on SDS gels (section 4.9.2).

4.9.1.4 Sample preparation for SDS-PAGE

Protein samples were diluted with PBS and either reducing or non-reducing 5x protein sample buffer (with or without β-mercaptoethanol, respectively) to a desired concentration and subsequently denatured by boiling at 95 °C for 5 min. Samples were briefly spinned to collect condensation, gently mixed by pipetting and immediately used for SDS-PAGE or stored at -20 °C for later usage.

4.9.2 SDS-polyacrylamide gel electrophoresis (SDS-PAGE)

Using SDS-polyacrylamide gel electrophoresis (SDS-PAGE), proteins were separated in acrylamide gels based on their electrophoretic mobility. The gels consisted of an upper stacking component (large pore size, pH 6.8) and a lower separating component (smaller pore size, pH 8.8). Gels were run in SDS-PAGE running buffer, with stacking gels at around 50 V and separating gels at higher voltage of around 100 V. For estimation of molecular weights,

standards covering a high (200, 116, 97, 66, 45 kDa) or low (97, 66, 45, 31, 22, 14 kDa) molecular weight range were chosen.

4.9.3 Acrylamide gel colloidal coomassie staining

Acrylamide gels were treated with colloidal coomassie for unspecific detection of proteins. Colloidal coomassie staining has the advantage to be much more sensitive than a detection with normal coomassie, resulting in an intensive blue staining. After SDS-PAGE, gels were briefly washed in dH_2O to remove residual SDS and transferred to colloidal coomassie solution. The staining dish was covered to prevent evaporation of methanol. Gels were incubated O/N on a shaker, washed twice in dH_2O and dried between two sheets of cellophane foil in a vacuum dryer.

4.9.4 Acrylamide gel silver staining

Silver staining of proteins in acrylamide gels was carried out using a technique modified according to Ansorge (Ansorge, 1985). This very sensitive method allows visualisation of even small amounts of protein in the ng range. Briefly, proteins were fixed, washed and incubated with 0.01 % (w/v) potassium permanganate in order to oxidise amino acid residues and thereby enhancing negative charges. After several washing steps, gels were treated with 0.2 % (w/v) silver nitrate in order to incorporate silver ions into proteins. By addition of a formaldehyde containing developer solution, silver ions were reduced and protein bands became visible. Afterwards, gels were washed and dried between cellophane foils using a vacuum dryer.

4.9.5 Western blotting and immunodetection

Western blotting technique was carried out to transfer proteins from acrylamide gels to a nitrocellulose membrane by applying an electric field. Gels were blotted at 340 mA for 1 h in a tank blot system using WB transfer buffer. After blotting, nitrocellulose membranes were briefly washed in PBS, stained with Ponceau S to mark the protein standard and blocked with WB blocking buffer for at least 30 min at RT. Generally, WB washing and blocking solutions contained PBS as base component, however, only for detection of murine NGAL protein TBS was used instead of PBS. Furthermore, the WB blocking solution for NGAL contained 5 % milk powder instead of BSA. Subsequent to the blocking step, membranes were incubated with primary antibodies (section 3.8) dissolved in WB blocking solution O/N at 4 °C, followed by washing in WB washing solution. Secondary antibodies conjugated with either horseradish-peroxidase (HRP) or alkaline phosphatase (AP; section 3.8) were dissolved in WB blocking buffer and applied at RT for 2 h. After washing, the blots were developed using either a chemiluminescent substrate for HRP-coupled antibodies (combined with ChemiDoc XRS equipment and Quantity One software) or a colourimetric substrate consisting of nitro blue tetrazolium chloride (NBT) and 5-bromo-4-chloro-3-indolyl phosphate *p*-toluidine salt (BCIP).

4.10 Histology

4.10.1 Cryostat sectioning

To obtain tissue sections for histological and immunofluorescence stainings, tissues were dissected, fixed with 4 % PFA/PBS and residual aldehydes were quenched with 50 mM ammonium chloride/PBS. Fixation times depended on tissue sample and size. Cryoprotection was obtained using 15 % (w/v) and 30 % (w/v) sucrose/PBS. All steps of tissue pretreatments were performed at 4 °C. After cryoprotection, tissues were embedded in Tissue-Tek O.C.T. compound, frozen on dry ice and stored at -80 °C until sectioning. 10-25 µm thick cryosections were obtained at a cryostat at a temperature range between -20 °C and -18 °C (temperature depending on the type of tissue), transferred to gelatin-coated glass slides, dried and stored at -20 °C.

In case that tissue sections were required for later *in-situ* hybridisation experiments, all equipment and solutions were RNase-free (section 4.1.11). Furthermore, dissection procedures were carried out as fast as possible to avoid RNA degradation. Also, the tissue pre-treatment and embedding procedures were modified by omission of the ammonium chloride quenching step and by performing a more rapid freezing process in dry ice-cooled pentane. Finally, tissue sections were mounted on uncoated, positively-charged glass slides, dried and stored at -70 °C.

4.10.2 Microtome sectioning

Tissues that were difficult or incapable to section by cryostat, e.g. hydronephrotic kidneys, were embedded in sliceable glycol methacrylate plastic and sectioned using a microtome. For this purpose, tissues were dissected and fixed in 4 % PFA/PBS at 4 °C. Afterwards, tissues were washed in PBS, dehydrated in a graded ethanol series (30 % EtOH/PBS; 50 % EtOH; 60 % EtOH; 70 % EtOH; 80 % EtOH; 90 % EtOH; 99 % EtOH) and embedded in Technovit 7100 according to manufacturer's instructions. Technovit 3400 based on methylmethacrylate plastic was used for mounting the cured tissue specimens to Technovit histoblocs which were required for fastening the specimens to the microtome. 5 µm thin sections were obtained and transferred to a pre-heated water bath. By means of a brush, the sections were then mounted on uncoated glass slides and dried on a slide dryer. Slides were stored at RT.

4.10.3 Nissl thionin staining

The Nissl staining is based on the binding capacity of basic dyes, e.g. thionin, to nucleic acids and was carried out on brain sections. 25 µm thick brain cryosections were defatted by incubation in 50 % (v/v) chloroform/50 % (v/v) ethanol solution for two times for 30 min. Rehydration of the sections was performed using decreasing alcohol concentrations (100 % EtOH; 96 % EtOH; 70 % EtOH; 50 % EtOH) for 5-10 min each, followed by dH_2O two times for 2 min. The staining procedure was performed for 30 min using Nissl thionin solution. Subsequently, sections were rinsed three times in dH_2O and dehydrated by an increasing ethanol series (50 % EtOH; 70 % EtOH; 96 % EtOH; 100 % EtOH), with 2 min for each step. After

a 5 min clearance in xylene, sections were mounted using Entellan or Roti-Histokitt. Slides were stored at RT.

4.10.4 Haematoxylin & eosin staining

The haematoxylin & eosin (H&E) staining is a widely used staining method in histology. The staining makes use of a two dye application. The dye haemalum provides a nuclear basophilic stain, whereas the dye eosin is used as a counterstain. Microtome sections were stained in H&E Gill's haematoxylin solution for 15 min, washed in tap water for 10 min and decolourised by brief dipping into H&E acid ethanol. Subsequently, the slides were rinsed in tap water and in dH_2O. Blueing of the staining was achieved by a two minute incubation in Scott's tap water substitute. Thereafter, the slides were rinsed twice in dH_2O, counterstained in H&E eosin solution for 2 min and dehydrated by incubation in 96 % EtOH and 100 % EtOH for 2 min each. The sections were cleared in xylene for 2 min each, mounted with Entellan or Roti-Histokitt and stored at RT.

4.10.5 Immunofluorescence staining

Immunofluorescent stainings were performed on tissue cryosections. Frozen sections were thawed and treated with 50 mM ammonium chloride/PBS for 10 min at RT to quench residual aldehydes. Then, the tissue sections were treated differently according to the host in which the antibodies had been raised.

For all antibodies that had not been raised in mouse, the procedure continued as follows: the tissues were permeabilised and blocked using the Triton X-100 and goat serum containing IF blocking solution for 1 h at RT. Thereafter, the primary antibodies were diluted in IF blocking solution, applied to the sections and incubated O/N at 4 °C. Three washing steps with IF washing solution at RT for 15 min each followed to remove unbound antibodies. In a next step, secondary antibodies with a fluorescent conjugate were diluted in IF blocking solution and incubated with the slides at RT for 2 h. Subsequently, the nuclear marker 4',6-Diamidino-2-phenylindole (DAPI) was applied to the slides as 1:1,000 dilution in IF blocking solution. Then, the slides were washed three times in IF washing solution, washed once in PBS and mounted with Immu-Mount.

For immunofluorescent stainings with antibodies raised in mouse, the Vector M.O.M. Immunodetection Kit was used for blocking steps and antibody dilution in order to prevent binding of the secondary anti-mouse antibody to endogenous immunoglobulins in the tissue. However, the kit was not used according to manufacturer's instructions but with the following modified protocol: first, cryosections were permeabilised using the IF washing solution for 15 min at RT. Then, the sections were blocked by incubation in IF M.O.M. blocking solution for 1 h at RT. Afterwards, the antibodies were diluted in IF M.O.M. antibody solution and incubated on the slides O/N at 4 °C. After washing with IF washing solution, the secondary antibody diluted in IF M.O.M. antibody solution was applied at 2 h at RT. DAPI staining, washing and mounting steps were performed according to the protocol mentioned above.

4.11 *In situ* hybridisation (ISH)

Using *in situ* hybridisation (ISH), mRNA expression was localised in tissue cryosections by hybridisation of DIG-labelled riboprobes to target transcripts and subsequent immunohistochemical detection.

Since RNA is prone to degradation by RNases, special care was taken to work under RNase-free conditions according to the RNA work guidelines as stated in section 4.1.11.

4.11.1 ISH probe generation

Riboprobes used for ISH were designed to be exon-exon overlapping to prevent hybridisation to gDNA in the tissue. Probe length was between 500 and 1,000 bp to incorporate a sufficient amount of digoxigenin (DIG) for adequate signal output and to allow permeabilisation into the tissue.

In a first step, probe DNA sequences with either T7 or SP6 RNA polymerase promoter sequences were produced. Using *in vitro* transcription and digoxigenin (DIG)-labelled dUTPs, RNA polymerase promoter sequences at the 5' end of the DNA then gave rise to sense DIG-labelled riboprobes, while 3' promoter sequences generated antisense DIG-labelled riboprobes.

4.11.1.1 Probe DNA amplification

cDNA templates were amplified by proof-reading DNA polymerase Q5 according to manufacturer's instructions using primers with promoter sequences of either T7 or SP6 RNA polymerases (primer sequences listed in section 3.6). The vector pCMV-Sport6-mCLMP (cloned by Christopher Patzke) containing the full-length *Clmp* cDNA was used for amplification of *Clmp* probe DNA. The 731 bp amplicon (size excluding the promoter sequence) was identical to the already published probe sequence by Allen Brain Atlas (www.brain-map.org, riboprobe ID RP_080603_02_C03). Finally, the probe DNA sequences were purified by gel extraction.

4.11.1.2 *In vitro* transcription generating DIG-labelled riboprobes

To generate DIG-labelled riboprobes, 300 ng of probe DNA were used as template for *in vitro* transcription using 40 U of appropriate RNA polymerases SP6 or T7, the DIG RNA labelling mix and RNaseOUT. The *in vitro* transcription reaction mix was set up as recommended by manufacturer's instructions and was incubated for 2 h at 37 °C. Riboprobes were purified by means of the "*RNA Cleanup Protocol*" of RNeasy Mini Kit with combined on-column DNase I digestion using the RNase-free DNase Set. The RNA concentration of the eluate was measured using a Nano Drop spectrophotometer. Thereafter, formamide was added 1:1 to stabilise the riboprobes, which were finally stored in small aliquots at -70 °C.

4.11.1.3 Dot blot assay

The efficiency of DIG labelling was analysed by dot blot according to the manual in Roche's *"DIG Application Manual for Nonradioactive In Situ Hybridisation"*. Briefly, diluted aliquots of DIG-labelled riboprobes were spotted on a nylon membrane next to a diluted standard, the

purchased DIG-labelled control RNA. Probes were recognised by an anti-DIG antibody conjugated with alkaline phosphatase using solutions of the DIG Wash and Block Buffer Set and thereafter colourimetrically detected with NBT and BCIP.

4.11.2 *In situ* hybridisation

Tissue cryosections of 15 µm thickness were prepared as stated in section 4.10.1. Before the tissue sections were hybridised with DIG-labelled riboprobes, the sections had to undergo several pretreatment steps to avoid unspecific probe binding. After thawing, sections containing fatty tissue (e.g. periureteral fat) were treated with chloroform for 5 min and were then allowed to air-dry. Chloroform delipidised the tissue in order to prevent nonspecific background caused by lipid vesicles (Dijkman *et al.*, 2008). The chloroform treatment was omitted for brain sections. All tissue sections were then fixed for 10 min by 4 % (w/v) PFA/DEPC-PBS and washed three times in cold DEPC-PBS. A proteinase K treatment at this point was not carried out because such treatment had been experienced to give unspecific results. An acetylation step was performed in order to remove the positive charge of slides and tissues to prevent unspecific binding of the negatively charged probe. For this, sections were equilibrated in ISH acetylation buffer and thereafter positive charges were acetylated by incubation in 0.25 % (v/v) acetic anhydride in ISH acetylation buffer for 10 min. Afterwards, the tissue was permeabilised in 0.3 % (v/v) Triton X-100/DEPC-PBS for 20 min at 4 °C. Three subsequent washing steps with DEPC-PBS for 5 min each at 4 °C completed the tissue pretreatments.

In order to prepare tissue sections for the hybridisation, the slides were prehybridised in ISH hybridisation buffer at 65 °C for 1 h in a chamber humidified with 50 % formamide/5x DEPC-SSC. In the meantime, DIG-labelled riboprobes were thawed and diluted in ISH hybridisation buffer according to the following formula of Roche's manual "*Nonradioactive* In Situ *Hybridization - Frequently Asked Questions*" to determine the required riboprobe concentration: 0.1-0.5 ng/µl per kb DIG-labelled RNA. Thereafter, the probes were heated to 80 °C for 5 min and immediately put on ice. When the prehybridisation was completed, the diluted riboprobes were applied to the slides. The use of coverslips was omitted because coverslips used in earlier *in situ* hybridisations had not shown a signal improvement but instead they are reported to decrease the signal (Dijkman *et al.*, 2008). The hybridisation was carried out at 65 °C in a humidified chamber for a prolonged period of time of up to 40 h as has been reported useful for rare transcripts (Braissant & Wahli, 1998).

After hybridisation, it was no more required to work under RNase-free conditions due to the insusceptibility of the hybridised, double stranded RNA to degradation. Unhybridised riboprobes were removed by washing in ISH washing buffer I two times at 60 °C for 20 min each, followed by equilibrating in ISH RNase buffer and digestion for 15 min at 37 °C using 20 µg/ml RNase A in ISH RNase buffer. The sections were washed two times in ISH washing buffer II at 37 °C for 20 min each and washed two times in ISH washing buffer III at 37 °C for 20 min each. Then, the slides were washed in ISH MABT solution for 20 min at RT and blocked

in ISH blocking solution for at least 1 h at RT. An anti-DIG antibody conjugated with alkaline phosphatase was diluted 1:1,000 in ISH blocking solution, applied to the tissue sections and left O/N a 4 °C in a humidified chamber. The next day, unbound antibodies were removed by washing in ISH MABT solution at RT six times for 30 min each. Thereafter, sections were equilibrated in freshly-prepared ISH NTMT solution and alkaline phosphatase signals were detected by incubation in ISH NTMT solution supplemented with 0.225 mg/ml NBT, 0.175 mg/ml BCIP, and 1 mM levamisole for up to four days in the dark. After colourimetric detection, the slides were washed in 0.5 % (v/v) Tween 20/PBS five times for 10 min each at RT, rinsed three times in PBS and mounted with Immu-Mount.

4.12 Statistics

Statistical analysis was conducted using the software SigmaStat. First, a normality test was performed to test whether the values were Gaussian distributed. If the normality test passed, values of two groups with equal variances were compared using a two-tailed Student's *t*-test. In case of a failed normality test, statistical differences between two groups were analysed using the Mann-Whitney Rank Sum test. Values are presented as mean ± standard error of the mean (SEM). Statistically significant differences are denoted by asterisks with * indicating $P \leq 0.05$, ** indicating $P \leq 0.01$ and *** indicating $P \leq 0.001$.

5 RESULTS

5.1 *Clmp* knockout mouse generation

Mutant mice are widely used to investigate the function of a protein since they allow analysing the alterations in the animals' phenotypes caused by a modified gene expression. Among various genetic approaches, a complete knockout of a specific gene will reveal its function most apparently. At the beginning of this study, no *Clmp* mutant mice were available. In order to examine the function of CLMP, the aim was to generate a conventional *Clmp* knockout mouse line, which completely lacks the CLMP protein.

5.1.1 Targeting strategy

To generate a knockout of *Clmp*, the *Clmp* locus was analysed. The murine *Clmp* gene is localised on the forward strand of chromosome 9 and spans the bases 40,685,962-40,785,319. *Clmp* is encoded by seven exons, of which the first exon contains the ATG start codon. The targeting strategy aimed at deleting the start codon of the *Clmp* gene by replacing the entire sequence of exon 1 by a *loxP*-flanked *Neo* resistance cassette (FIGURE 2). A targeting vector considering these criteria was ordered at Vega Biolab.

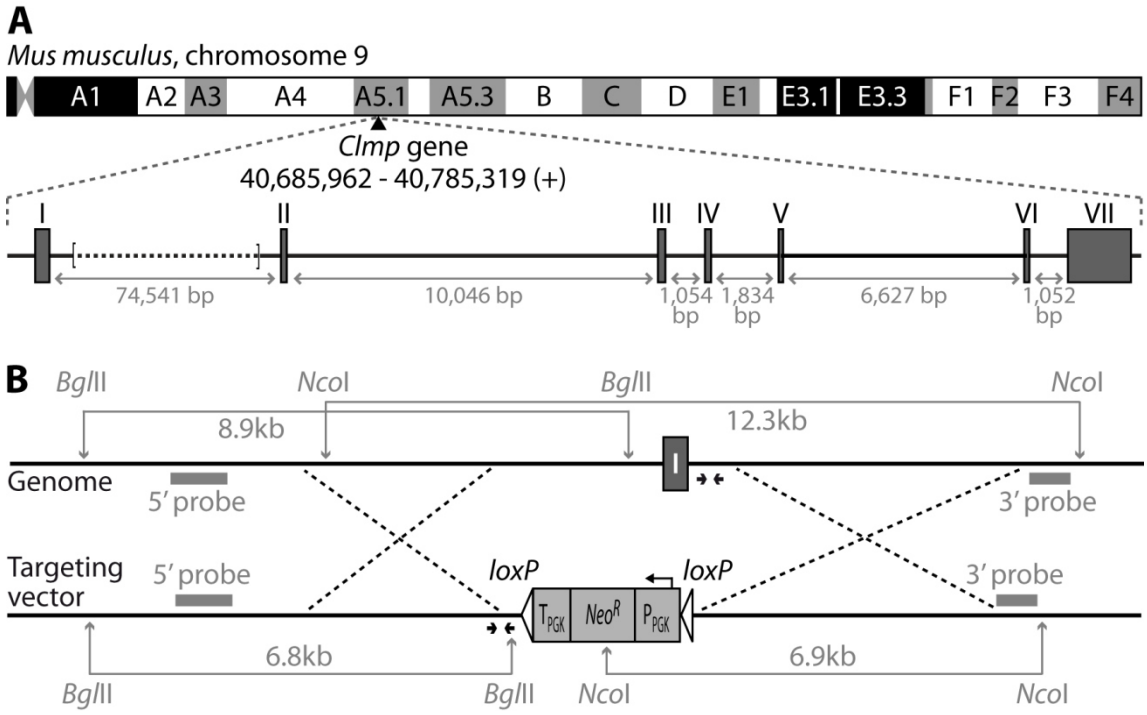

FIGURE 2. *Clmp* targeting strategy.

(A) The *Clmp* locus is on chromosomal band A5.1 of chromosome 9 and comprises seven exons, of which the first exon contains the ATG start codon. (B) The targeting strategy was designed to replace exon 1 by a *loxP*-flanked *Neo* cassette by homologous recombination in order to abolish *Clmp* expression. Binding sites of external 5' and 3' Southern probes, the respective restriction sites and fragment sizes are indicated in light grey. Primers for genotyping are shown by black arrows.

5.1.2 Targeting vector sequencing

The pVBTK-CLMP targeting vector was sequenced since no detailed sequence information had been provided by Vega Biolab. A 9,622 bp region spanning the *loxP*-flanked *Neo* cassette, the 3' homology arm and almost the entire 5' homology arm were sequenced using 32 oligonucleotides (FIGURE 3). The 5' homology arm comprised 3,000 bp, whereas the 3' homology arm consisted of 4,901 bp. In between the arms, a 2,262 bp sequence covered the *Neo* cassette and the two *loxP* sites. The *Neo* cassette was included in a reverse orientation, meaning the cassette was inserted as reverse complement sequence. The *Neo* cassette was composed of a 541 bp PGK-promoter, a 804 bp *Neo* resistance gene, and a 488 bp PGK-terminator, and was directly flanked by *loxP* sites. Between the 5' homology arm and the first *loxP* site there was a 337 bp insert, while a short 25 bp sequence was inserted between the second *loxP* site and the 3' homology arm. The sequence file with feature information can be accessed via the CD attached to the thesis (see section 8.1 for further information).

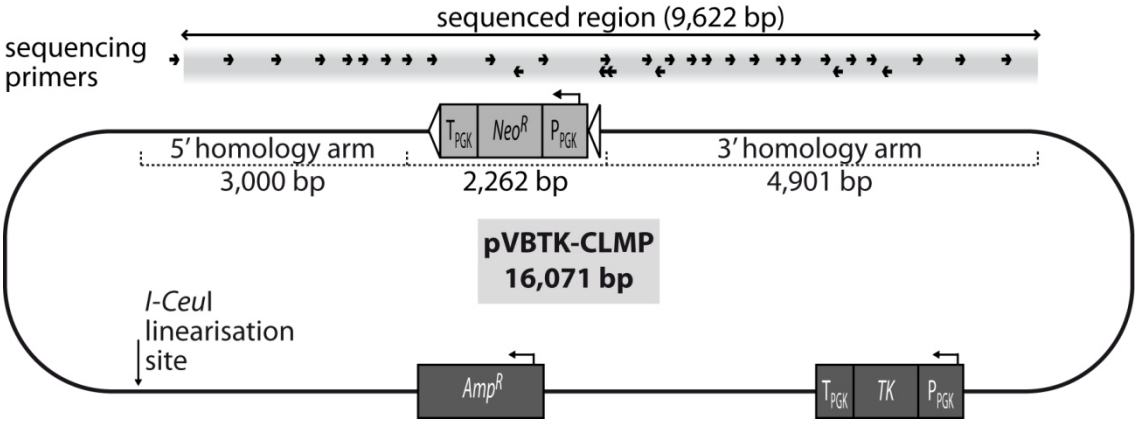

FIGURE 3. Sequencing the pVBTK-CLMP targeting vector.
The regions relevant for gene targeting by homologous recombination were sequenced. The 9,622 bp sequenced region comprised the 5' homology arm, the *loxP*-flanked *Neo* cassette and the 3´homology arm. Binding sites of 32 sequencing primers are indicated by black arrows. Figure is not to scale.

5.1.3 Homologous recombination of ES cells

The targeting vector was amplified for electroporation into E14.1 ES cells. Three electroporations were performed and 882 ES cells were screened for homologous recombination by Southern blot analysis using external probes that bind outside of the homologous arms. Due to the number amount of ES cells, the primary screen was conducted with only the 5' probe and revealed two positive clones (clones 9D and 2A; TABLE 1 and FIGURE 4A). The clone 9D was expanded and subjected to a Southern rescreen using both the 5' probe and the 3' probe. Both probes confirmed homologous recombination of targeting vector and ES cell genome by showing an upper band representing the wild type allele and a lower band representing the recombined allele (FIGURE 4B). Therefore, clone 9D ES cells were chosen for blastocyst injection and processed accordingly.

Electroporation	# of screened ES cells	# of positive clones
no. 1	294	0
no. 2	294	1 (clone 9D)
no. 3	294	1 (clone 2A)

TABLE 1. ES cell primary screen.
Three electroporations with 882 screened ES cells yielded two positive clones.

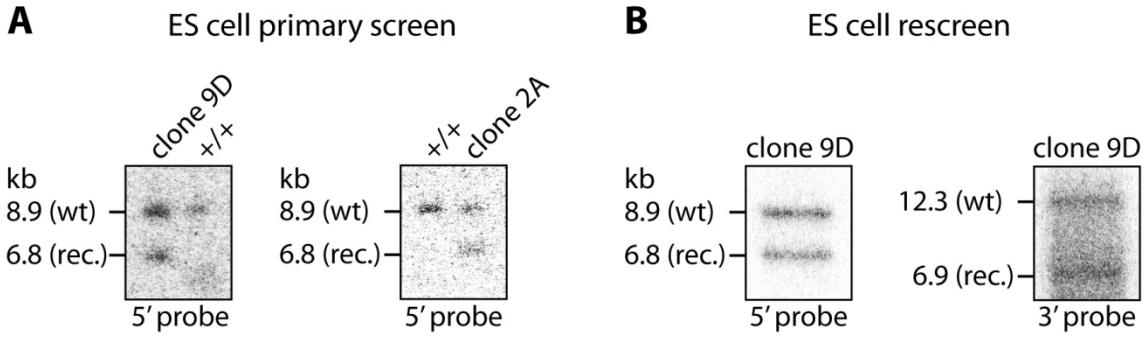

FIGURE 4. ES cell Southern blot screening.
(A) In comparison to wild type clones, clones 9D and 2A showed an additional recombinant band in Southern 5' probe hybridisations. (B) A rescreen with both 5' and 3' external probes validated a recombined allele by homologous recombination in clone 9D.

5.1.4 Production of chimaeric mice by blastocyst injection and generation of *Clmp* mutant mice

Based on the homologous recombination, clone 9D ES cells were injected into C57BL/6-blastocysts at the MDC Transgenic Core Facility. Six chimaeric male mice were generated, which were mated with C57BL/6 females to achieve germline transmission. In total, the six chimaeras produced 16 litters with 86 pups, of which only 20 pups were genotyped as *Clmp*$^{+/-}$ (TABLE 2).

Chimaera ID	# of litters	# of pups	# of pups with germline transmission
2041	1	4	0
2042	1	8	0
2043	5	34	8
2044	1	1	0
2045	5	26	9
2046	3	13	3

TABLE 2. Chimaeric germline transmissions.
Of six chimaeric male mice, only three produced heterozygous offspring by germline transmission.

The heterozygous pups derived from three chimaeras with the IDs 2043, 2045, and 2046 (FIGURE 5). However, it was decided to further breed offspring of only one chimaera to exclude phenotype differences. Finally, the knockout mouse strain was established solely by offspring of chimaera ID 2043, therefore the laboratory strain name was designated "*Clmp*-2043", while the international nomenclature is B6;129P2-*Clmp*^{tm1aFgr}. By crossing the *Clmp*-2043 mice to a *Cre*-Deleter strain, the *Neo* cassette was deleted in all cells by Cre-mediated excision. The offsprings of this breeding were used for further backcrossing to C57BL/6 background and determined strain "*Clmp*-KO", international nomenclature B6.129P2-*Clmp*$^{tm1a.1Fgr}$. FIGURE 6 provides a schematic overview of chimaera generation and strain derivation.

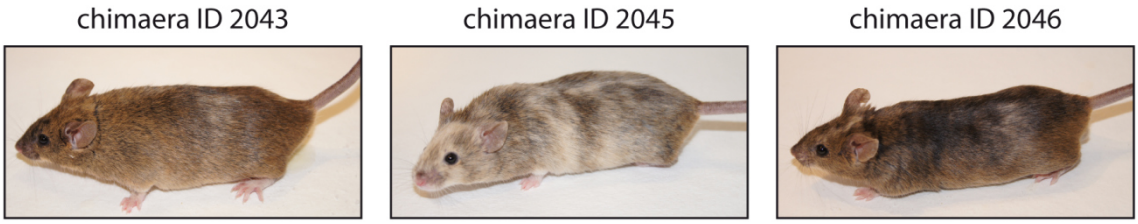

FIGURE 5. Chimaeric animals with germline transmission.
Coat colour chimaerism of chimaeras 2043, 2045 and 2046 showing germline transmission.

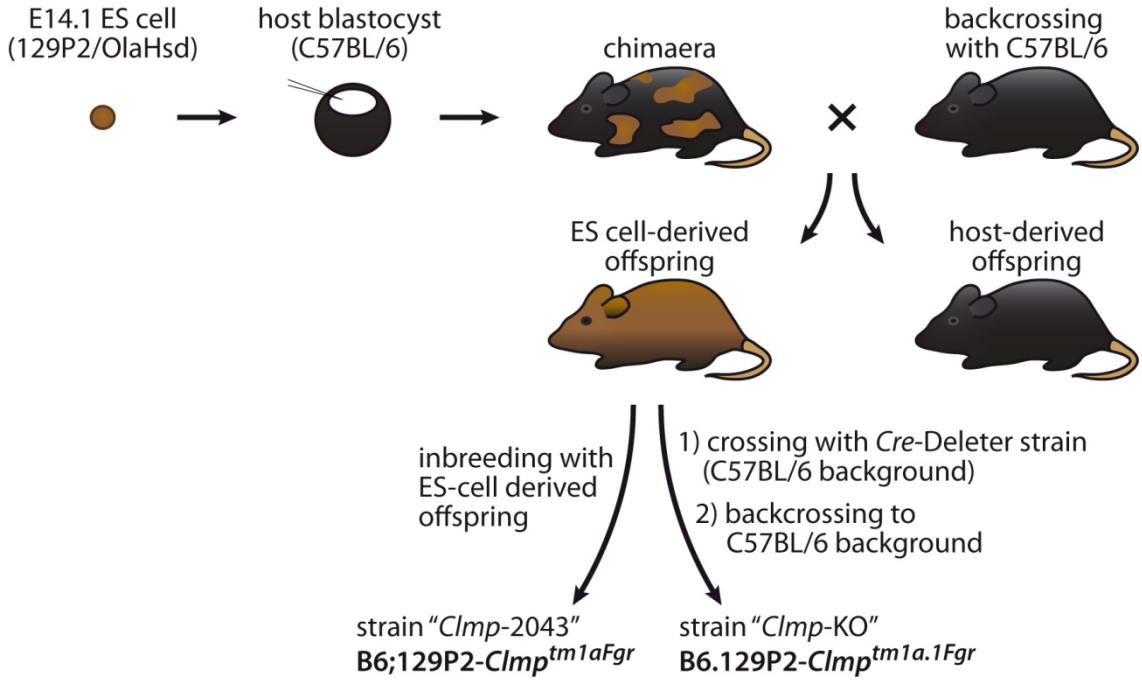

FIGURE 6. Generation of *Clmp* mutant mice.
For generation of *Clmp* knockout animals, targeted E14.1 ES cells were injected into C57BL/6 blastocysts. Coat colour chimaerism of born chimaeras was used to estimate the probability of germline transmission. ES-cell derived offspring was identified by genotyping and recognised by brown goat colour and founded the strain "*Clmp*-2043" (B6;129P2-*Clmp*^{tm1aFgr}). Simultaneously, heterozygous *Clmp*-2043 animals were crossed with *Cre*-Deleter strain to remove the *Neo* cassette from the genome and the resulting offspring was used for backcrossing to C57BL/6 genetic background, giving rise to the "*Clmp*-KO" strain (B6.129P2-*Clmp*$^{tm1a.1Fgr}$).

5.1.5 Verification of *Clmp* knockout

After generation of *Clmp* mutant animals, the knockout was validated on genomic, transcript and protein levels. To confirm the knockout on the genomic level, *Clmp* wild type, heterozygous and knockout animals were examined by Southern hybridisation and PCR genotyping. In Southern blot analysis, both external 5' and 3' probes revealed the absence of the wild type bands in *Clmp*$^{-/-}$ animals in comparison to their wild type and heterozygous littermates (FIGURE 7A). The same result was shown by PCR genotyping, as *Clmp*$^{+/+}$ and *Clmp*$^{+/-}$ animals presented a 459 bp wild type band, which was lacking in the *Clmp*$^{-/-}$ animal (FIGURE 7B). To test *Clmp* transcript expression, total RNA from wild type, heterozygous and knockout mice was reverse-transcribed into cDNA and analysed by PCR using *Clmp*- and β-*actin* (*Actb*)-

specific, exon-exon overlapping primers. While the amplification of *Actb* transcript showed the integrity of cDNA in all animals, *Clmp* transcripts could only be amplified in $Clmp^{+/+}$ and $Clmp^{+/-}$ mice but not in the knockout animal (FIGURE 7C). In order to investigate the CLMP protein expression, brain tissue from $Clmp^{+/+}$, $Clmp^{+/-}$ and $Clmp^{-/-}$ animals was prepared and subcellularly fractionated into membranous protein fractions and cytosolic protein fractions. Owing to its transmembrane domain, CLMP is expected to be found in the membrane fraction but not in the cytosolic fraction. Using the Rb 6504-anti-$CLMP_{cyt}$ antibody, Western blot analysis revealed a specific 46 kDa CLMP band in the membrane fractions of wild type and heterozygous mice, whereas no band could be identified in the membrane fraction of $Clmp^{-/-}$ animals (FIGURE 7D). Bands in cytosolic fractions of all animals are unspecific signals.

In conclusion, all approaches to validate a complete knockout of the *Clmp* gene were successful and confirmed the genetic knockout on genomic level by correct integration of the targeting vector into genome, as well as the functional knockout by absence of *Clmp* transcript and CLMP protein in homozygous animals.

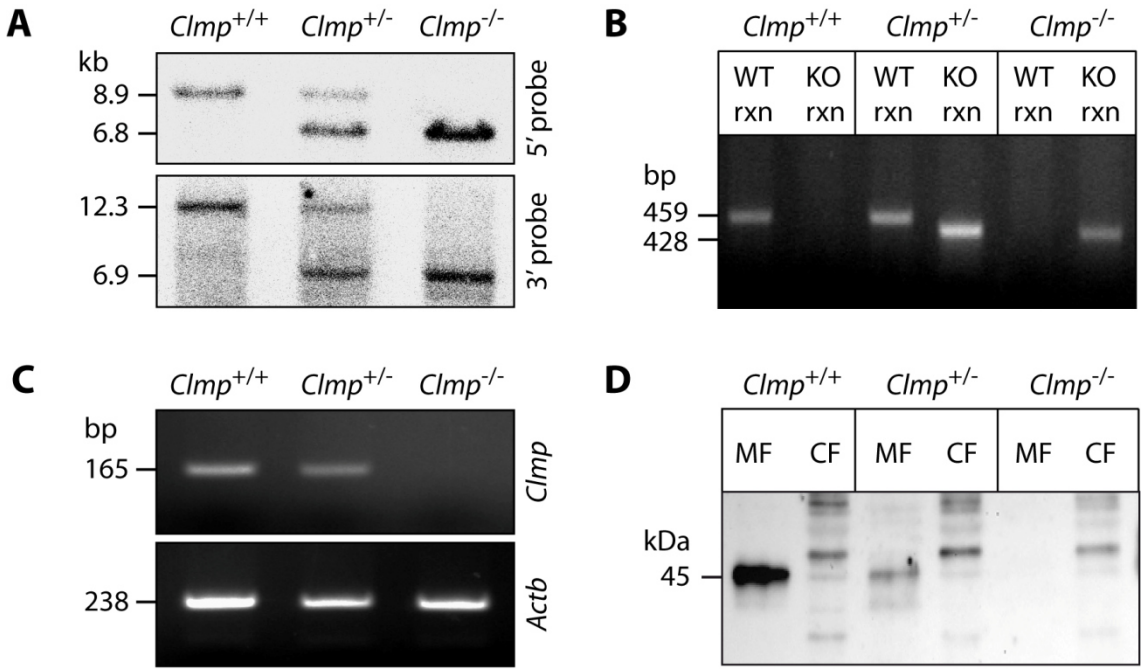

FIGURE 7. Validation of *Clmp* knockout mouse model.

The knockout of *Clmp* was analysed on genomic, transcript and protein level by comparison of homozygous mutants to wild type and heterozygous littermates. (A) Both Southern probes hybridised to DNA fragments of wild type allele in $Clmp^{+/+}$ and $Clmp^{+/-}$ mice, whereas in $Clmp^{-/-}$ animals only the recombinant allele was recognised. (B) The wild type allele could be amplified by PCR genotyping in wild type and heterozygous mice but not in homozygous mutants. (C) In comparison to control littermates, a 165 bp fragment of *Clmp* transcript could not be amplified from cDNA of $Clmp^{-/-}$ mice, although the cDNA integrity was fine due to *Actb* amplification. (D) Western blot analysis using a CLMP-specific antibody showed a 46 kDa CLMP band in brain membrane fractions from wild type and heterozygous littermates, whereas such band was lacking in the homozygous animal. WT, wild type reaction; KO, knockout reaction; MF, membrane fraction; CF, cytosolic fraction.

5.2 Body weight and survival rate analysis of *Clmp* mice

In order to test *Clmp* mutants for general phenotypic changes, the development of body weight and length was analysed first. Pups were monitored from day of birth on up to the day of weaning. Every day, the body weight and pre-weaning losses were noted and examined separately for the *Clmp*-2043 and *Clmp*-KO strains (FIGURE 8, TABLE S1 and TABLE S2). On the day of birth, knockout animals of the *Clmp*-2043 strain had a body weight similar to their littermate controls (control 1.538 ± 0.036 g, n = 42 vs. knockout 1.442 ± 0.078 g, n = 12). However, beginning from P 1 until the day of weaning, *Clmp*$^{-/-}$ pups failed to gain as much weight as their control littermates (P 22, control 11.033 ± 0.401 g, n = 24 vs. knockout 8.100 g, n = 1). Reductions in mutant body weight were highly significant (FIGURE 8A and TABLE S1). Simultaneous to the reduction in body weight, the survival rate of *Clmp*-2043 knockout pups drastically decreased after birth. While 94.74 % of the newborn mutants survived P 0, only 36.84 % survived until P 10 and only 31.58 % were still alive at P 22. In contrast, 89.50 % of control littermates were still alive at P 22 (FIGURE 8A'). Similar body weight and survival results were obtained for the *Clmp*-KO strain, of which pups of generations N1-N5 were examined. However, even at the day of birth, CLMP-deficient pups of the *Clmp*-KO strain had significantly less body weight (1.292 ± 0.026 g, n = 13) as compared to their control littermates (1.465 ± 0.030 g, n = 48; FIGURE 8B and TABLE S2). In the following days up to the day of weaning, mutant pups were not able to catch up with the controls and remained with a highly significantly diminished body weight (P 22, control 9.136 ± 0.234 g, n = 39 vs. knockout 6.600 ± 0.100 g, n = 2). Correspondingly, knockout pups showed a high rate of pre-weaning loss. At P 0, 100.00 % of *Clmp*$^{-/-}$ pups were alive, however only 50.00 % were alive at P 10 and as few as 14.29 % survived until P 22 (FIGURE 8B'). Please note that due to the high rate of pre-weaning deaths, the number of animals used for body weight measurements correspondingly decreased with every day.

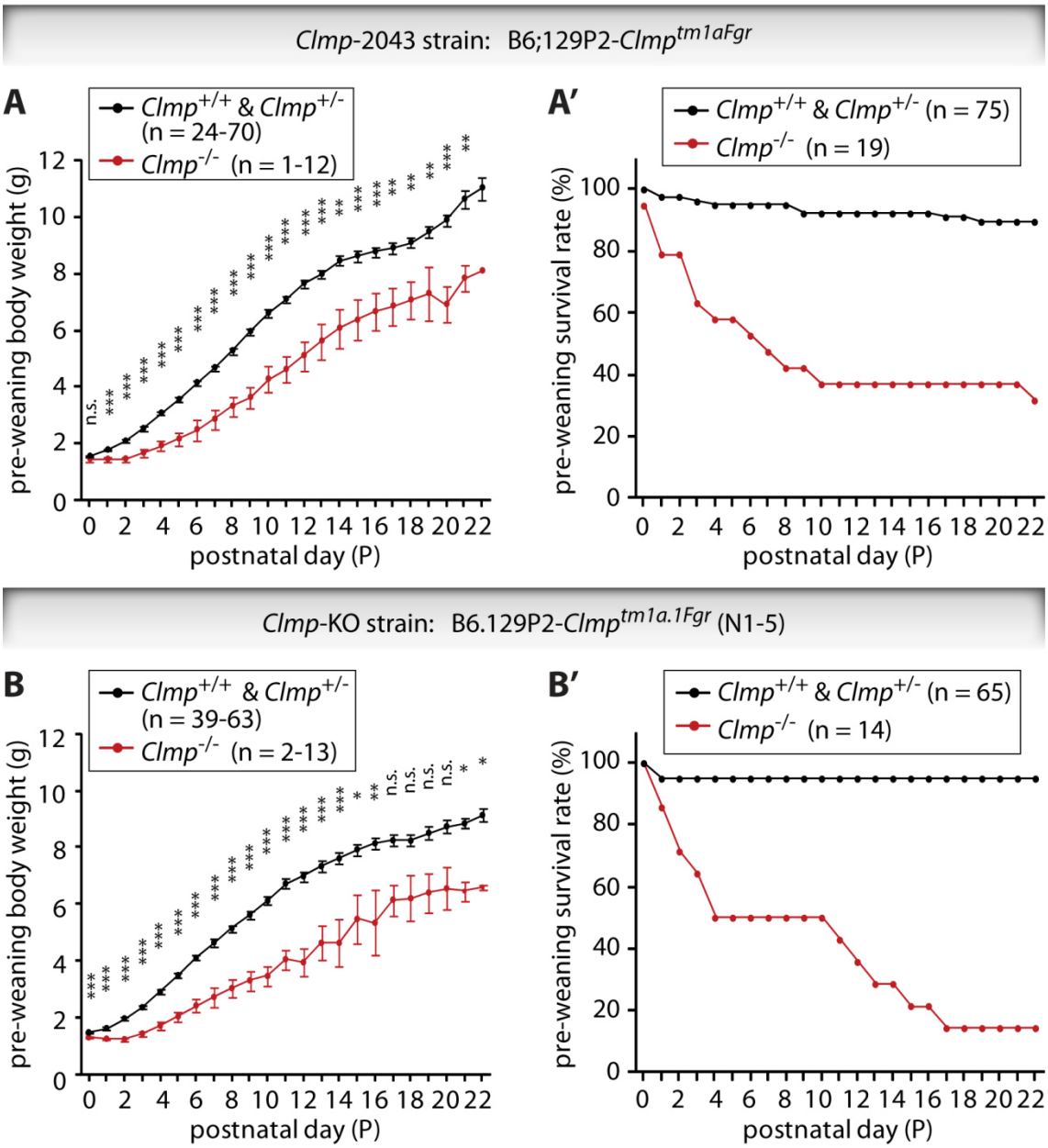

FIGURE 8. Body weight and survival of pups.

During early postnatal development, *Clmp* knockout pups of both strains exhibit significantly less body weight as compared to littermate controls. The defect in gaining weight is accompanied by a pronounced rate of pre-weaning death in both strains.

FIGURE 9 provides exemplary photos of *Clmp*$^{-/-}$ pups and their wild type littermates at early postnatal stages P 1, P 2, P 3, and P 7. As shown by FIGURE 10, the white appearance of stomachs of P 1 neonates indicates normal feeding with milk by mothers. Although mutant and wild type pups are almost not distinguishable at P 1 at first sight, the shapes of CLMP-deficient pups are slimmer. The delayed body growth becomes even more apparent at later stages. Despite the reduction in body size, mutant pups do not have any striking changes in their outward appearances.

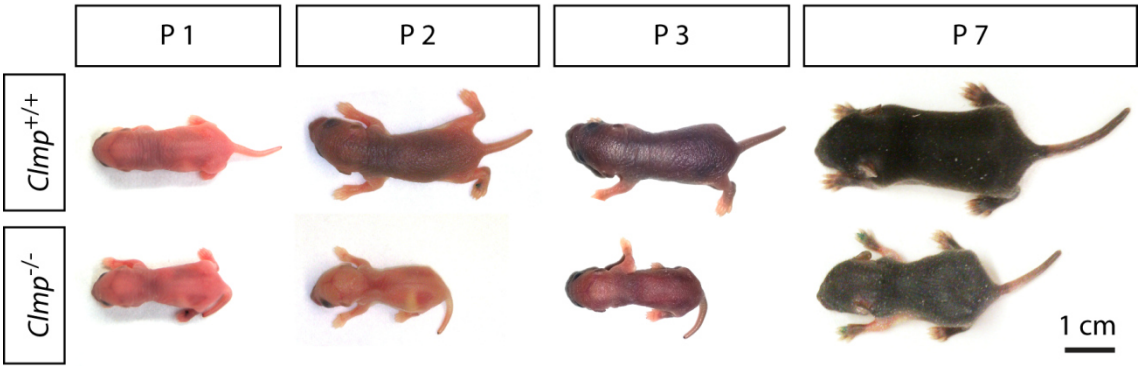

FIGURE 9. Delayed body growth of *Clmp* mutants.
The loss of CLMP becomes apparent by a retarded body growth at early postnatal stages. Mutant pups are smaller and have a slimmer shape than littermate controls.

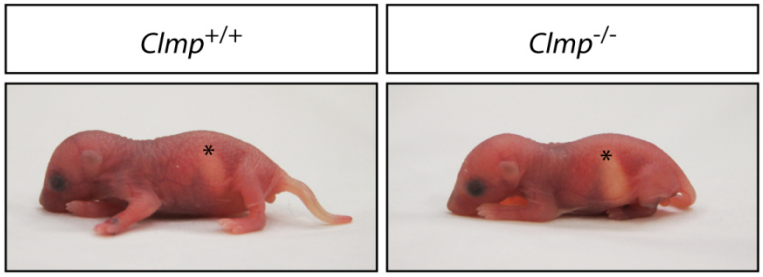

FIGURE 10. Neonates display a stomach filled with milk.
After birth, wild type and mutant P 1 pups are fed by their mothers as demonstrated by the white milk-filled stomachs indicated by asterisks.

After weaning at the age of three weeks, the body weights and lengths of surviving juvenile mice were monitored every seven days up to the seventeenth week of life (FIGURE 11, TABLE S3 and TABLE S4). In comparison to wild type and heterozygous control littermates, *Clmp*$^{-/-}$ mice had significantly less body weight between postnatal days P 35 and P 77. At P 35, control animals had a mean weight of 20.897 ± 0.676 g (n = 32), whereas knockouts weighed only 18.194 ± 0.855 g (n = 18). At P 77, CLMP-deficient mice weighed 25.646 ± 0.877 g (n = 24) and thus were still significantly lighter than their littermates with 27.886 ± 0.673 g (n = 36). After P 77, the decrease in body weight was still present but was not significant anymore. Despite the reduced body weight, mutant animals were able to gain weight during development comparable to control littermates (FIGURE 11A and TABLE S3). Similar to the body weight, *Clmp* mutants exhibited a reduced naso-anal body length, although this difference was only significant at some stages (FIGURE 11B and TABLE S4). At P 35, controls and knockouts had a comparable length of 8.375 ± 0.138 cm (n = 28) and 8.000 ± 0.154 cm (n = 15), respectively. At P 77, however, the body length was significantly reduced in mutant animals (8.955 ± 0.104 cm, n = 22) as compared to their littermate controls (9.25 ± 0.100 cm, n = 34). At P 105, the last day of measurements, the body lengths of control mice (9.357 ± 0.096 cm, n = 28) and mice lacking CLMP (9.184 ± 0.134 cm, n = 19) almost converged (FIGURE 11B and TABLE S4).

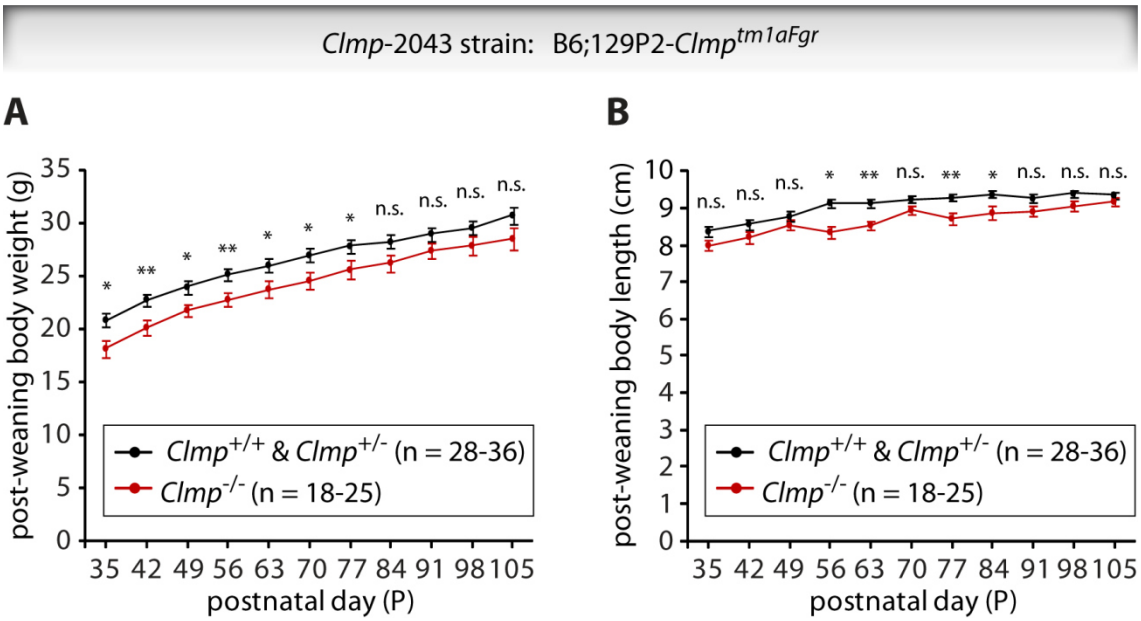

FIGURE 11. Body weight and naso-anal length development of surviving juvenile animals.
During juvenile and adult development, surviving CLMP-deficient animals gain weight but fail to meet the body weights of littermate controls. In the period between P 35 and P 77, body weights of *Clmp* mutants are significantly reduced as compared to control animals. Simultaneously, naso-anal body lengths of *Clmp* knockout mice are shorter, but almost comparable to littermates.

In a next step, the reproduction of adult animals was analysed. Heterozygous males were crossed to heterozygous females and numbers of newborn and weaned animals were noted for each genotype (TABLE 3). About 18-19 % of newborn pups of both strains were *Clmp*$^{-/-}$ genotype, which does not quite match the expected Mendelian ratio of 25 % but may be in the

TABLE 3. Reproduction of heterozygous to heterozygous matings.
Newborn (P 0) and weaned (P 21) offspring was analysed for genotypic distribution according to Mendelian ratios. The percentage of born knockout animals of both strains not quite matches the expected ratio of 25 %. In contrast, the ratio of surviving, weaned CLMP-deficient animals of the *Clmp*-2043 strain is much less than expected.

Parental cross		Offspring					
***Clmp*-KO**		**# total litters**	**# total born**	**genotype**	**# born**	**% born**	**% expected**
♂	♀						
Clmp$^{+/-}$	*Clmp*$^{+/-}$	34	256	*Clmp*$^{+/+}$	71	27.73 %	25 %
				Clmp$^{+/-}$	136	53.13 %	50 %
				Clmp$^{-/-}$	49	19.14 %	25 %
***Clmp*-2043**		**# total litters**	**# total born**	**genotype**	**# born**	**% born**	**% expected**
♂	♀						
Clmp$^{+/-}$	*Clmp*$^{+/-}$	33	218	*Clmp*$^{+/+}$	63	28.90 %	25 %
				Clmp$^{+/-}$	115	52.75 %	50 %
				Clmp$^{-/-}$	40	18.35 %	25 %
***Clmp*-2043**		**# total litters**	**# total weaned**	**genotype**	**# weaned**	**% weaned**	**% expected**
♂	♀						
Clmp$^{+/-}$	*Clmp*$^{+/-}$	51	267	*Clmp*$^{+/+}$	85	31.84 %	25 %
				Clmp$^{+/-}$	162	60.67 %	50 %
				Clmp$^{-/-}$	20	7.49 %	25 %

range of biological diversity. In contrast, monitoring the genotypic distribution of animals that survived until weaning at P 21 showed a strong discrepancy between the percentage of observed and expected *Clmp* knockout mice. Of 267 weaned animals, 31.84 % were wild type, 60.67 % were heterozygous, and only 7.49 % were homozygous. Compared to the Mendelian ratio, $Clmp^{+/+}$ and $Clmp^{+/-}$ animals were more frequent than expected, whereas the number of knockout animals was underrepresented, which is consistent with the loss of $Clmp^{-/-}$ animals at pre-weaning stages, as illustrated in FIGURE 9.

Additionally to heterozygous to heterozygous matings, male and female *Clmp* knockout animals were crossed to C57BL/6 mice to analyse whether *Clmp* mutants are able to reproduce. However, neither male nor female breedings produced pregnancies and thus no litters (TABLE 4). Although the number of breedings was limited, the lack of offspring strongly hints to infertility of both male and female $Clmp^{-/-}$ mice.

TABLE 4. Reproduction of homozygous *Clmp* mutants.
In breedings with C57BL/6 animals, male and female mutants (*Clmp*-2043) were not able to reproduce.

Parental cross		Breedings		Offspring		
♂	♀	# mutants	# breedings	# pregnancies	# litters	# pups
$Clmp^{-/-}$	C57BL/6	4	8	0	0	0
C57BL/6	$Clmp^{-/-}$	2	2	0	0	0

5.3 Analysis of visceral organ alterations in *Clmp* mice

In a next approach, animals of the *Clmp*-2043 strain that survived to adulthood were dissected between P 97 and P 140, and visceral organs were collected to determine their wet weights. Due to the decreased body weight of *Clmp* mutants, all organ weights were normalised to the body weight and length of each dissected animal for better comparison (TABLE 5). The brains of CLMP-deficient animals were smaller and had significantly less weight (0.601 ± 0.015 g, n = 15) as compared to control mice (0.531 ± 0.016 g, n = 10; P = 0.005). However, since brain size correlates with body size, neither the normalisation of brain weight to body weight nor to body length obtained statistical significance (P = 0.586 and P = 0.122, respectively). In contrast to the brain, the weights of dissected stomachs and intestines were significantly higher in the absence of CLMP (4.563 ± 0.210 g, n = 12) as compared to controls (3.322 ± 0.150 g, n = 18; P < 0.001), and high statistical significance remained even after normalisation to both body weight (P < 0.001) and body length (P < 0.001). When compared to control hearts (1.181 ± 0.008 g, n = 16), heart weight were highly reduced in knockout animals (0.155 ± 0.010 g, n = 11), however this difference was not significant. Similarly to the gastrointestinal tract, mutant kidneys with a mean weight of 0.837 ± 0.062 g (n = 22) were highly significantly heavier than control kidneys weighing 0.224 ± 0.007 g (n = 36; P < 0.001). The tremendous difference in kidney weight reached high significance after normalisation to body weight (P < 0.001) and body length (P < 0.001). Liver weights were not altered between control (1.389 ± 0.058 g, n = 16) and knockout mice (1.292 ± 0.077 g, n = 11). In contrast, lung and spleen wet weights

were significantly decreased in the absence of CLMP (0.210 ± 0.006 g, n = 11, and 0.087 ± 0.010 g, n = 11, respectively) when compared to the mean weights of control mice (0.245 ± 0.008 g, n = 17, and 0.114 ± 0.010 g, n = 16, respectively). These differences, however, were not significant anymore after normalisation to body weights and body lengths.

While some organs did not show changes in gross anatomy, the wet weight of stomach and intestine as well as the wet weight of kidneys were highly significantly increased in *Clmp*$^{-/-}$ mice. Due to the strong weight alterations, these organs were further investigated in the following sections. Furthermore, although the mutant brains were decreased in size that correlated with the reduced animal size, the brain was also subjected to further evaluation.

TABLE 5. Wet weight analysis of visceral organs of the *Clmp*-2043 strain at P 97 - P 140.
St., stomach; Int., intestine; Ctrl., control; KO, knockout; *t*, *t*-test; MW, Mann Whitney Rank Sum test; n.s., not significant; * indicating P ≤ 0.05, ** indicating P ≤ 0.01 and *** indicating P ≤ 0.001.

Organ	Genotype	Organ weight (g)		Ratio organ weight/ body weight		Ratio organ weight/ body length	
Brain	Ctrl. (n = 15)	0.601 ± 0.015	P = 0.005	0.022 ± 0.001	P = 0.586	0.066 ± 0.008	P = 0.122
	KO (n = 10)	0.531 ± 0.016	** [*t*]	0.021 ± 0.001	n.s. [*t*]	0.061 ± 0.005	n.s. [*t*]
St. + Int.	Ctrl. (n = 18)	3.322 ± 0.150	P < 0.001	0.124 ± 0.005	P < 0.001	0.365 ± 0.014	P < 0.001
	KO (n = 12)	4.563 ± 0.210	*** [*t*]	0.183 ± 0.008	*** [*t*]	0.529 ± 0.022	*** [*t*]
Heart	Ctrl. (n = 16)	1.181 ± 0.008	P = 0.056	0.007 ± 0.000	P = 0.353	0.020 ± 0.001	P = 0.184
	KO (n = 11)	0.155 ± 0.010	n.s. [MW]	0.006 ± 0.000	n.s. [*t*]	0.018 ± 0.001	n.s. [*t*]
Kidney	Ctrl. (n = 36)	0.224 ± 0.007	P < 0.001	0.008 ± 0.000	P < 0.001	0.025 ± 0.001	P < 0.001
	KO (n = 22)	0.837 ± 0.062	*** [MW]	0.033 ± 0.002	*** [MW]	0.097 ± 0.007	*** [MW]
Liver	Ctrl. (n = 16)	1.389 ± 0.058	P = 0.217	0.050 ± 0.002	P = 0.694	0.152 ± 0.006	P = 0.838
	KO (n = 11)	1.292 ± 0.077	n.s. [MW]	0.051 ± 0.003	n.s. [*t*]	0.150 ± 0.009	n.s. [*t*]
Lung	Ctrl. (n = 17)	0.245 ± 0.008	P = 0.003	0.009 ± 0.000	P = 0.422	0.026 ± 0.001	P = 0.056
	KO (n = 11)	0.210 ± 0.006	** [*t*]	0.008 ± 0.000	n.s. [*t*]	0.024 ± 0.001	n.s. [*t*]
Spleen	Ctrl. (n = 16)	0.114 ± 0.010	P = 0.049	0.004 ± 0.000	P = 0.312	0.013 ± 0.001	P = 0.079
	KO (n = 11)	0.087 ± 0.010	* [MW]	0.003 ± 0.000	n.s. [MW]	0.010 ± 0.001	n.s. [MW]

5.3.1 No obvious change of *Clmp* mutant brain anatomy

Since CLMP's closest homologue CAR is strongly expressed in the developing brain (Hotta *et al.*, 2003; Patzke *et al.*, 2010), the gross brain anatomy of *Clmp*$^{-/-}$ animals was examined. Assuming that alterations in brain anatomy manifesting during development would still be present in adult brains, 25 µm coronal sections of P 107 brains were produced and stained using the nuclear Nissl thionin staining. All sections of wild type and mutant brains were compared to each other using a mouse brain atlas (Paxinos & Franklin, 2012). However, no gross changes could be observed between the genotypes, as all prominent brain areas were present and comparable in size and structure (FIGURE 12). Using the Nissl staining method, only gross changes in brain structure could be investigated but in order to identify detailed changes in brain anatomy, further experiments would be required. Due to the normal appearance of CLMP-deficient brains and due to the presence of more significant organ alterations of gastrointestinal tract and kidneys, no further investigations were carried out on mutant brains.

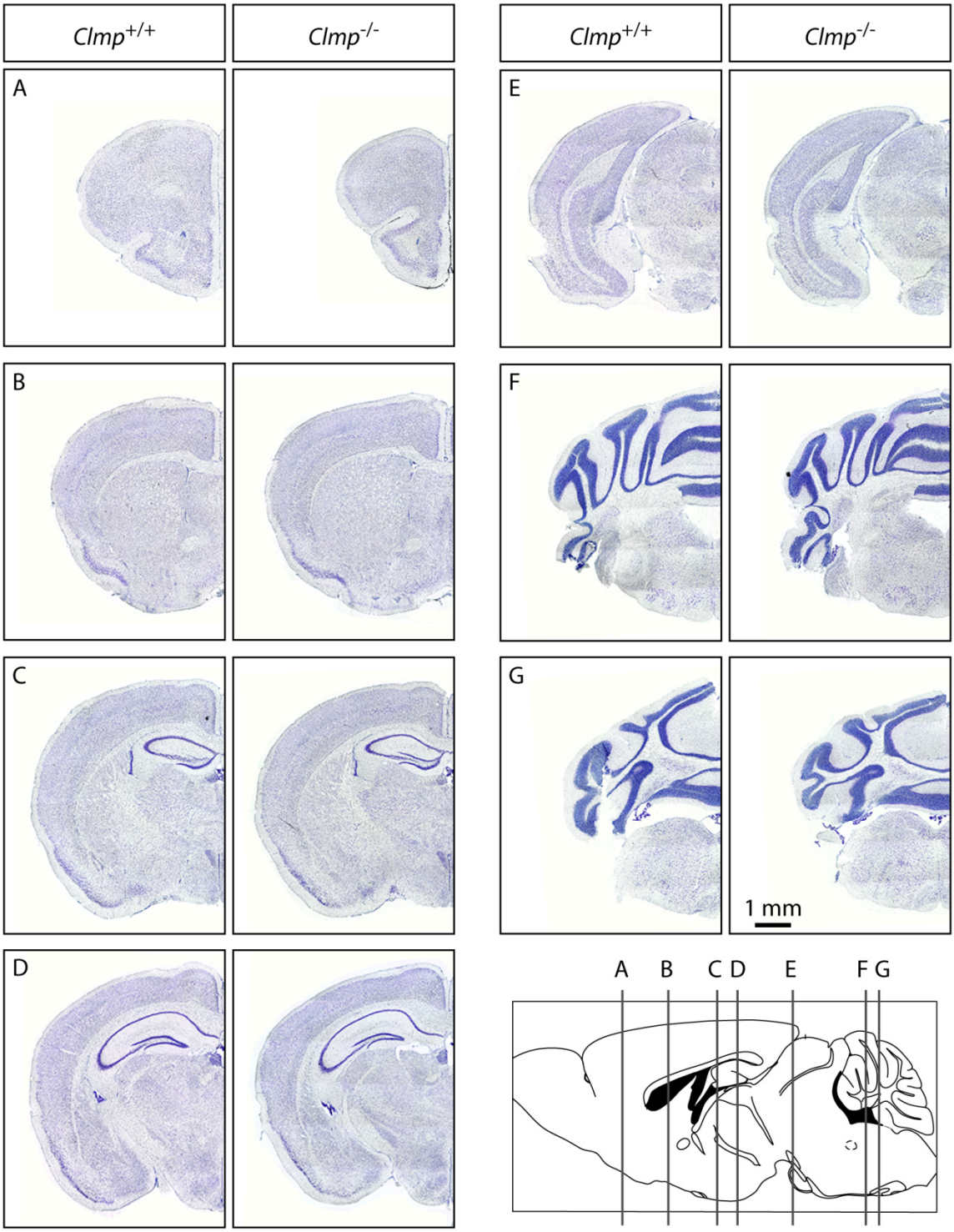

FIGURE 12. Nissl staining shows normal gross brain anatomy at P 107.
Coronal 25 µm thick brain slices of P 107 old wild type and knockout mice of the *Clmp*-2043 strain were Nissl stained. Comparing to a mouse brain atlas, brain sections were analysed for alterations in gross brain anatomy. Approximate positions of the sections A-G are indicated in the brain scheme at the bottom on the right. No gross differences in brain structure could be identified.

5.3.2 *Clmp* mutants show intestinal abnormalities

During analysis of organ wet weights, stomachs and intestines of knockout mice were highly significantly heavier than of littermate controls (TABLE 5). Due to this striking observation and

because CLMP has been implicated in human CSBS patients (Van der Werf *et al.*, 2012), the analysis of mutant intestines was expanded. In a first set of experiments, the gastrointestinal tract comprising the stomach and the entire intestine were dissected from adult littermates of the *Clmp*-2043 strain (age between P 97 and P 140). For better comparison of intestinal structure and size, animals were kept without food over night before dissection and dissected intestines were kept swimming in a PBS-containing dish to prevent stretching of the intestine.

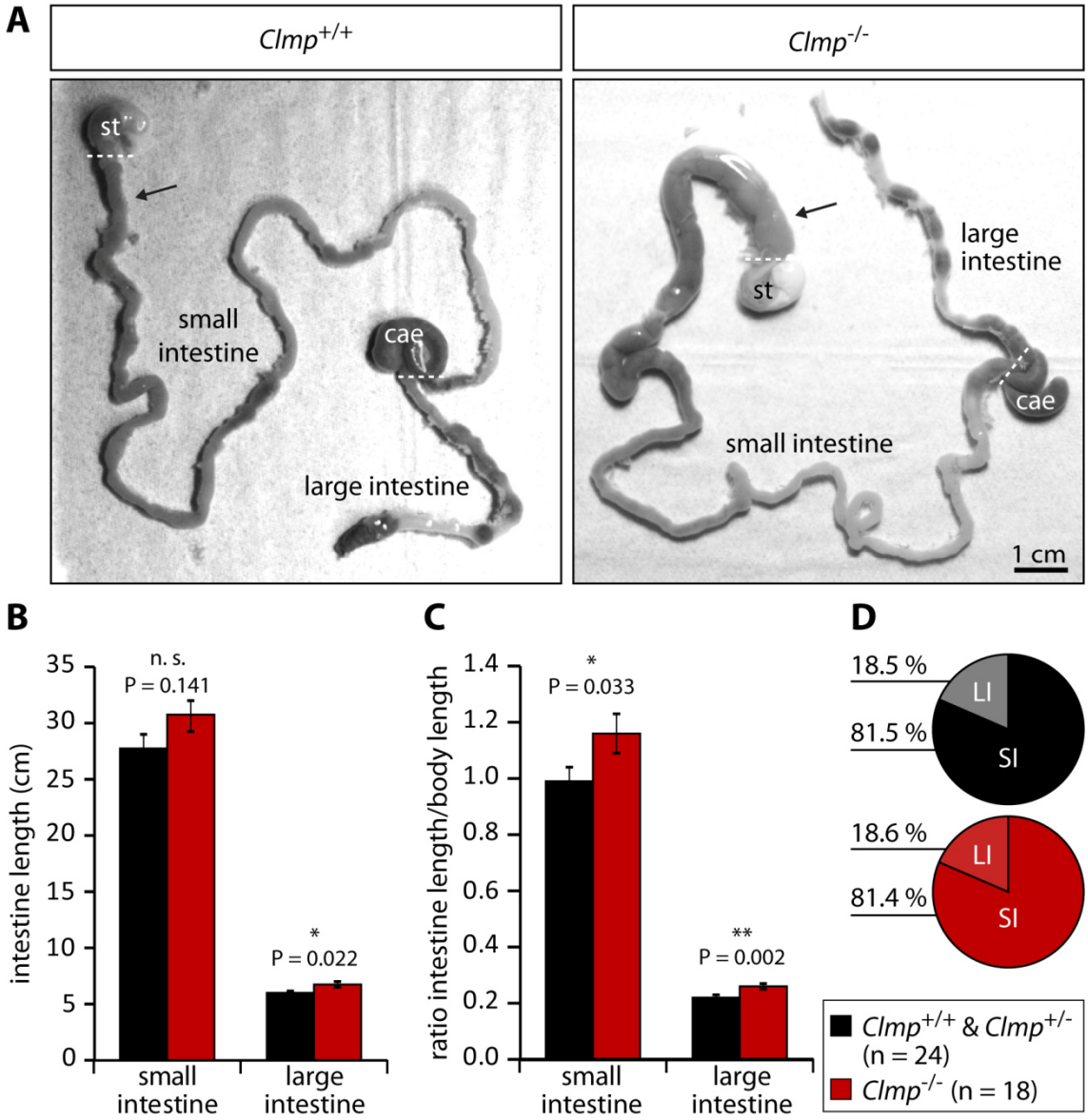

FIGURE 13. Intestine length analysis in adult *Clmp*-2043 animals.
(A) Intestines were dissected from P 97-P 140 old *Clmp*-2043 littermates and the lengths of small and large intestines were determined. Note that *Clmp*$^{-/-}$ animals exhibit a dilated duodenum (arrow). (B) In the absence of CLMP, intestines are longer, with a significantly extended the large intestine. (C) By normalisation to body length, a significant increase of small and large intestines became evident. (D) Proportions of small to large intestines were not altered in *Clmp* mutants. st, stomach; cae, caecum; SI, small intestine; large intestine.

Interestingly, the duodenum, which represents the first part of the small intestine directly after the stomach, was dilated in 100 % of dissected *Clmp* mutants (FIGURE 13A). Since the absence of CLMP in zebrafish has been described to cause an intestinal shortening (Van der Werf *et al.*, 2012), the lengths of intestines from *Clmp*$^{-/-}$ mice were compared to those of littermates (FIGURE 13). The small intestine was measured from the duodenal beginning directly after the stomach up to the caecum, the large intestine was measured from the caecum across the colon up to the rectum. In contrast to the zebrafish study, the small and large intestines of CLMP-deficient mice were not shortened. Instead, the mutant intestines were actually longer, which was even statistically significant for the large intestine (FIGURE 13B). Small intestines of wild type and heterozygous control animals had a length of 27.670 ± 1.364 cm (n = 24), whereas small intestines reached a mean length of 30.650 ± 3.390 cm (n = 18) in the absence of CLMP. The large intestines of control mice with a length of 6.120 ± 0.195 cm (n = 24) were significantly shorter than the large intestines of *Clmp* mutants, which were 6.918 ± 0.285 cm (n = 18) long. Given that *Clmp* knockout mice were reduced in body weight, intestinal lengths were normalised to the body length. Doing so, both the longer small and large intestines of *Clmp*$^{-/-}$ mice obtained statistical significance as compared to intestines of littermate controls (FIGURE 13C). The ratio of small and large control intestines normalised to body length were 3.046 ± 0.140 cm and 0.663 ± 0.024 cm (n = 18), respectively. However, normalisation yielded significantly higher ratios of 3.520 ± 0.162 cm and 0.793 ± 0.032 cm (n = 18) for small and large knockout intestines. Despite the prolonged intestines in *Clmp*$^{-/-}$ animals, the ratios of small intestine to large intestine are similar in both control and knockout mice, indicating normal intestinal proportions (FIGURE 13D).

Throughout the intestine dissections, a thickened duodenum was observed in adult knockout animals (FIGURE 13A). Also, juvenile CLMP-deficient mice showed a duodenal dilation as can be seen in exemplary photos of P 43 old *Clmp*-2043 littermates in FIGURE 14. Furthermore, when the abdominal cavity was opened, the loss of CLMP appeared to alter the arrangement of the intestine. In comparison to control intestine (FIGURE 14A), the mutant intestine looked swollen and somehow folded in a different way. For instance, the caecum was not visible and covered by intestinal folds (FIGURE 14C). Additionally, in comparison to the wild type and heterozygous littermates, a pyloric stenosis might be observed in the absence of CLMP (small images in FIGURE 14B' and FIGURE 14D', respectively), which needs further investigation (also personal communication with Dr A. Friebe, University of Würzburg). Even though *Clmp*$^{-/-}$ animals exhibit an intestinal phenotype, no further investigation on mutant intestines was carried out because research on *Clmp* knockouts was concentrated on the urinary system, as is described in the following sections.

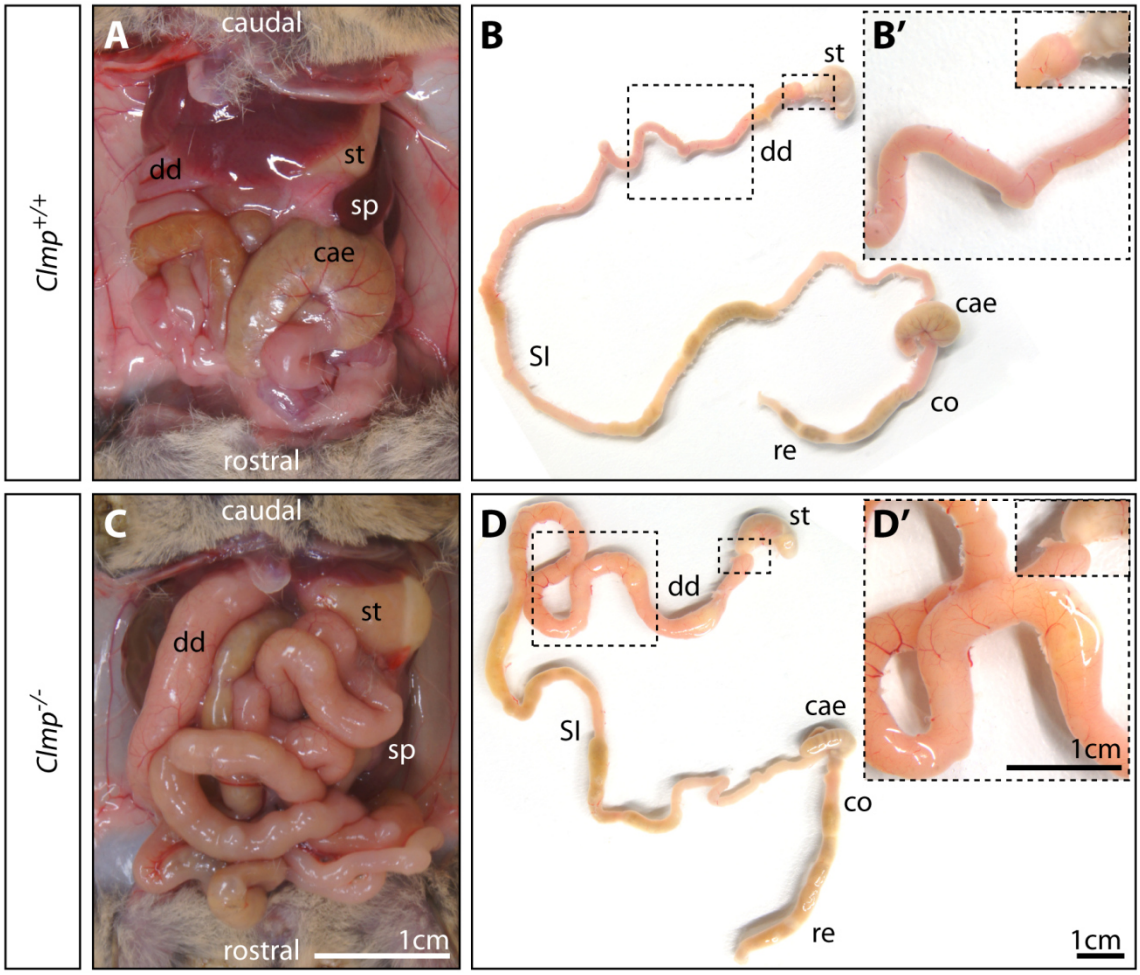

FIGURE 14. Intestinal folding and duodenal dilation in *Clmp* knockout mice.
View into the opened abdominal cavities of P 43 old wild type (A) and knockout (C) mice of the *Clmp*-2043 strain showing a thickened duodenum and a different enteric folding in the absence of CLMP. In contrast to the residual CLMP-deficient intestinal portions, the duodenum is the only dilated part (D) and is almost twice as thick as in the control (B). Images in B' and D' represent the dashed boxes in B and D, respectively, and provide a closer look at the duodenum and the junction between stomach and duodenum. Note that in comparison to the wild type (B', small image) a pyloric stenosis might be observed in the mutant animal (D', small image). st, stomach; sp, spleen; dd, duodenum; cae, caecum; co, colon; re, rectum; SI, small intestine.

5.3.3 *Clmp* mutants develop bilateral hydronephrosis

While dissecting kidneys from *Clmp*$^{-/-}$ animals, it quickly became evident that the increased weight of the kidneys described in TABLE 5 was not due to a simple increase in kidney size. In contrast, kidneys were swollen like a balloon filled with fluid, with the renal tissue reduced to a thin layer, a pathologic condition that is known as hydronephrosis (FIGURE 15). Hydronephrosis is caused by a failure in the drainage of urine, which accumulates in and distends and dilates the renal pelvis and calyces. Regardless from the animals' sex, 100 % of dissected *Clmp* knockouts suffered from severe bilateral hydronephrotic kidneys. Concurrently, reproductive organs appeared maldeveloped in mutant animals and most likely explain the observed infertility of male and female *Clmp*$^{-/-}$ mice shown in TABLE 4.

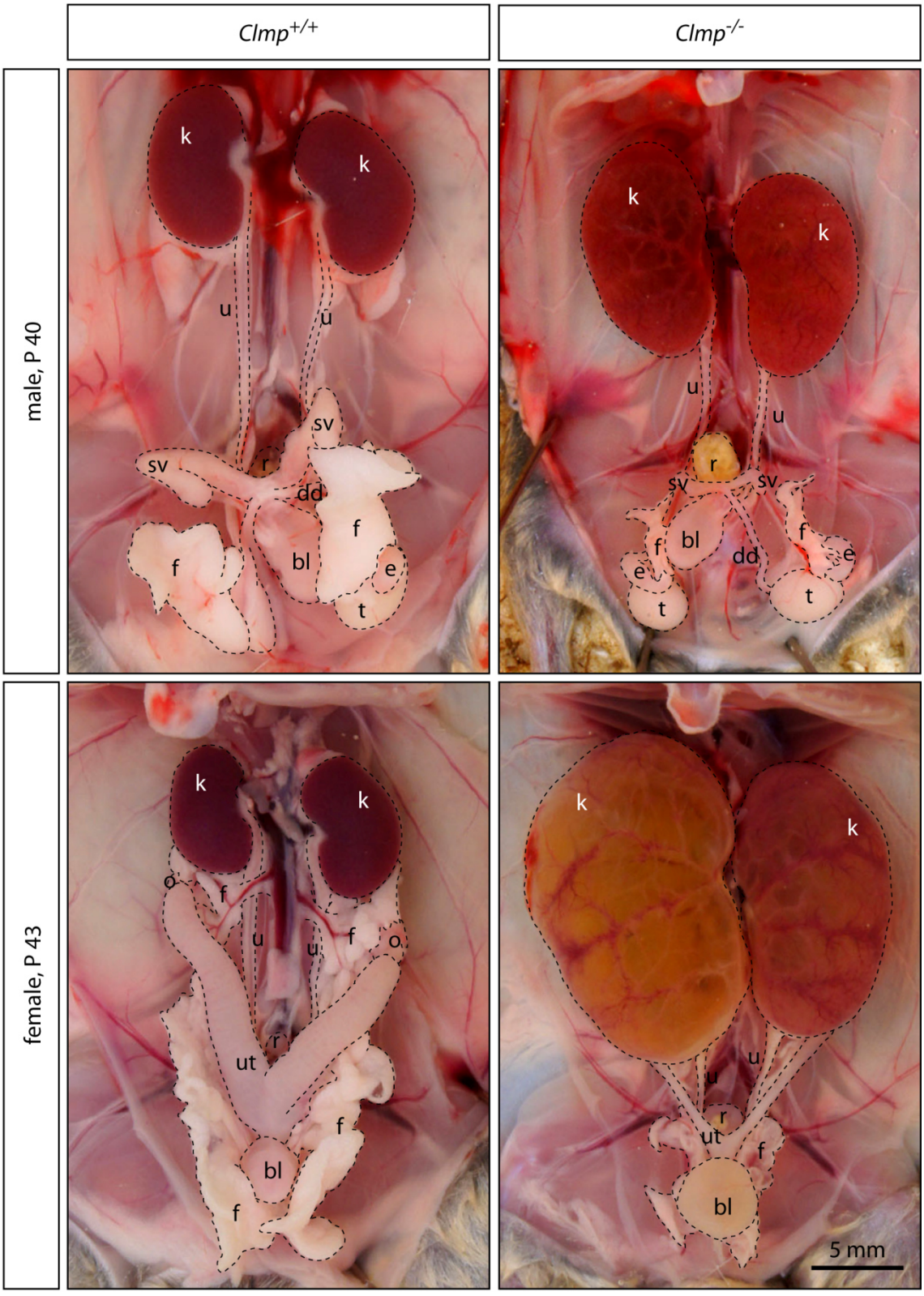

FIGURE 15. Dissected *Clmp* mutant animals display severe bilateral hydronephrosis.
Representative photos of juvenile animals of the *Clmp*-2043 strain showing highly hydronephrotic kidneys in *Clmp* mutants. Hydronephrosis developed bilaterally in both genders, while the ureters were not dilated. Additionally, reproductive organs of the male and female *Clmp* knockouts failed to develop as the wild type. Please note that ovaries and fallopian tubes were present in the mutant female but were covered by kidneys. k, kidney; u, ureter; bl, bladder; sv, seminal vesicle; dd, ductus deferens; t, testis; e, caput of the epididymis; f, fat; r, rectum; ut, uterus; o, ovary and associated fallopian tube.

Since bilateral hydronephrosis was initially discovered in adult *Clmp* mutant animals, the next step was to identify the onset of hydronephrosis. Blocks of the urinary system consisting of kidneys, ureters, and bladders were dissected from pups of both *Clmp* strains at early postnatal stages (FIGURE 16) and histological stainings were carried out on renal sections of selected postnatal stages (FIGURE 17). At the day of birth, the outward appearance of kidneys was normal in blocks of both control and knockout pups (FIGURE 16). Corresponding mutant kidney sections, however, already exhibited a dilation of the renal pelvis. Even at late embryonic stage E 18, histological stainings on cryosections revealed extended renal pelvis (FIGURE 17). In plastic sections of P 0 *Clmp*$^{-/-}$ kidneys, the nephron-containing renal parenchyma and the collecting duct system were still present, although the cortical and medullar layers appeared a bit thinner than in the kidneys of control newborn pups (FIGURE 17). One day later at P 1, in blocks a slight degree of transparency was visible in mutant kidneys as compared to controls, which became more apparent at P 2 (FIGURE 16). At postnatal day P 3, kidneys of *Clmp*$^{-/-}$ pups already possessed a high degree of hydronephrosis (FIGURE 16 and FIGURE 17). The dilation of the renal pelvis had become aggravated and the layers of renal tissues had become thinned out. Especially the nephron numbers in the cortex were markedly reduced. To conclude, loss of CLMP causes early development of bilateral hydronephrosis that could be observed as early as the day of birth. Typical characteristics of hydronephrosis like thinning of the renal parenchyma and dilation of renal pelvises were present, implicating the *Clmp* knockout lines as mouse model for congenital bilateral hydronephrosis.

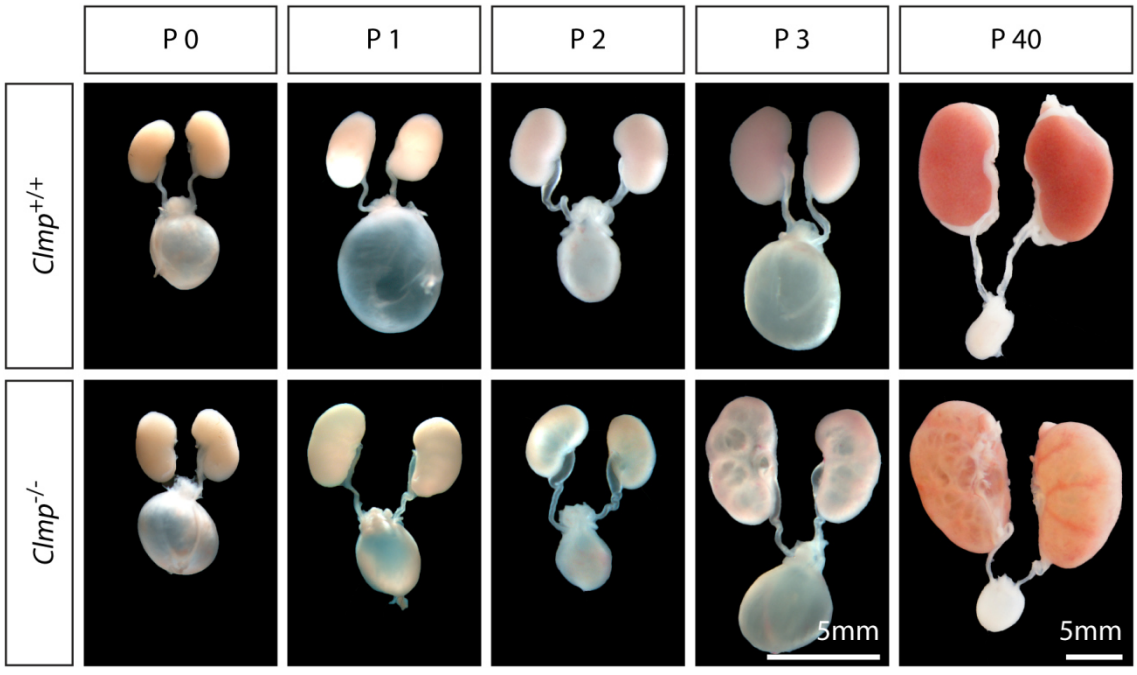

FIGURE 16. Kidney-ureter-bladder blocks at early postnatal and juvenile stages.
Bilateral hydronephrosis developed at early postnatal stages and could be recognised by eye at P 1 by a beginning of renal transparency, which became stronger at later stages and represented the dilation of renal pelvises with concurrent reduction in renal parenchyma. Note that ureteral diameters were not changed and the volume of bladder filling was independent of hydronephrosis and instead was influenced by dissection conditions, as some pups micturated before or during dissection.

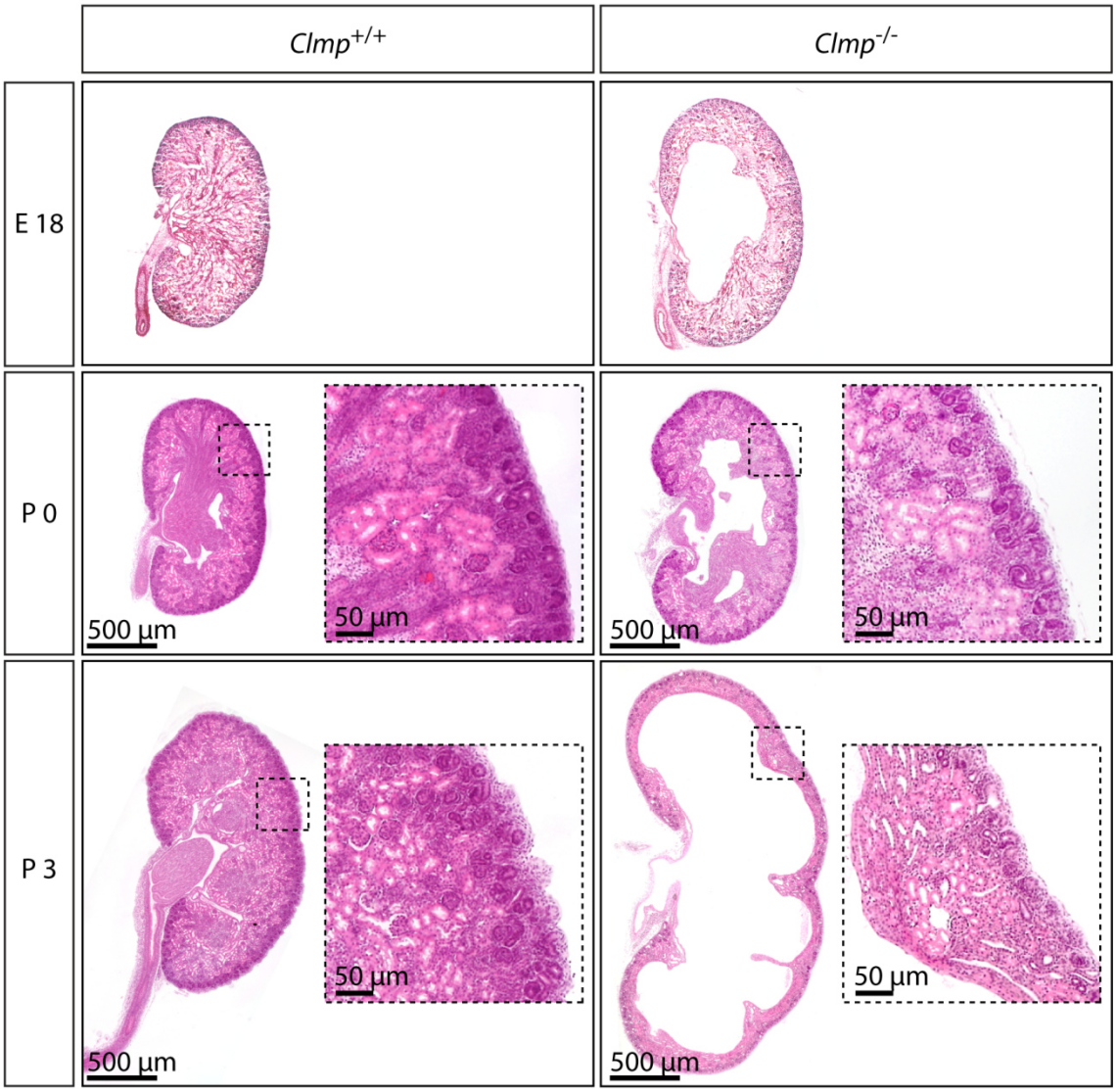

FIGURE 17. H&E stainings of kidney plastic sections.
Representative images of 5 µm thin renal plastic sections obtained from animals of the *Clmp*-KO strain, generation N4, were stained by haematoxylin and eosin. The histological staining revealed the early onset of hydronephrosis at E 18 and the rapid aggravation by dilation of the renal pelvis and calyces, which was accompanied by thinning in renal parenchyma.

5.4 Hydronephrosis due to kidney malfunction or obstruction?

In a first step of identifying the cause of hydronephrosis in *Clmp*$^{-/-}$ animals, renal function was estimated by determining urinary parameters. Changes in urine composition provide information about a failure during blood filtration and tubular reabsorption. However, based on the early mortality of *Clmp* knockout mice, it was difficult to obtain enough urine for an automated urinalysis in early postnatal and juvenile stages. Therefore, mouse urine was collected in a period of 8 h from adult animals (P 107) of the *Clmp*-2043 strain and analysed manually by Labor 28, Berlin. Urinary ingredients like electrolytes, proteins, glucose, urea, and glucose as well as the pH were determined (FIGURE 18). Interestingly, none of the urinary parameters were significantly altered in the absence of CLMP. The electrolytes sodium, potassium, magnesium, calcium, chloride, and phosphate were comparable in control and

knockout animals. Furthermore, the pH as well as glucose and urea levels were unchanged. Urinary protein concentration was highly, but not significantly reduced in *Clmp* mutant mice. Finally, levels of urinary creatinine, a common biomarker for estimation of renal health, were examined. Considering the early onset of hydronephrosis and the loss of renal parenchyma, urinary creatinine was expected to be elevated in adult *Clmp* knockout mice. Surprisingly, creatinine levels were however similar in urines of both control and knockout animals. As a result, the analysed urinary parameters did not indicate an impairment in renal function despite the huge anatomic change in adult *Clmp*$^{-/-}$ animals.

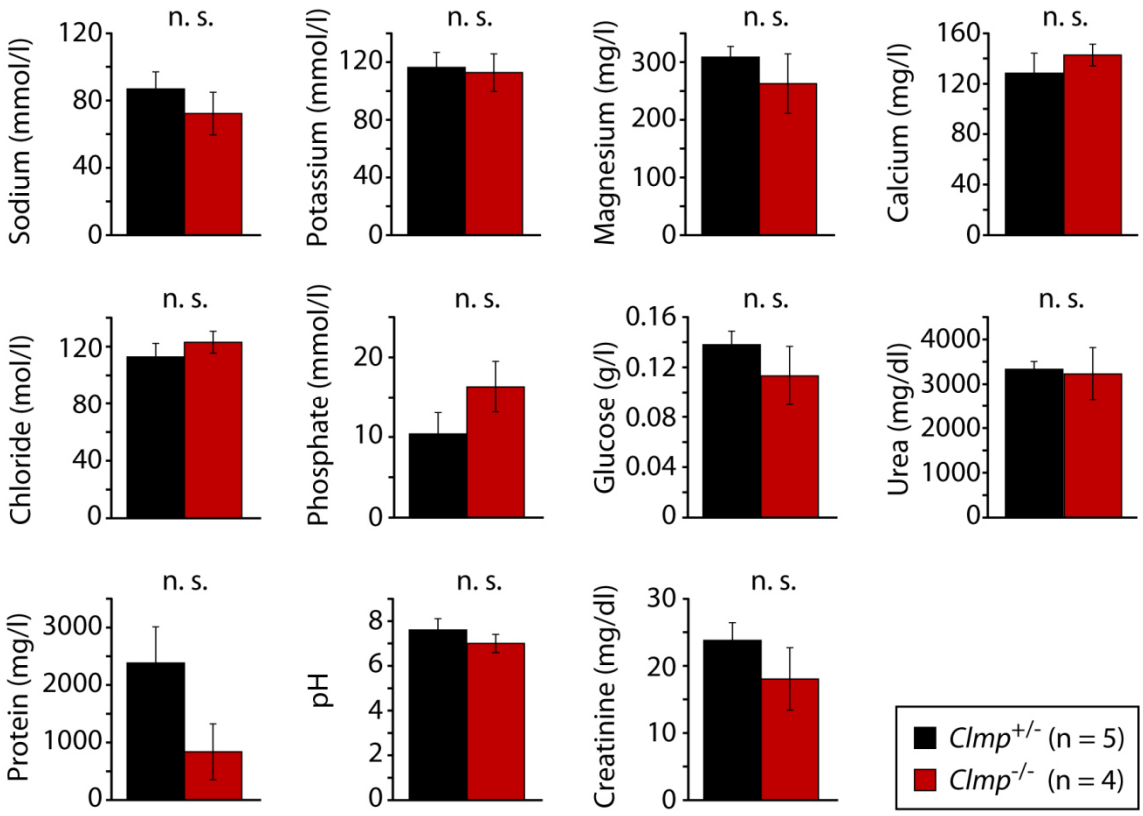

FIGURE 18. Urinary parameters of adult *Clmp*-2043 mice.
Several parameters were determined in urine from P 107 old animals of the *Clmp*-2043 strain by Labor 28, Berlin. Neither the pH nor the electrolytes, urinary glucose, urea, protein, and creatinine levels were altered in the absence of CLMP.

To investigate renal injury further, the secretion of neutrophil gelatinase-associated lipocalin (NGAL, also known as lipocalin 2) was examined in urine samples at different developmental stages. NGAL has recently been used as biomarker for different types of kidney injury, including the prediction of antenatal hydronephrosis (Mori & Nakao, 2007; Singer *et al.*, 2013; Lucarelli *et al.*, 2014; Noyan *et al.*, 2015). In contrast to the determination of urinary parameters in FIGURE 18, detection of urinary NGAL was carried out by Western analysis and has the advantage that only a little amount of urine is required. Equal volumes (10 µl) of urine from early postnatal, juvenile and adult *Clmp*$^{+/+}$, *Clmp*$^{+/-}$, *Clmp*$^{-/-}$ animals were separated on a

non-reducing SDS-PAGE and their NGAL levels were compared to recombinant NGAL standards (FIGURE 19). While wild type and heterozygous animals had rather low NGAL levels, NGAL amounts were clearly increased in urine samples from CLMP-deficient mice, even in early postnatal development. Thus, although creatinine levels were comparable in adult control and mutant littermates (FIGURE 18), elevated urinary NGAL in *Clmp*$^{-/-}$ mice strongly indicates ongoing injury in hydronephrotic kidneys, which might be associated with the loss of renal parenchymal tissue.

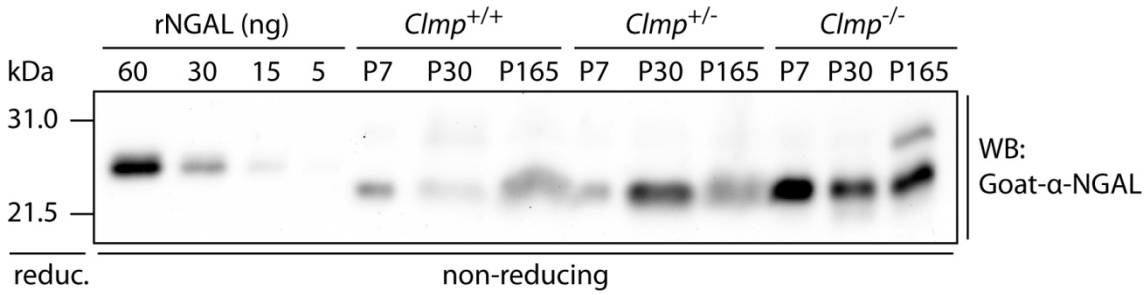

FIGURE 19. Detection of urinary NGAL in early postnatal, juvenile, and adult animals.
Urine was directly taken from the urinary bladder of dissected animals by punctuation with a syringe. Equal urine volumes of P 7 (*Clmp*-KO strain), P 30, and P 165 (*Clmp*-2043 strain) old mice were loaded to a non-reducing SDS-PAGE, and NGAL was detected in comparison to defined recombinant NGAL amounts. In the absence of CLMP, urinary NGAL amounts were higher than in control samples.

In the literature, hydronephrosis has mostly been described as obstructive condition, where urinary drainage is impaired by a blockage in the urinary system. After collection in the renal pelvis, urine is transported to the urinary bladder via the ureter. The ureteropelvic junction (UPJ) and the vesicoureteric junction (VUJ) are the junctions that connect the renal pelvis to the ureter and the ureter to the urinary bladder, respectively. A physical barrier at these junctions results in an accumulation of urine in the renal pelvis and is often reported as cause for obstructive hydronephrosis in humans (Rasouly & Lu, 2013). To investigate whether *Clmp* mutant animals suffer from obstructive hydronephrosis, ink was injected into the renal pelvis of E 18 embryos and ink propagation to the urinary bladder was observed (FIGURE 20). Independent from the genotype, ink flow was not compromised and was easily propagated to the urinary bladder after application of little pressure. While the ink filled the renal pelvis, the mutant pelvis appeared to be wider than the control pelvises, indicating an onset of hydronephrosis at even late embryonic stages. Conclusively, a physical barrier did not account for the development of bilateral hydronephrosis in *Clmp* knockout animals.

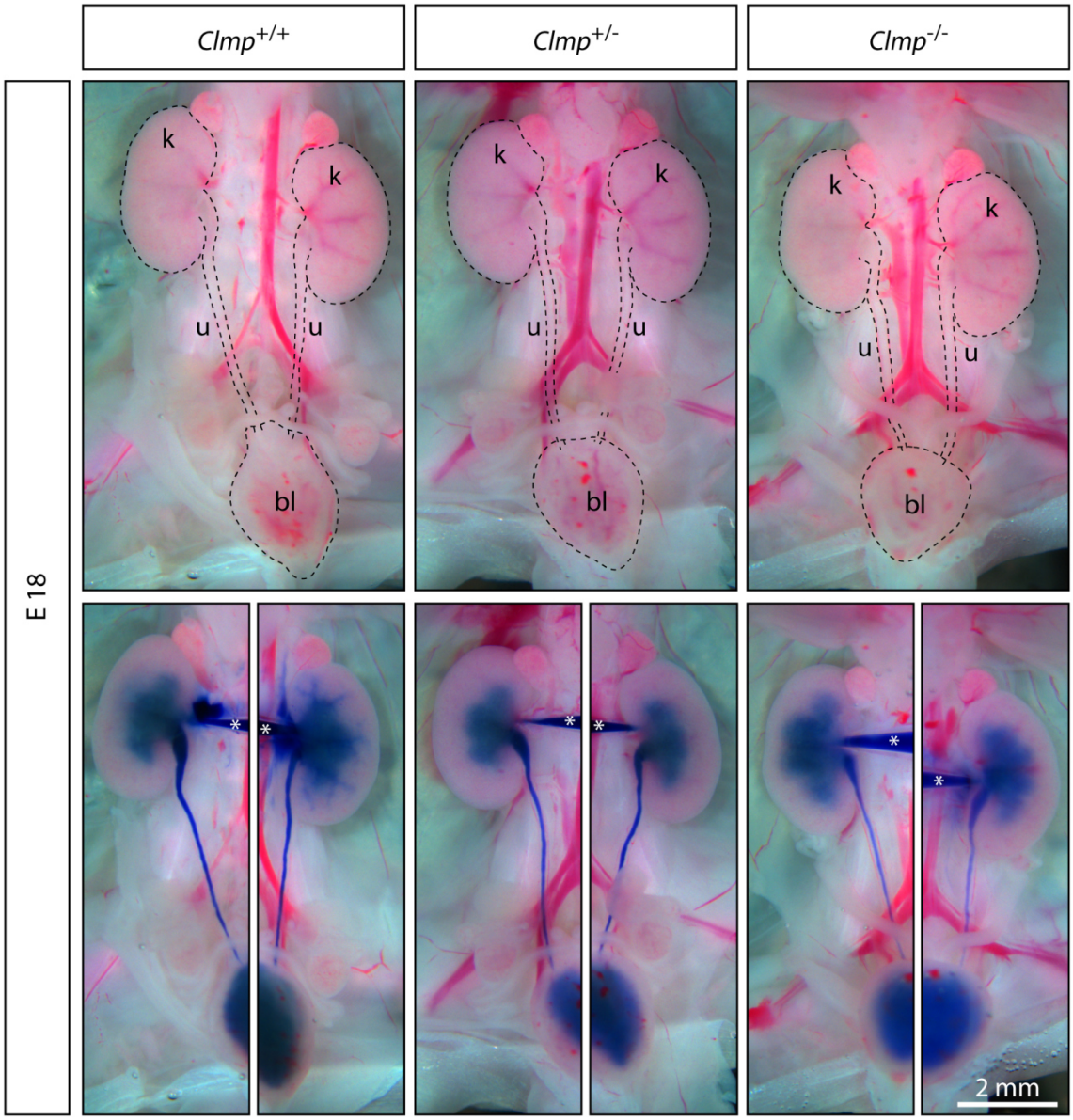

FIGURE 20. Intrapelvic ink injections reveal no physical obstruction.
Urinary systems of E 18 embryos of the *Clmp*-KO strain were exposed (top) and ink was injected into the renal pelvises by a pulled micropipette (white star) with little pressure to achieve propagation to the urinary bladder via the ureters (bottom). In all preparations, ink flow was not impaired by physical barriers. Comparing the ink distribution in mutant renal pelvises to control pelvises, the onset of hydronephrosis might already occur at late embryonic stages. k, kidney; u, ureter; bl, urinary bladder.

5.5 Analysis of ureteral anatomy by immunofluorescence

Since previous experiments indicated that bilateral hydronephrosis in *Clmp* knockout animals is non-obstructive, a next set of experiments was carried out to examine defects in ureteral structure and function. The ureter functions as a tube and actively transports urine from the renal pelvis to the urinary bladder. This mechanism called peristalsis is characterised by a unidirectional contraction wave of ureteral smooth muscle tissue. Smooth muscle cells define one of the prominent ureteral cell types, and absence or maldevelopment of ureteral smooth muscle has been reported to cause hydronephrosis in mice (Mahoney *et al.*, 2006; Caubit *et*

al., 2008; Yan *et al.*, 2014). To examine whether an impaired smooth muscle development might account for the urine accumulation in the renal pelvis, the anatomy of transverse sections was compared between control and mutant ureters. The normally developed, mature ureter is a tube whose lumen is surrounded by a transitional epithelial layer called urothelium that consists of inner umbrella cells, intermediate and outer basal cells. The urothelium is lined by a stromal cell layer, which in turn is covered by an inner circular and an outer longitudinal smooth muscle cell layer. All cell types of ureteral urothelium are recognised by detection of cytokeratin 8, while stromal cells are marked by retinaldehyde dehydrogenase 2 (RALDH 2). In contrast, α-smooth muscle actin (α-SMA) is specifically expressed in differentiated smooth muscle cells.

The anatomy of proximal, medial and distal parts of the ureter was analysed by immunofluorescent stainings of transverse sections using antibodies specifically recognising cytokeratin 8, RALDH 2, and α-SMA. Transverse cryosections were obtained from newborn or P 1 littermates, because older stages with advanced hydronephrosis might exhibit anatomical impairments secondary to urine accumulation. FIGURE 21 provides exemplary immunofluorescent stainings obtained from comparable sections of P 1 pups of the *Clmp*-KO strain. Please note that generally ureteral appearance in comparable sections of control and knockout specimens varied in regard to overall size, layer thickness and lumen diameter. Especially in CLMP-deficient preparations, some proximal ureters showed little dilation (e.g. FIGURE 21C in contrast to FIGURE 21A), which was however not observed in the majority of the sections. Still, all control and mutant ureteral sections shared a strong signal of α-SMA-positive smooth muscle layer and cytokeratin 8-positive urothelium as can be seen in FIGURE 21B and FIGURE 21D, respectively. Between the smooth muscle ring and the urothelium, the stromal cell layer is located. Stainings of the marker RALDH 2, however, did not produce constantly reliably signals in ureteral sections. In some preparations, RALDH 2-positive ring structures were clearly seen in between the α-SMA-positive and the cytokeratin 8-positive cell layers in both control and knockout preparations, while in others RALDH 2 signals were absent in either of the genotypes (figures not shown). Nevertheless, in double stainings of cytokeratin 8 and α-SMA, the stromal cell layer could yet be identified without RALDH 2 counterstaining in both control and CLMP-deficient sections (FIGURE 21B and FIGURE 21D, respectively). Thus, immunofluorescent analysis showed that the major cell layers of the ureter – the thick contraction-executing smooth muscle ring, the stromal cell layer as well as the urothelium functioning as permeability barrier – are present in mutant ureters, revealing no change in gross ureteral anatomy. Therefore, the development of hydronephrosis cannot be explained by a complete loss of a specific cell layer and may instead arise from a functional defect rather than from an anatomical defect.

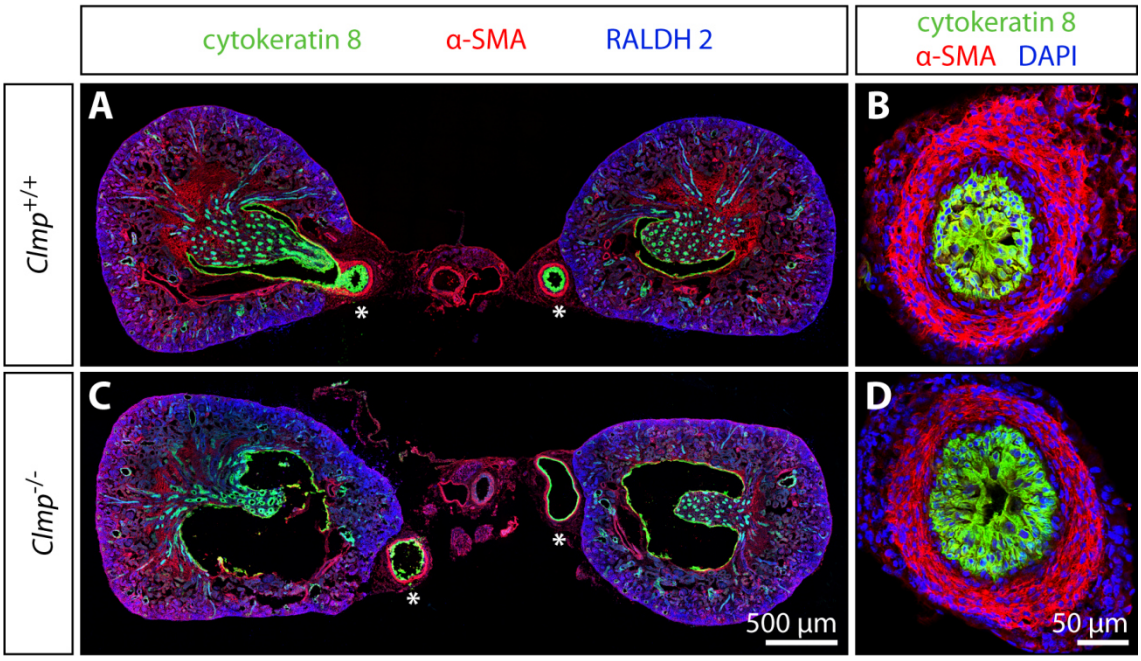

FIGURE 21. Gross ureteral anatomy analysed by immunofluorescence.
Transverse sections from P 1 pups of the *Clmp*-KO strain were stained with ureteral markers cytokeratin 8, α-SMA, and RALDH 2. (A, C) Overview sections reveal hydronephrotic kidneys which exhibit an epithelial layer lining the renal pelvis and RALDH 2-positive renal cortical stroma. Ureters marked by white asterisks were dilated in the mutant sections presented here, which however was not the case in the majority of the analysed sections. (B, D) Representative ureteral transverse sections obtained from other pups revealed the presence of outer smooth muscle ring, stromal layer and inner urothelium in control and mutant ureters. α-SMA, α-smooth muscle actin; RALDH 2, retinaldehyde dehydrogenase 2.

5.6 Impaired ureteral peristalsis in *Clmp* mutants

As previously described, peristaltic contraction waves occur unidirectionally in order to propel urine from the renal pelvis to the urinary bladder. Since no gross anatomical alterations were observed in mutant ureters, the functionality of ureteral peristalsis was examined in a next set of experiments. During embryonic development, ureters form as the distal stalk of the ureteric bud elongates towards the bladder. Around E 14.5 to E 15.5, ureteral smooth muscle and stromal cells start to differentiate from mesenchymal cells surrounding the ureteral stalk, while the epithelial stalk itself differentiates into the urothelium (Airik & Kispert, 2007; Rasouly & Lu, 2013; Bohnenpoll & Kispert, 2014). At later embryonic stages, ureters begin with peristaltic contractions in order to transport urine whose production starts at E 16.5. Ureteral peristalsis is regulated by several factors including innervating nerve fibres, however peristalsis can also be driven independently from neural control and can instead be initiated spontaneously by pacemaker cells (Santicioli & Maggi, 1998; Lang *et al.*, 2006). In several studies, isolated ureters dissected from E 15.5 mouse embryonic urinary systems begin to spontaneously contract after several days *in vitro* when kept in culture on a filter membrane at the liquid-air interface (David *et al.*, 2005; Caubit *et al.*, 2008; Cain *et al.*, 2011). In order to similarly investigate spontaneous peristalsis, ureters from E 15.5 urinary tracts of the

Clmp-2043 and the *Clmp*-KO strains were cultured *ex vivo*. Ureteral explants of all genotypes elongated during culture and were comparable in length (FIGURE 22A). Furthermore, outward appearances were similar among control and mutant ureters. After four days in culture, ureteral wild type and heterozygous explants from both *Clmp* strains started to spontaneously develop peristaltic waves. At DIV 5, contraction waves were monitored by 270 ms interval time-lapse recordings and analysed. Contractions started at the proximal site and unidirectionally propagated towards the distal ureter end (FIGURE 23A and FIGURE 23A'; see also supplemental VIDEO 1 and VIDEO 2). Importantly, peristaltic waves started not before a previous wave had completed. Furthermore, changes in ureteral diameter during contraction were comparable to the literature (Bush *et al.*, 2006). Because both *Clmp* strains exhibited equal peristaltic waves, the strains were pooled for further analysis. Frequency and speed were calculated and did not differ between $Clmp^{+/+}$ and $Clmp^{+/-}$ ureter explants (FIGURE 22B and FIGURE 22C, respectively). In contrast to control ureters, 100 % of mutant ureters (26 ureters from 13 embryos) did not produce peristaltic waves at all. Instead, small fibrillation-like contractions were observed that never shaped a proximal-to-distal contraction wave. Mutant contractions were slow, locally restricted and failed to strongly reduce the ureteral lumen diameter. However, contractions were continuously observed non-stop and also several contractions could occur simultaneously at multiple sites of the ureter (FIGURE 23B and FIGURE 23B'; see also supplemental VIDEO 3 and VIDEO 4). Since the local contractions in ureters lacking CLMP were weak and occurred slowly, the ureteral phenotype can be best demonstrated in videos, therefore the reader is highly recommended to watch the supplemental videos on the CD attached to this thesis (see section 8.1 for further information). To conclude, the overall impaired and uncoordinated contractions in CLMP-deficient ureters do promote the impression that urine drainage is not functional in $Clmp^{-/-}$ animals. Thus, the loss of CLMP leads to a functional obstruction which results in accumulation of urine and thereby finally causes hydronephrosis.

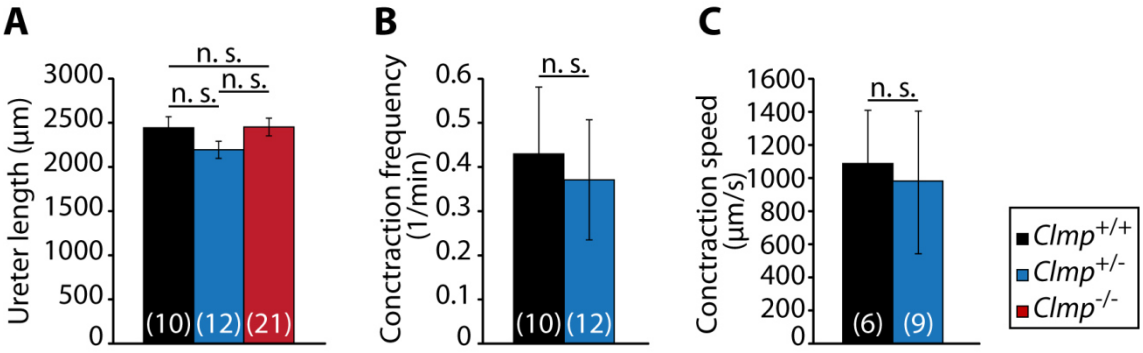

FIGURE 22. Parameters of ureteral explant appearance and peristalsis.
After five days in culture, isolated ureters dissected at E 15.5 were analysed for (A) ureter length, (B) contraction frequency, and (C) contraction speed. Please note that $Clmp^{-/-}$ did not exhibit peristaltic contractions that could be examined for frequency and speed. Numbers of investigated specimens are indicated in brackets. n. s., not significant.

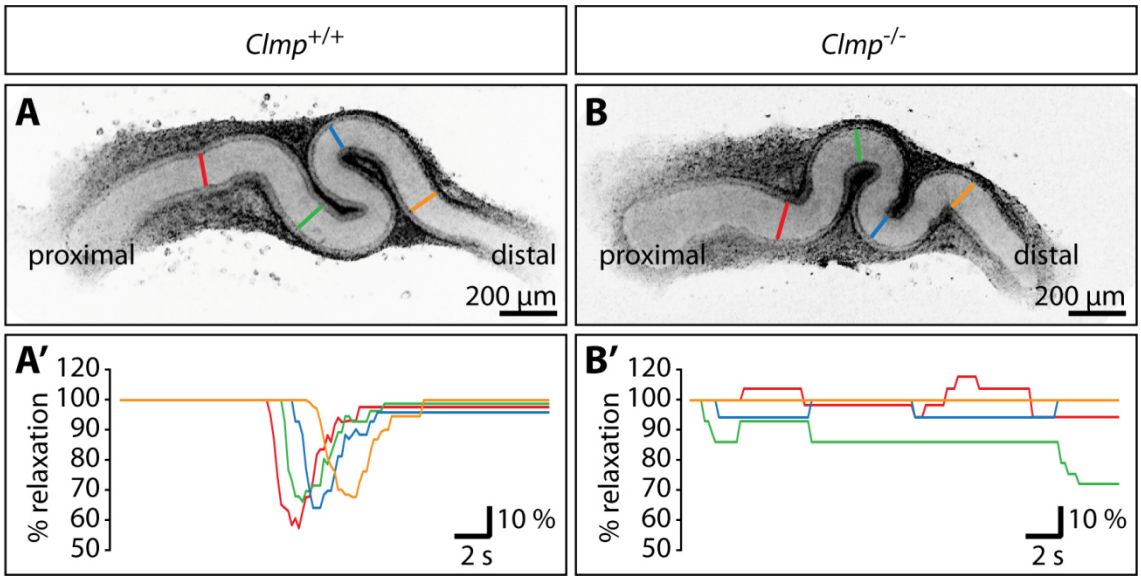

FIGURE 23. Ureteral peristaltic diameter changes.
Outward appearances were comparable in ureter explants as shown by representative images from E 15.5 *Clmp*$^{+/+}$ (A) and *Clmp*$^{-/-}$ (B) embryos at day *in vitro* (DIV) 5. Wild type ureters produced proximal-to-distal oriented, peristaltic contractions. (A') A single peristaltic wave is plotted as % relaxation of the ureteral lumen diameter at the respective sites indicated in (A). Contraction intensities were comparable to the literature (Bush *et al.*, 2006). (B') Contrarily, mutant ureters did not conduct peristaltic movements but uncoordinated, fibrillation-like contractions that did not constrict the lumen diameter as intense as the control.

The observation that ureteral peristalsis is impaired in *Clmp* knockout animals raises the question about the underlying mechanisms. Generally, contractions are initiated by electrical activity arising from pacemaker cells at the renal pelvis and conducted to ureteral smooth muscle, consisting of mainly so-called typical smooth muscle cells. The smooth muscle cells form a functional syncytium and anterogradely propagate the electrical signal to the distal ureter. The electrical excitation of smooth muscle cells triggers intracellular Ca^{2+}influx which is coupled to immediate contractions (Santicioli & Maggi, 1998; Bohnenpoll & Kispert, 2014).

Since contractions in CLMP-deficient ureters were not completely absent but rather uncoordinated and continuous, and given that the closest homologue of CLMP, CAR, is implicated in modulating electrical activity in the brain (Rathjen laboratory, unpublished observation, personal communication), a potential defect in signal propagation in smooth muscle cells was taken into account. Therefore, the ureteral Ca^{2+} signalling was analysed by electrophysiologist Dr René Jüttner, who has profound experience in calcium imaging. Ureter explants taken for previously described peristaltic studies were loaded with Ca^{2+}-sensitive indicator Fura-2 at DIV 5 and examined by whole-mount calcium imaging. Ca^{2+} transients were recorded at different regions of interest (ROI) and by plotting calcium transients of the different ROIs over time, Ca^{2+} waves were defined when over 50 % of ROIs were synchronously active (FIGURE 24). As expected, CLMP-deficient ureters were not able to produce Ca^{2+} waves that are required for synchronous contractions. In contrast, mutant ureteral explants only exhibited only few and weak Ca^{2+} transients. Taken together, these data suggest that ureteral

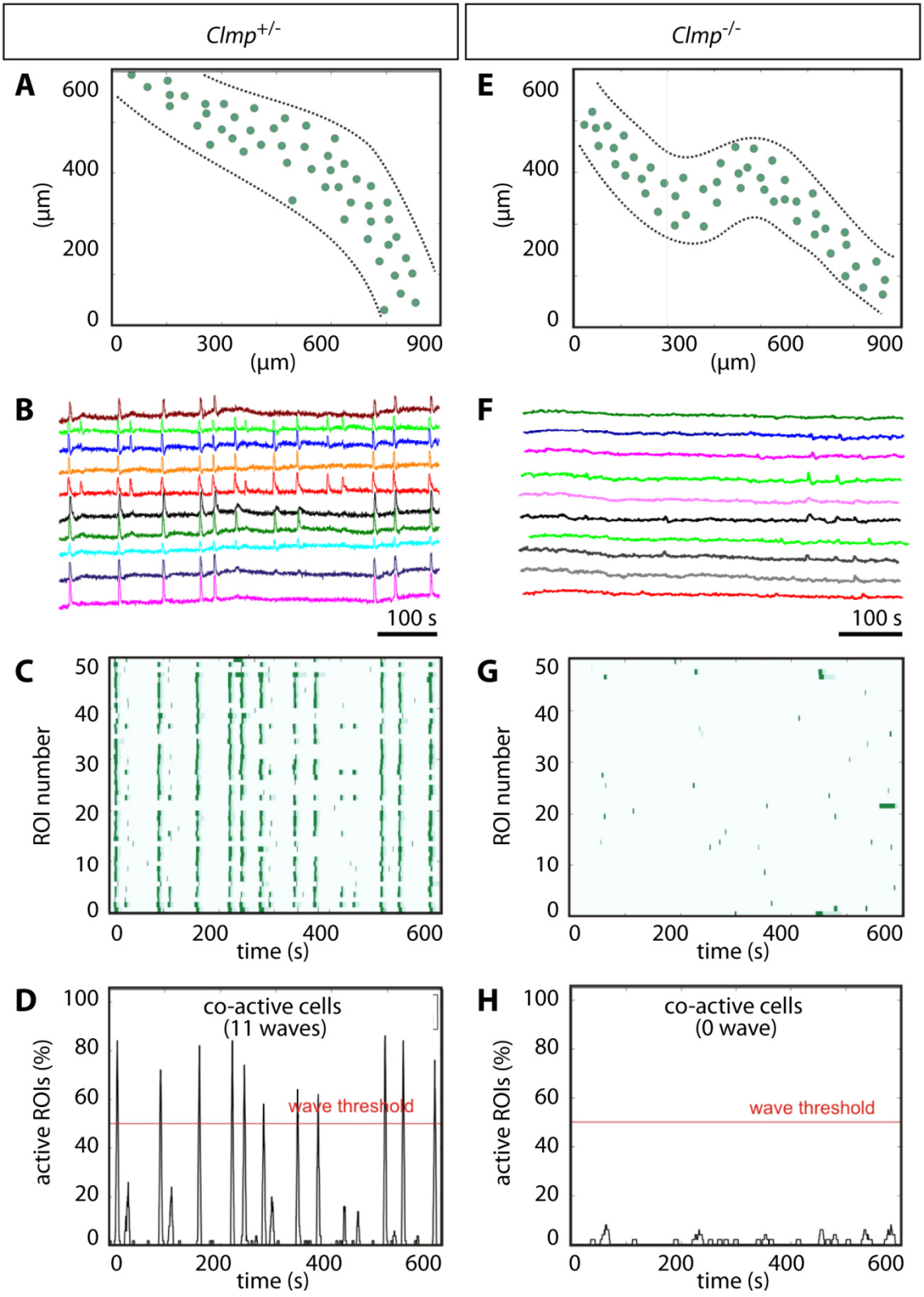

FIGURE 24. Calcium imaging reveals lack of Ca^{2+} waves in CLMP-deficient ureter explants. Ureteral *Clmp*$^{+/-}$ (A-E) and *Clmp*$^{-/-}$ (F-J) explants were loaded with the Ca^{2+}-sensitive indicator Fura-2 at DIV 5 and Ca^{2+} waves were analysed by calcium imaging performed by Dr René Jüttner. (A, E) Schematic representation of ureter tissue with 50 regions of interest (ROI; green dots; 20 µm x 20 µm), from which Ca^{2+} transients were recorded. Examples of Ca^{2+} transients (B, F), heatmaps (C, G) and waveograms (D, H) are shown for *Clmp*$^{+/-}$ and *Clmp*$^{-/-}$ ureters, respectively. Estimated velocity of the Ca^{2+} wave in *Clmp*$^{+/-}$ ureteral explant is 73.55 ± 5.22 µm/s.

peristalsis is severely impaired in *Clmp*$^{-/-}$ ureters due to uncoordinated smooth muscle contractility and associated compromised Ca^{2+} signalling. Whether Ca^{2+} signalling is the primary defect causing impaired peristalsis or rather a secondary effect remains to be clarified. In order to design suited experiments, it has to be first determined which ureteral cell types express CLMP.

5.7 Generation of antibodies against CLMP

In order to analyse CLMP expression in the urinary tract, polyclonal antibodies raised against the cytoplasmic tail and the extracellular domain of CLMP were generated in rabbits. First, rabbits were immunised with the $mCLMP_{cyt}$ antigen to generate sera against the cytoplasmic region. Later in the course of this study, another series of rabbit immunisations was carried out using the $mCLMP_{ex}$-hFc antigen in order to produce antibodies specifically recognising the extracellular region of CLMP.

5.7.1 Purification of CLMP antibodies

Rabbit antisera were purified by affinity chromatography. In a first step, complete IgG molecules were purified using a protein A-coupled matrix. After affinity chromatography, antibody purifications were analysed by SDS gel coomassie stainings revealing IgG heavy and light chains (FIGURE 25). If desired, some IgG antibody fractions were further purified by using tag- and antigen-coupled affinity columns (TABLE 6).

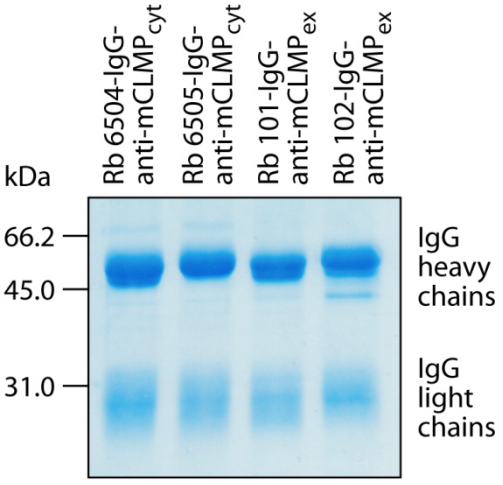

FIGURE 25. Protein A-purified antibodies.
Purified antibodies were separated by SDS-PAGE and tested for IgG heavy and light chains by coomassie staining.

TABLE 6. Overview of antibody purifications.

Antibody designation	Immunising antigen	Matrix-coupled molecules		
		Protein A	Tag	Antigen
Rb 6504-IgG-anti-$mCLMP_{cyt}$	$mCLMP_{cyt}$	yes	GST	-
Rb 6504-AP-anti-$mCLMP_{cyt}$	$mCLMP_{cyt}$	yes	GST	$mCLMP_{cyt}$
Rb 6505-IgG-anti-$mCLMP_{cyt}$	$mCLMP_{cyt}$	yes	GST	-
Rb 101-IgG-anti-$mCLMP_{ex}$	$mCLMP_{ex}$-hFc	yes	-	-
Rb 101-AP-anti-$mCLMP_{ex}$	$mCLMP_{ex}$-hFc	yes	IgG 1	$mCLMP_{ex}$
Rb 102-IgG-anti-$mCLMP_{ex}$	$mCLMP_{ex}$-hFc	yes	-	-

5.7.2 Testing antibodies for specificity

After purification, antibodies were tested for specificity in either Western and/or immunofluorescence applications.

5.7.2.1 Western blots

To examine whether antibodies were suitable for specific recognition of CLMP in Western blots, several approaches were undertaken. In a first step, the $mCLMP_{cyt}$ antigen was separated via SDS-PAGE and after blotting, nitrocellulose stripes were incubated with different dilutions of antibodies Rb 6504-IgG-anti-$mCLMP_{cyt}$ and Rb 6505-IgG-anti-$mCLMP_{cyt}$ (FIGURE 26). Both antibodies recognised around 40 ng of cytoplasmic region of CLMP even at low antibody concentrations of 0.06 µg/ml, however Rb 6504-IgG-anti-$mCLMP_{cyt}$ provided a much higher detection intensity. Therefore, this antibody was chosen for further purification by antigen-coupled sepharose affinity chromatography and generated the purified Rb 6504-AP-anti-$mCLMP_{cyt}$.

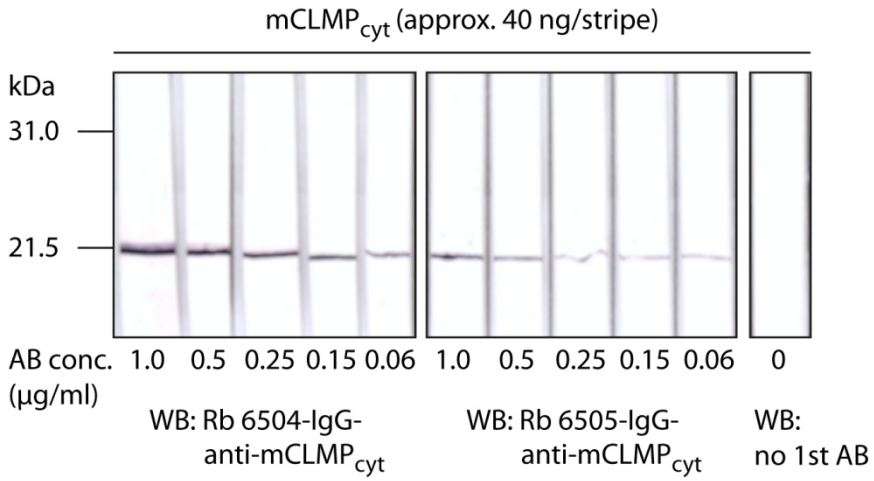

FIGURE 26. Recognition of the cytoplasmic fragment of murine CLMP in Western blot.
The cytosolic CLMP fragment from mouse was detected by serial dilutions of Rb 6504-IgG-anti-$mCLMP_{cyt}$ and Rb 6505-IgG-anti-$mCLMP_{cyt}$ antibodies with higher signal intensity obtained using the former Rb 6504-IgG-anti-$mCLMP_{cyt}$ antibody. AB, antibody; conc., concentration.

To test specificity of the purified antibody Rb 6504-AP-anti-$mCLMP_{cyt}$, COS-7 cells were transfected with the cDNA encoding full-length CLMP by technician Anne Banerjee. Protein lysates of untransfected and transfected COS-7 cells were prepared and separated by SDS-PAGE with or without β-mercaptoethanol. As illustrated by FIGURE 27, Western blot analysis with Rb 6504-AP-anti-$mCLMP_{cyt}$ revealed specific recognition of CLMP in transfected, but not untransfected samples. Furthermore, the omission of β-mercaptoethanol in the sample buffer led to a band shift in the SDS gel due to uncleaved disulphide bridges resulting in an incomplete unfolding of the protein.

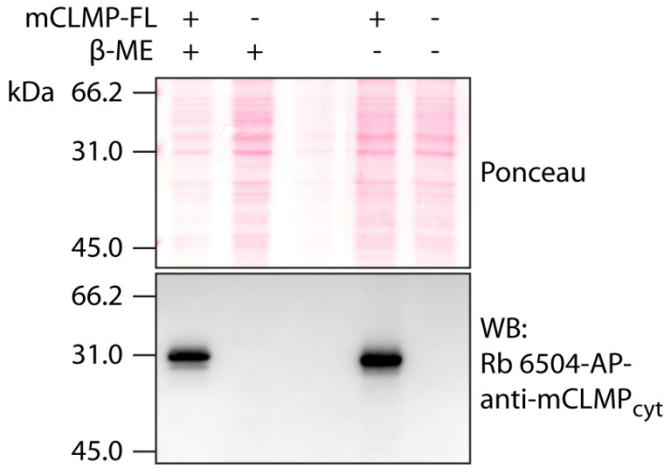

FIGURE 27. Recognition of CLMP in transfected COS-7 cells.
Lysates of untransfected COS-7 cells and COS-7 cells transfected with full-length CLMP (mCLMP-FL) were separated by SDS-PAGE in presence or in absence of β-mercaptoethanol (Ponceau staining, top). The antibody Rb 6504-IgG-anti-mCLMP$_{cyt}$ antibody did not detect proteins in untransfected samples but specifically recognised CLMP in samples lysates obtained from transfected cells. βME, β-mercaptoethanol.

Shortly after affinity purification of Rb 6504-AP-anti-mCLMP$_{cyt}$, IgG fractions were purified from antisera of rabbits Rb 101 and Rb 102, generating the antibodies Rb 101-IgG-anti-mCLMP$_{ex}$ and Rb 102-IgG-anti-mCLMP$_{ex}$. To test whether these antibodies are able to detect endogenous CLMP, they were used for detection of CLMP in brain samples since CLMP has been reported to be expressed in the brain (Raschperger *et al.*, 2004; Eguchi *et al.*, 2005). In a first approach, brains from early postnatal C57BL/6 mice (P 1 and P 10) were subcellularly fractionated to receive specific signals for the transmembranous CLMP protein in the membrane fraction but not in the cytosolic fraction (FIGURE 28). The Rb 6504-AP-anti-mCLMP$_{cyt}$ antibody detected a band with the appropriate molecular weight of 46 kDa in the membrane fraction but not in the cytosolic fraction, as expected. Contrarily, both Rb 101-IgG-anti-mCLMP$_{ex}$ and Rb 102-IgG-anti-mCLMP$_{ex}$ antibodies detected several bands at inappropriate sizes and also bands at around 46 kDa, however, in both subcellular fractions, concluding that both antibodies did not specifically recognise CLMP in these samples.

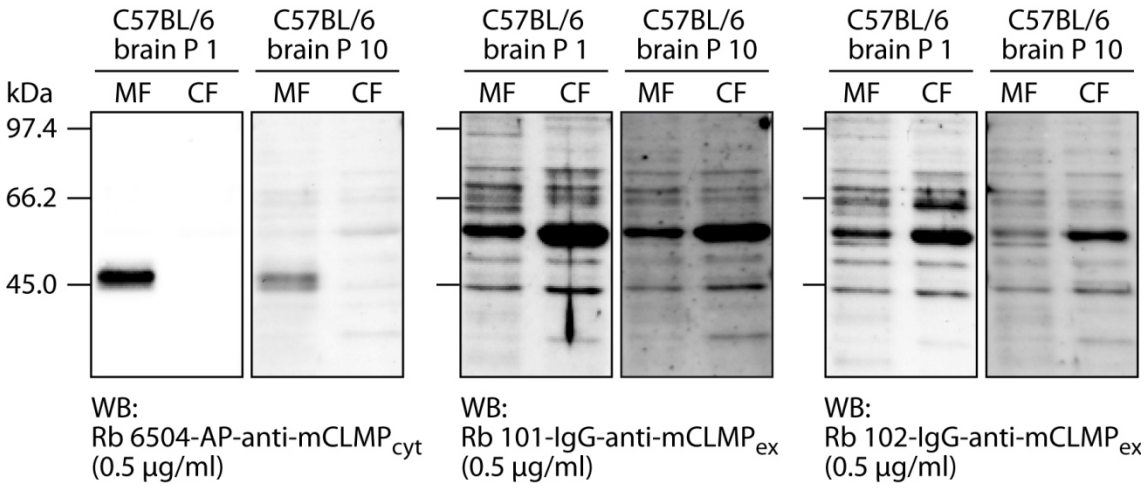

FIGURE 28. Recognition of CLMP in subcellular brain fractions.
Brains from P 1 and P 10 C57BL/6 pups were subcellularly fractionated and 5 µg protein were loaded per lane. While antibody Rb 6504-AP-anti-mCLMP$_{cyt}$ detected a band at the appropriate molecular weight of 46 kDa in membrane fractions, blots using antibodies Rb 101-IgG-anti-mCLMP$_{ex}$ and Rb 102-IgG-anti-mCLMP$_{ex}$ resulted in many unspecific bands. MF, membrane fraction; CF, cytosolic fraction.

To further prove that the 46 kDa band recognised by Rb 6504-AP-anti-mCLMP$_{cyt}$ antibody was specific, it was examined whether the band could also be detected under deglycosylated and non-reduced conditions. CLMP has been shown to be *N*-glycosylated (Gundry *et al.*, 2009) and deglycosylation at these sites would result in a change in molecular weight. Furthermore, samples were treated with or without β-mercaptoethanol to reveal a band shift similarly to the shift shown in FIGURE 27. PNGase F-treated and untreated membrane fractions of E 15 C57BL/6 brains were loaded with or without β-mercaptoethanol to SDS gels, and antibodies Rb 6504-AP-anti-mCLMP$_{cyt}$, Rb 101-IgG-anti-mCLMP$_{ex}$ and Rb 102-IgG-anti-mCLMP$_{ex}$ were used for detection. In addition, the antibody Rb 80-anti-mCAR$_{ex}$ recognising the *N*-glycosylated transmembranous CAR protein was used as control (FIGURE 29). The blot using Rb 80-anti-mCAR$_{ex}$antibody confirmed successful deglycosylation of the brain samples by resulting in a reduction of molecular weight and furthermore, the lack of β-mercaptoethanol in the sample buffers caused a band shift as expected. Similar results were obtained by detection of CLMP using antibody Rb 6504-AP-anti-mCLMP$_{cyt}$. The putatively CLMP-representing 46 kDa band detected in untreated samples was reduced by PNGase F treatment to approximately 41 kDa, which corresponds to the molecular mass calculated from amino acid sequence analysis (www.uniprot.org, entry Q8R373). Also, a band shift could be observed under non-reducing conditions without β-mercaptoethanol. Thus, these data further indicate the specificity of Rb 6504-AP-anti-mCLMP$_{cyt}$ antibody in Western blots. On the contrary, both antibodies

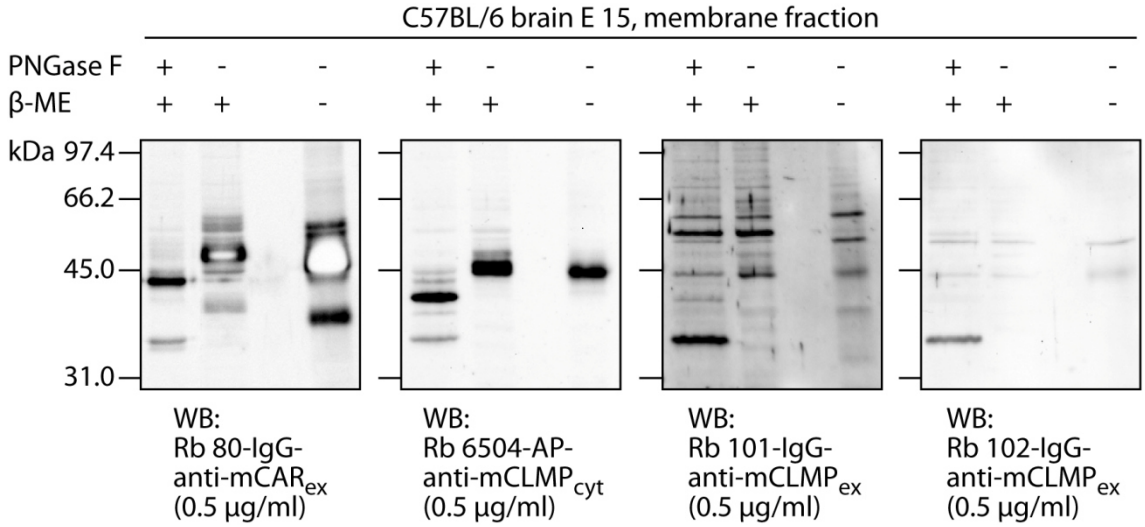

FIGURE 29. Recognition of CLMP in deglycosylated and non-reduced brain membrane fractions.

Membrane fractions of E 15 C57BL/6 brains were treated with or without PNGase F for deglycosylation or β-mercaptoethanol, respectively. A protein amount of 5 µg was loaded for reduced samples, whereas 8 µg protein were loaded in samples lacking β-mercaptoethanol. Among the blots for CLMP detection, only bands recognised by antibody Rb 6504-AP-anti-mCLMP$_{cyt}$ showed appropriate molecular masses. The detection of CAR protein using Rb 80-IgG-anti-mCAR$_{ex}$ served as control; white areas in the bands are due to blot overdevelopment. Please note that the 36 kDa bands in deglycosylated samples represent the unspecific recognition of PNGase F. βME, β-mercaptoethanol; CAR, coxsackie-adenovirus receptor; PNGase F, peptide-N-glycosidase F.

Rb 101-IgG-anti-mCLMP$_{ex}$ and Rb 102-IgG-anti-mCLMP$_{ex}$ did not produce the expected results. Neither deglycosylation nor non-reducing conditions led to appropriate band shifts, supporting the impression that both antibodies raised against the extracellular CLMP domain are not suitable for Western analyses. To finally verify that the 46 kDa band recognised by Rb 6504-AP-anti-mCLMP$_{cyt}$ represents CLMP protein, subcellular fractions of brain from *Clmp*$^{+/+}$, *Clmp*$^{+/-}$ and *Clmp*$^{-/-}$ E 15 embryos were separated by SDS-PAGE, transferred to nitrocellulose membrane and incubated with Rb 6504-AP-anti-mCLMP$_{cyt}$ antibody (FIGURE 30). As in the previous blots, the antibody detected the 46 kDa band in wild type and heterozygous membrane fractions. Importantly, no such band was detected in samples obtained from knockout brains. Taken together, the results obtained from the different Western blots presented in this section confirm that antibody Rb 6504-AP-anti-mCLMP$_{cyt}$ specifically detects CLMP in membrane fractions (at least in brain samples) and can be used for Western analyses.

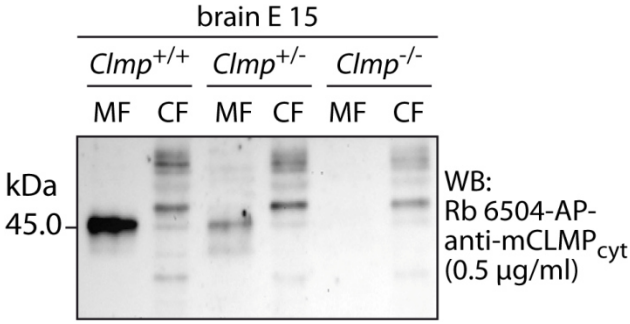

FIGURE 30. Specificity of Rb 6504-AP-anti-mCLMP$_{cyt}$ validated in brain samples of *Clmp* mutants.
Rb 6504-AP-anti-mCLMP$_{cyt}$ detected a 46 kDa band in membrane fractions of wild type and heterozygous E 15 brains, whereas no bands were recognised in membranous preparations from mutant brains. MF, membrane fraction; CF, cytosolic fraction.

5.7.2.2 Immunofluorescence

To investigate whether antibodies raised against the extracellular CLMP region specifically recognise CLMP in immunofluorescent stainings, a series of immunofluorescence stainings were performed. In a first approach, antibodies were tested to detect CLMP in overexpressing cells. For this, COS-7 cells were transfected with full-length CLMP and stained with different dilutions of antibodies Rb 6504-AP-anti-mCLMP$_{cyt}$, Rb 101-IgG-anti-mCLMP$_{ex}$, Rb 101-AP-anti-mCLMP$_{ex}$ and Rb 102-IgG-anti-mCLMP$_{ex}$. The two IgG fractions of antibodies Rb 101 and Rb 102 comparably detected transfectants best at a dilution of 1.25 µg/ml (FIGURE 31), whereas the affinity-purified versions of Rb 6504 and Rb 101 did not give any positive stainings (not shown). Due to the positive staining results obtained from Rb 101-IgG-anti-mCLMP$_{ex}$ and Rb 102-IgG-anti-mCLMP$_{ex}$, further immunofluorescent stainings using these two antibodies were carried out to detect CLMP in primary cell cultures and cryosections (TABLE 7). Since CLMP-deficient mouse strains had not been available at that time point, antibody testing was initiated in tissues from C57BL/6N mouse strain. First, dissociated cultures of embryonic brain tissues dissected at E 15 were stained, as previous Western blots indicated expression of CLMP in embryonic brains (section 5.7.2.1). Unfortunately, these primary cultures did not reveal CLMP-positivity (not shown, TABLE 7). In a next step, cryosections of C57BL/6N mice were analysed by immunofluorescence. However, no specific immunoreactivity could be observed in tissues from either embryonic or postnatal stages, even in brain tissues no clear positive signals could

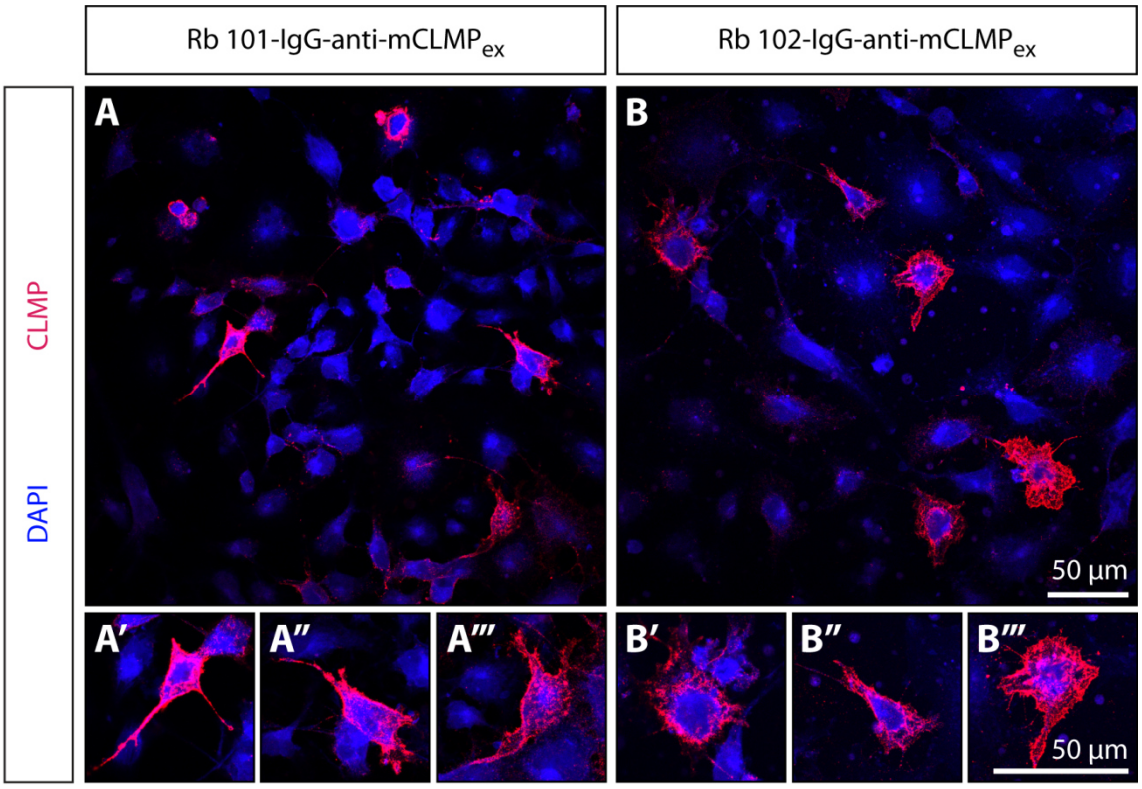

FIGURE 31. Recognition of transfected mCLMP$_{fl}$ by antibodies purified from rabbits Rb 101 and Rb 102.

Transfected COS-7 cells expressing full-length CLMP were detected by antibodies Rb 101-IgG-anti-mCLMP$_{ex}$ (A and detailed images A', A'', A''') and Rb 102-IgG-anti-mCLMP$_{ex}$ (B and detailed images B', B'', B''') at a dilution of 1.25 µg/ml, whereas any dilutions of antigen-purified antibodies Rb 6504-AP-anti-mCLMP$_{cyt}$ and Rb 101-AP-anti-mCLMP$_{ex}$ were not able to stain transfectants (not shown).

be obtained (not shown, TABLE 7). Once *Clmp* mouse strains had been generated, specificity testing was expanded by the direct comparison of wild type and/or heterozygous tissues to *Clmp* knockout tissue. Analysed tissues ranged from whole embryos up to newborn brains, duodenum and urinary tracts consisting of kidneys, ureters, and urinary bladders. Interestingly, some faint but specific-looking immunofluorescent signals could be observed in some tissue structures from *Clmp*$^{+/+}$ or *Clmp*$^{+/-}$ animals, e.g. in the duodenal muscle layer. The direct comparison of stainings in control cryosections to comparable *Clmp*$^{-/-}$ cryosections, though, ruled out that the monitored signals were specific, since the same staining results were seen in *Clmp* knockout tissues (not shown, TABLE 7). Therefore, it was concluded that antibodies Rb 101-IgG-anti-mCLMP$_{ex}$ and Rb 102-IgG-anti-mCLMP$_{ex}$ are indeed able to specifically recognise CLMP in transfected cells, but are not suited for CLMP expression analysis in neither primary cell cultures nor cryosections. Given that Western analyses revealed expression of CLMP in membrane fractions brain tissue, but such expression could not be detected by equivalent immunostainings, the data suggest that CLMP expression might be too weak to be detected by cryosections and instead subcellular fractionation of protein lysates sufficiently enriched CLMP protein amounts for detection by Western blots.

TABLE 7. Immunofluorescence stainings of different tissues and stages using antibodies Rb 101-IgG-anti-mCLMP$_{ex}$ and Rb 102-IgG-anti-mCLMP$_{ex}$.

Staining	Tissue	Plane	Stage
primary cell cultures	cerebral cortex	-	E 15, DIV 5; DIV 7
C57BL/6N	hippocampus	-	E 15, DIV 7
cryosections	embryo	sagittal	E 15
C57BL/6N	whole brain	sagittal	E 16; E 18; P 1
	whole brain	coronal	P 1
	cerebellum	sagittal	P 2; P 15; adult
cryosections	embryo	sagittal	E 15
Clmp$^{+/+}$ and/or *Clmp*$^{+/-}$ vs. *Clmp*$^{-/-}$	abdomen	transverse	E 18
	urinary tract	transverse	P 0
	whole brain	sagittal	P 0
	duodenum	cross	P 0

5.8 Expression analysis of CLMP protein and transcript in urinary tract

5.8.1 Western blot expression analysis

Since previous antibody tests revealed that Rb 6504-AP-anti-mCLMP$_{cyt}$ was the only purified antibody suitable for expression analyses, this antibody was used to investigate CLMP expression in membrane fractions of kidney, ureter, and urinary bladder at various stages. Unfortunately, no 46 kDa bands could be detected in Western blots of these samples, while simultaneous stainings with reference protein E-cadherin ruled out the possibility that failed detection was due to a fault during protein purification procedures (not shown). The inability of CLMP detection in samples of urinary tract raised the question whether CLMP was indeed expressed in these tissues. As expression could not be analysed on protein level, investigation of *Clmp* transcript expression was conducted to obtain better detection sensitivity.

5.8.2 RT-PCR expression analysis

The detection of gene transcripts by RT-PCR is a highly sensitive technique that was used to definitely answer the question whether *Clmp* was weakly or not at all expressed in developmental stages of the urinary tract. Kidneys, ureters, and urinary bladders from C57BL/6N animals at E 15, P 0, P 7, P 30, and P 60 were dissected rapidly, but as precisely as possible to avoid contamination from undesired tissue. Total RNA of these tissues were purified and the mRNA was reverse-transcribed using Oligo(dT)$_{18}$ primers. A comparable amount of resulting cDNA was tested for *Clmp* transcript by designing specific exon-exon overlapping primers and cDNA integrity was verified by concurrent analysis of *Actb* expression (FIGURE 32). RT-PCR analysis revealed *Clmp* expression in the urinary tract. In the kidney, *Clmp* was found primarily in early developmental stages (E 15, P 0, P 7), whereas *Clmp* expression declined at later stages P 30 and P 60 (FIGURE 32). Ureteral *Clmp* expression was detected in all tested stages, similarly to the urinary bladder. Although comparing the ratios of *Clmp* and *Actb*

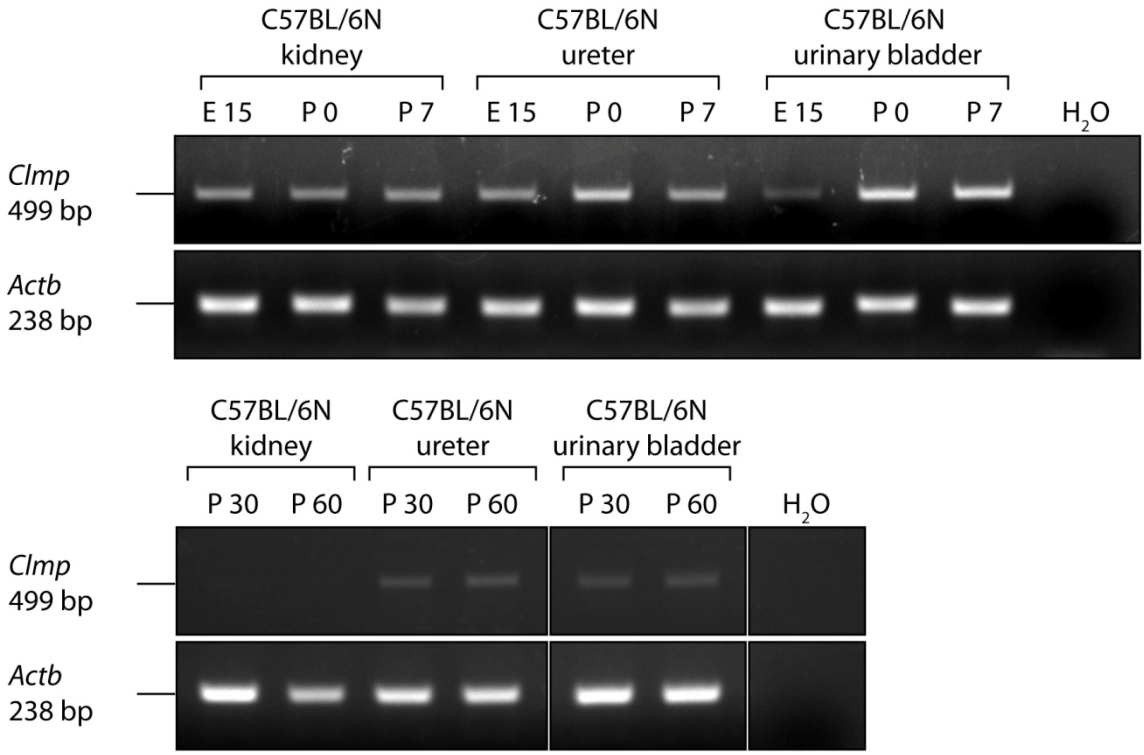

FIGURE 32. Reverse transcription-PCR analysis of *Clmp* expression in murine urinary tract. Comparable cDNA amounts were used as template for amplification of *Clmp* and *Actb* transcripts in kidney, ureter, and urinary bladder samples from E 15, P 0, P 7, P 30, and P 60 old C57BL/6N mice. A reaction sample with H_2O instead of cDNA served as negative control. *Clmp* was expressed throughout the development in ureter and urinary bladder, whereas the kidney expression was restricted to earlier developmental stages. Compared to *Actb* reference, *Clmp* was rather weakly expressed in urinary tract.

band intensities gave the impression that *Clmp* might be more strongly expressed in early developmental stages as compared to later stages, this RT-PCR was not suitable for quantitative analyses. Nonetheless, this RT-PCR approach was able to validate *Clmp* expression in the urinary tract, though the direct comparison of *Clmp* band intensities to *Actb* references suggests that *Clmp* is indeed a weakly expressed gene. Database entries proposed that *Clmp* might be expressed by more than one transcript. Additionally to the published sequence with the accession number NM_133733.4, the two transcript variants X1 and X2 (XM_006510602.1 and XM_006510603.1, respectively) have been predicted by automated computational analysis. As the primers used for previous RT-PCR experiments also bind to X1 and X2 sequences, all three transcript variants might have been detected in RT-PCR. To investigate expression of putative transcripts X1 and X2, primers specific to either the original *Clmp* transcript, the predicted variant X1 or the variant X2 were designed and used for amplification of ureter cDNA of P 60 C57BL/6N mice (FIGURE 33). An annealing temperature gradient was performed in order to offer different primer binding conditions. However, only the original *Clmp* transcript could be amplified, but not either of the predicted transcripts. Taken together, this RT-PCR approach suggests that the predicted *Clmp* transcripts X1 and X2 are not expressed at least in the ureters of adult animals.

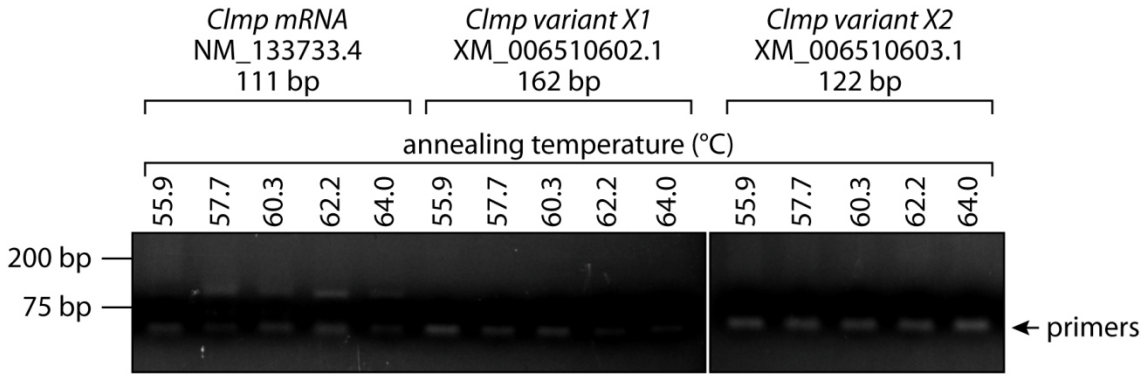

FIGURE 33. No ureteral expression of predicted X1 or X2 *Clmp* transcript variants.
Clmp expression in P 60 C57BL/6N cDNA was examined using transcript-specific primers at different annealing temperatures. While appropriate 111 bp fragments of the original *Clmp* mRNA were amplified, no amplicons of neither predicted variants (X1, 162 bp; X2, 122 bp) could be observed.

5.8.3 *In situ* hybridisation expression analysis

RT-PCR analyses revealed expression of *Clmp* in the urinary tract at various developmental stages. Unfortunately, this method does not provide information about the cellular localisation of *Clmp*. For further investigation of the murine phenotype caused by the loss of CLMP, it is, however, required to uncover the cell types expressing *Clmp* in the urinary system. Since its expression on protein level could not be analysed on tissue sections as generated antibodies were either not sensitive enough or CLMP expression was too weak for immunodetection (sections 5.7.2.2), the remaining technique to answer the essential expression profile was *in situ* hybridisation. *In situ* hybridisation is a common technique to histologically analyse mRNA expression by hybridisation of labelled riboprobes to complementary transcripts in tissue sections.

Thus, a first step was to design riboprobes that complementarily bind the *Clmp* transcript. The published *Clmp* mRNA, whose expression was verified in urinary system (section 5.8.2), contains 2,929 bp and consists of seven exons. The coding sequence reached from a rear part of exon 1 up to the beginning of exon 7, leaving a 371 bp long 5´non-coding region and an even longer 3´non-coding tail with 1,436 bp. The riboprobe used in this study was already published by Allen Brain Atlas (www.brain-map.org, riboprobe ID RP_080603_02_C03) and was designed to hybridise to a sequence covering the coding region in exons 6 and 7 and a part of the 3´non-coding region and had an overall length of 731 bp (FIGURE 34).

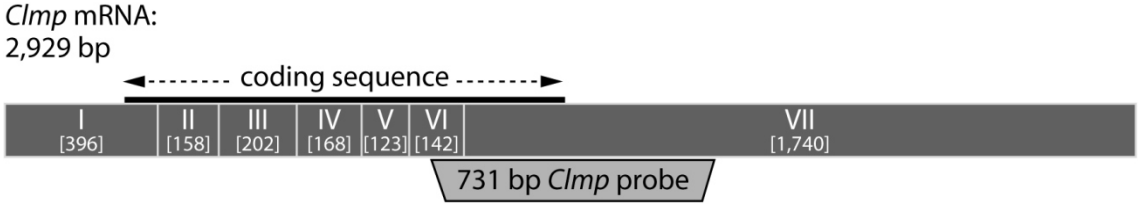

FIGURE 34. Localisation of riboprobe binding site on *Clmp* transcript.
The 731 bp *Clmp* riboprobe hybridises to a sequence spanning parts of exons 6 and 7 and the coding region and the 5‘ non-coding region. Numbers in brackets indicate exon sizes in base pairs.

Two variants of *Clmp* riboprobes were generated. First, an antisense sequence was produced that was complementary to and thus hybridised with the *Clmp* mRNA. In addition, a sense riboprobe was generated that was identical to the mRNA sequence and thus was not able to hybridise to the transcript and served as negative control. Both antisense and sense riboprobes were labelled by digoxigenin (DIG) during *in vitro* transcription. Labelling procedures were monitored in dot blot analyses by comparison to purchased DIG-labelled control RNA (FIGURE 35).

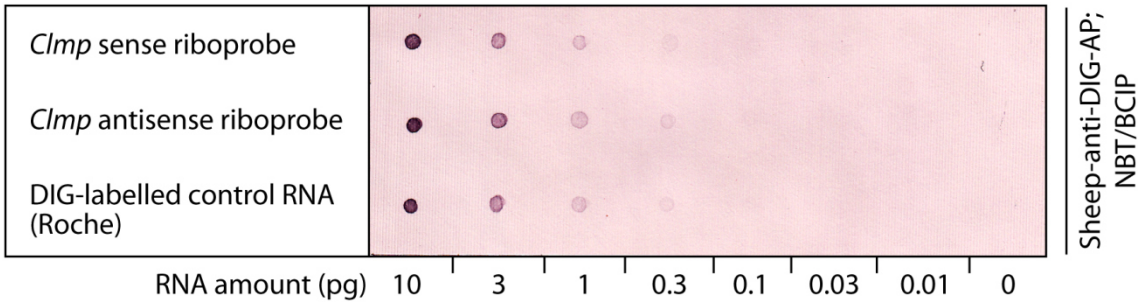

FIGURE 35. Dot blot control of riboprobe DIG labelling.
Serial dilutions of DIG-labelled probes were spotted on positively charged nylon membrane and detected by NBT and BCIP. Comparison to purchased DIG-labelled control RNA revealed successful DIG labelling.

After testing correct labelling of riboprobes, the probes were used for *in situ* hybridisation. Tissue cryosections were prepared from brains and urinary tracts of $Clmp^{+/+}$ and $Clmp^{-/-}$ at early postnatal stages P 0 till P 1. Brain sections were included as positive control since previous Western experiments validated the expression of CLMP protein at these stages (section 5.7.2.1), whereas sections from *Clmp* mutants served as negative control. All tissue sections were hybridised with antisense and sense riboprobes for double checking, expecting only positive results in cryosections from $Clmp^{+/+}$ mice hybridised with *Clmp* antisense probe, whereas all sections hybridised with *Clmp* sense probe and all sections from *Clmp* knockout mice should not produce any staining. Several attempts of *in situ* hybridisation were undertaken during this study, but unfortunately most of them led to unspecific stainings. For instance, the use of coverslips during hybridisation as well as tissue pretreatments without chloroform or with proteinase K digestion produced unspecific signals, which became apparent by staining of sections hybridised with sense probes or obtained from knockout mice (not shown).

Among the series of hybridisations, only the last one showed promising results. In this last attempt, hybridisation with *Clmp* antisense probe generated a weak, but distinct staining in wild type P 0 brain sections, whereas CLMP-deficient brain sections were not stained (FIGURE 36). Furthermore, hybridisation with the sense probe left clean sections without signals (not shown), supporting the impression that the hybridisation conditions used in this attempt delivered specific signals.

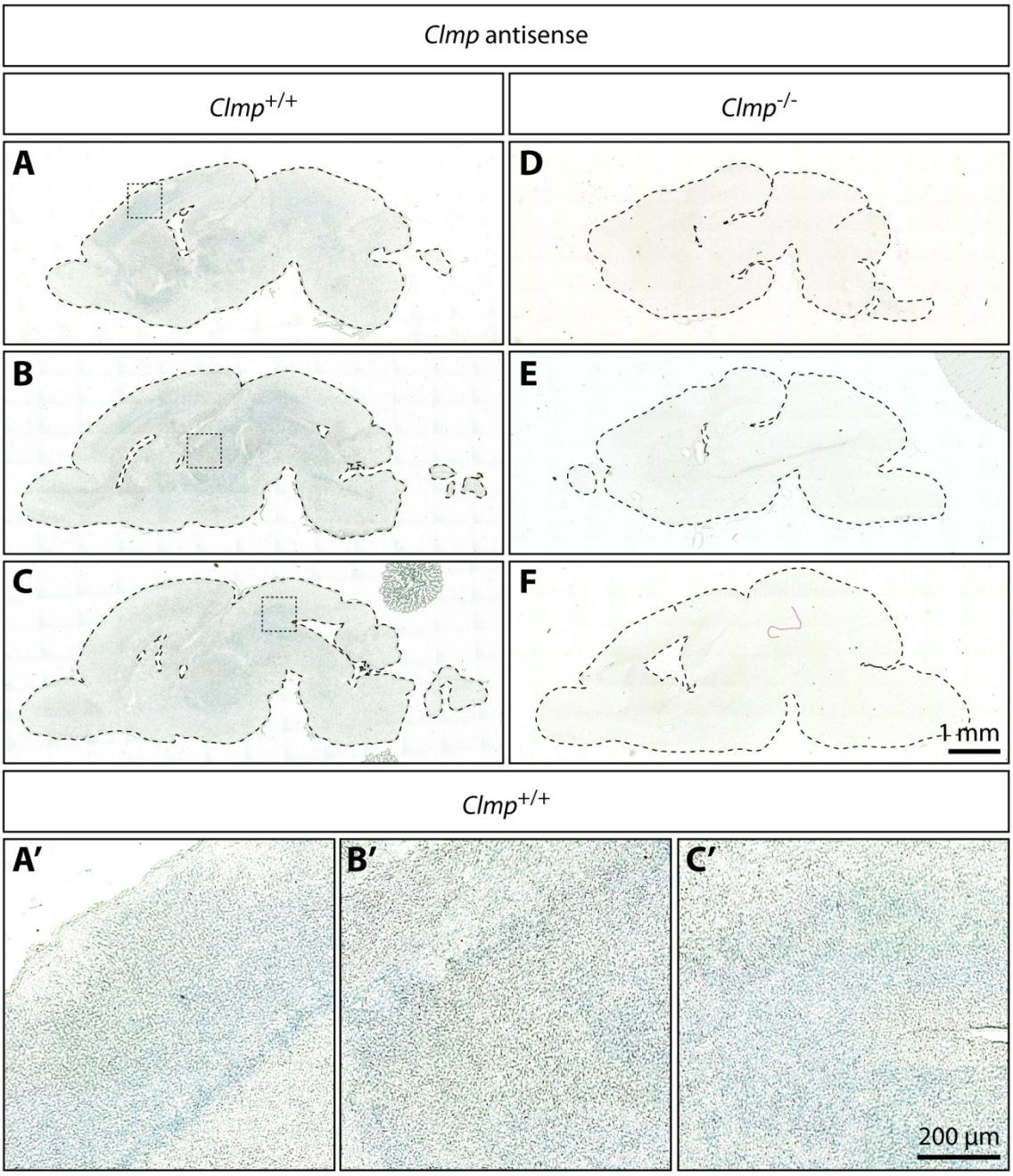

FIGURE 36. *In situ* hybridisation of sagittal brain sections.
Brain cryosections obtained from newborn (P 0) *Clmp* wild type and knockout mice were hybridised with *Clmp* sense probe (no signals, not shown) and *Clmp* antisense probe. The antisense probe specifically stained brain regions in wild type sections (A, B, C, and detailed views A', B', and C'), whereas no signals were observed in mutant sections (D, E, F).

Simultaneous with the brain sections, transverse cryosections covering the kidneys and ureters from newborn pups were also hybridised under the same conditions. Wild type and knockout tissues were hybridised with both sense and antisense probes. However, none of the hybridised sections showed any staining, instead all sections were left clean (FIGURE 37, sections with sense probe not shown). While the clean sections hybridised with sense probe and sections obtained from mutant mice were as expected, the wild type sections hybridised

with *Clmp* antisense probe were contrarily expected to expose *Clmp* expression in the urinary tract. Thus, there is a discrepancy as the antisense hybridisation on brain sections produced a specific-looking staining which was absent in urinary tract cryosections. Please note that the hybridisation results presented here (FIGURE 36 and FIGURE 37) derived from only one trial of *in situ* hybridisation. It is therefore not noteworthy to mention that the results obtained in this single experiment have to be repeated. However, since a lot of *in situ* hybridisations with altered conditions have been tried yet to achieve specific stainings, this last trial might after all prove that the generated DIG-labelled riboprobes are indeed able to produce specific stainings (at least in brain sections) and that further attempts using the generated probes are not only required but worth trying out further in order to finally reveal *Clmp* expression in the urinary tract.

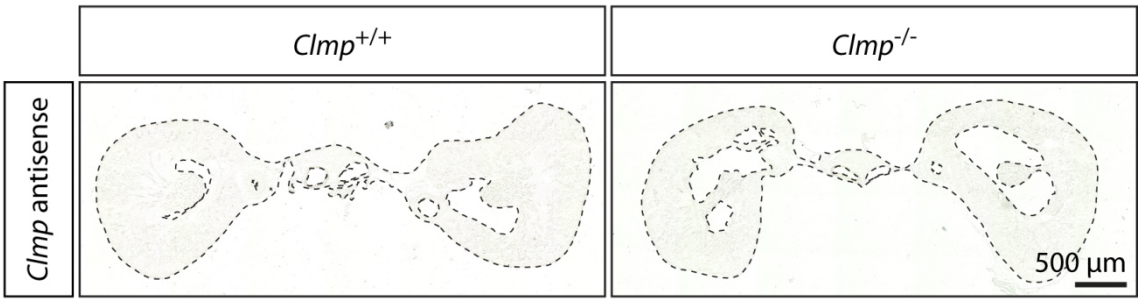

FIGURE 37. *In situ* hybridisation of transverse urinary tract sections.
Transverse cryosections of urinary tracts from *Clmp*$^{+/+}$ and *Clmp*$^{-/-}$ newborn pups were hybridised with *Clmp* sense riboprobe (no staining, not shown) and *Clmp* antisense riboprobe. Mutant antisense sections remained clean after the staining procedure as expected. Contrary to the staining signals obtained in brain sections, hybridisation with *Clmp* antisense probe did not produce any visible staining in wild type urinary tract sections.

6 DISCUSSION

CLMP is an IgCAM whose biological function has not been entirely unravelled yet despite several studies stating that CLMP localises to intercellular contact sites, mediates cell-adhesive functions, and is implicated in obesity, ovulation and the gastrointestinal disease CSBS (Hida *et al.*, 2000; Raschperger *et al.*, 2004; Eguchi *et al.*, 2005; Sze *et al.*, 2008*a*; Van der Werf *et al.*, 2012; Li *et al.*, 2014). This study aimed at shedding light on the functional role of murine CLMP by analysing the global absence of CLMP in a constitutive *Clmp* knockout mouse model and by investigating the phenotype-associated expression pattern of CLMP.

6.1 Deletion of *Clmp* results in multiple phenotypes

At the beginning of this study, no mouse models with constitutive or conditional deletions of *Clmp* were available. Therefore, the generation of a mouse model lacking CLMP might provide substantial insight into the function of CLMP in a living organism. In this study, a constitutive *Clmp* knockout mouse line was established by genetic targeting of the start codon-containing first exon of the *Clmp* gene. Technically, electroporation of the targeting vector into ES cells enabled the replacement of *Clmp* exon 1 by a *loxP*-flanked *Neo* cassette by homologous recombination. The homologous recombination of targeting vector and genome was verified by Southern blot analysis in ES cells prior to blastocyst injection. In the mouse, the deletion of *Clmp* was validated at genomic, transcript and protein levels (section 5.1). Phenotypic analysis of the CLMP-deficient mouse revealed a delay in body growth and a poor postnatal survival rate as compared to wild type and heterozygous littermate controls (section 5.2). In addition, dissections of *Clmp*$^{-/-}$ mutants uncovered gastrointestinal and renal anatomic abnormalities (sections 5.3.2 and 5.3.3). Further research was focused on the renal phenotype associated with peristaltic defects in the urinary system (sections 5.4, 5.5, and 5.6). On the basis of this autosomal recessive phenotypic diversity and significance, Online Mendelian Inheritance in Man (OMIM; http://omim.org) database and literature were screened for already known human diseases and syndromes, which cover the combination of the multiple phenotypes observed in *Clmp*$^{-/-}$ knockout mice. However, database queries and literature searches have not detected any diseases or syndromes that match exactly the concurrent impairments of growth, survival, gastrointestinal and urinary tract phenotypes of CLMP-deficient mice, which might indicate a genetic redundancy of CLMP, or a rare, yet unpublished or early lethal disorder in humans. In the following sections, the results obtained in this study are discussed in the context of relevant published literature.

6.2 Delayed body growth, high mortality and a putative link to abnormalities in the gastrointestinal tract

During postnatal development, CLMP-deficient animals had difficulties in gaining body weight and in survival (section 6.2). This is a very dominant phenotype that limits further phenotypic analyses since the majority of *Clmp*$^{-/-}$ animals dies early after birth and only 15-30 % of knockout mice survive until adulthood (FIGURE 8). The reduction in body weight and the high mortality rate are consistent with the observation that heterozygous-to-heterozygous matings did not recover the expected Mendelian ratio of 25 % weaned *Clmp* mutant mice. While at birth about 18 % of neonates were of *Clmp*$^{-/-}$ genotype, after three weeks of life only about 7 % of weaned animals were *Clmp* knockouts (TABLE 3), indicating that mortality primarily occurs at early postnatal stages. Surviving juvenile and adult *Clmp* knockout animals were used for experiments, however, the question arises whether these mutants survived due to less severely developed phenotypes and/or a spontaneous resolve of phenotypic symptoms. For instance, the body weight of surviving CLMP-deficient mice approached the weight of wild type and heterozygous littermates up to a non-significant level from P 84 on (FIGURE 11). Thus, it might be possible that surviving mice are able to somehow compensate the loss of CLMP, which usually leads to early postnatal death in the majority of animals, by yet unknown mechanisms. Therefore, results obtained in these juvenile and adult survivors should be interpreted on a basis of such a compensational potential. Importantly, another constitutive knockout mouse model of *Clmp* has been generated in the course of a large scale knockout screen, which confirmed a decreased body weight and reduced viability in homozygous *Clmp* mutants (Tang *et al.*, 2010). Unfortunately, the phenotypic observations were not investigated further in this study. After all, it is certain that CLMP displays an essential factor for murine development and survival.

To date, it can only be speculated about the underlying cause of body growth delay and poor survival of *Clmp*$^{-/-}$ mice. It might initially be suggested that the development of bilateral hydronephrosis causes this phenotype in *Clmp* mutants. Onset of bilateral hydronephrosis could be observed as early as embryonic stage E 18. In neonates, the dilation of renal pelvises rapidly increased (FIGURE 16 and FIGURE 17). How much such fast hydronephrotic development affects body growth and by which degree such defect might cause lethality in neonates remains to be determined. However, very severe dimensions of hydronephrotic kidneys resembling fluid-filled balloons with a only a very thin renal parenchyma were found in surviving juvenile and adult *Clmp* knockout animals (FIGURE 15), indicating that survival might not be compromised despite this severity and other reasons than hydronephrosis might account for impairments in body growth and survival.

Many genetically targeted mouse models have been reported to challenge similar problems with body growth and survival and the reasons can be very diverse and complex (Turgeon & Meloche, 2009). In both *Clmp* strains, abnormal suckling behaviour, one of the primary explanations for early postnatal lethality, can be ruled out since all knockout pups showed

stomachs filled with milk comparably to wild type and heterozygous littermates (FIGURE 10). The observation of milk-filled stomachs in *Clmp* mutant pups, though, does not exclude the possibility that these pups have nutritional problems. After intake, food is converted into chyme in the stomach, and passage through the pylorus, a contractile muscular junction between the stomach and the small intestine, is required for the chyme to arrive at the intestine for further digestion and nutrient absorption. On the background that homozygous *Clmp* lethality primarily emerges from the day of birth on and foetal nutrition by placenta and umbilical cord is replaced by gastrointestinal tract function in neonates, defects in pyloric function, enteric peristalsis and/or nutrient absorption might account for impaired body growth and postnatal lethality.

Since ureteral explants revealed impaired peristaltic contractions in the *Clmp* mutants (section 5.6), it might be suggested that a similar defect might be present in the gut peristalsis. Recent preliminary experiments carried out in Dr Andreas Friebe's laboratory at the University of Würzburg analysing intestinal peristalsis in $Clmp^{+/+}$ (n = 2) and $Clmp^{-/-}$ (n = 2) pups did not reveal apparent differences in spontaneous and evoked contractility and relaxation in duodenum and colon. In the stomach fundus and corpus, similar recordings did not reveal contractile abnormalities, either (Dr A. Friebe, data not shown, personal communication). Interestingly, Dr Friebe identified a pyloric stenosis associated with absence of milk in the gut in the two analysed CLMP-deficient pups, which means an obstruction of the pyloric lumen and in turn hindrance of chyme to pass from stomach to duodenum. In fact, in some dissections of $Clmp^{-/-}$ neonates used for other experiments in this study, a dark green-coloured viscous mass had been observed at different regions within the gut lumen (figures not shown), indicating difficulties in excretion of the first stool, namely meconium. In addition, the duodenal lumens of neonate dissections turned out to be yellowish in some *Clmp* knockouts instead of being white in colour due to the presence of milky chyme as found in wild type and heterozygous littermates (figures not shown). Although further investigations are required to determine whether a pyloric stenosis is indeed present in all *Clmp* mutants, pyloric stenosis might represent a possible explanation for the delay in body growth and early postnatal mortality in CLMP-deficient animals due to inability to absorb nutrients and, in turn, starvation and dehydration.

Pyloric stenosis is the key pathologic condition in the pathogenesis of infantile hypertrophic pyloric stenosis (IHPS) whose complex aetiology involving genetic and environmental factors has not been completely identified yet. IHPS neonate patients present with projectile postprandial vomiting symptomatic of gastric outlet obstruction in the first weeks of life and require surgical intervention or alternatively atropine therapy to avoid electrolyte and acid-base imbalances and dehydration (Ranells *et al.*, 2011; Peeters *et al.*, 2012). If the deletion of *Clmp* indeed causes pyloric stenosis, it will be interesting and necessary to determine whether *Clmp* might be a potential candidate gene of the congenital IHPS disease.

6.3 The constitutive *Clmp* knockout mouse strain might not be a suitable model for CSBS

Recently, mutations in *CLMP* have been described to be implicated in an autosomal recessive form of CSBS (Van der Werf *et al.*, 2012). Seven CSBS patients from five families have been reported to carry different point mutations or deletions in the gene encoding CLMP that have not been found in healthy individuals. Three patients possessed single homozygous point mutations in either exon 3 or exon 5, leading to either missense or nonsense transcripts. Another patient was compound heterozygous with a paternal frameshift mutation causing a stop codon in exon 3 and a maternal splice site mutation probably resulting in exclusion of exon 6 during transcription. Furthermore, three patients had homozygous deletions in either intron 1 or exon 2 (Van der Werf *et al.*, 2012). All of the described *CLMP* mutations were assumed to result in a loss of function of CLMP. Indeed, for the one homozygous nonsense point mutation it has been shown that surface expression is abrogated in CHO and T84 cells transfected with this mutant *CLMP* cDNA (Van der Werf *et al.*, 2012). The described point mutations and deletions in the *CLMP* gene in humans might represent a functional knockout of *CLMP*, however it remains to be determined which precise impact the mutated transcripts and putatively translated mutated proteins have on the organism and whether this resembles a complete deletion of *CLMP*. To date, effects on the gastrointestinal tract by loss or mutagenesis of CLMP have not been reported in mammalian model organisms. A knock-down of *clmp* in zebrafish has been the only attempt to study the role of CLMP in CSBS *in vivo* (Van der Werf *et al.*, 2012). Lack of CLMP resulted in a developmental delay with a significant reduction in body size. The intestine length in the zebrafish *clmp* morphants was also reduced, however this shortened gut size was proportional to the overall smaller body length. Despite the gut length inconsistency among the zebrafish morphants and CSBS patients, the authors stated some similarities between the CLMP zebrafish model and the clinical CSBS phenotype due to a lack of goblet cells in the zebrafish midintestine, which is supposed to resemble the human small bowel (Van der Werf *et al.*, 2012).

In order to evaluate whether the deletion of *Clmp* in the mouse results in a CSBS-like phenotype, a closer look was taken at the gastrointestinal tract in CLMP-deficient mice and their wild type and heterozygous littermates. Weight analyses revealed a highly significantly increased wet weight of dissected entities of stomach and whole intestine in adult *Clmp*$^{-/-}$ animals as compared to control littermates (TABLE 5). The significance continued after normalisation to the body weight and to the body length of the respective dissected animal (TABLE 5). As CSBS patients present with a significantly shorter small intestine, the length of the intestines in adult mice was measured after dissection. Unexpectedly, but consistent with the heavier weight of stomach and intestine, the length of the small bowel and the large bowel were even longer in *Clmp* mutant animals as compared to control littermates. The increase in gut length was significant when normalised to the body length of the animals. Furthermore, the proportions of small intestine to large intestine were not altered in CLMP-deficient mice

(FIGURE 13). Although it is still unclear why the intestine in *Clmp* mutant mice is elongated, this observation is in contrast to the reported zebrafish *clmp* morphants having a reduced gut length, which was proportional to the overall zebrafish length (Van der Werf *et al.*, 2012). Taken together, these results show that the ablation of *Clmp* in the mouse does not reproduce the characteristic pathogenic condition of CSBS, the reduction in small bowel length, and thus adult constitutive *Clmp* knockout animals may not be a suitable model for analysis of CSBS.

Why there are such opposing impacts in human CSBS patients with *CLMP* mutations and mice constitutively lacking CLMP remains to be determined but different approaches of explanation might be reasonable. First of all, it might be tempting to speculate that there simply are differences among the species, as has been shown for CLMP orthologue expression in heart and brain with high abundance in the mouse but low expression in humans (Raschperger *et al.*, 2004; Eguchi *et al.*, 2005). In fact, expression of CLMP in the murine small intestine has not been proven yet except for one oligonucleotide microarray study, which analysed transcriptomes of interstitial cells of Cajal (ICC) in murine small intestine and detected *Clmp* to be differentially expressed in ICC of the deep muscular plexus (ICC-DMP; Chen *et al.*, 2007). Intramuscular ICC-DMP have been reported to establish synaptic contacts with nerve terminals of enteric motor neurons and thereby mediate intestinal motor function (Wang *et al.*, 2003; Iino *et al.*, 2004; Ward *et al.*, 2006). ICC-DMP of the small intestine in the mouse arise from enteric smooth muscle cells between postnatal days P 0 and P 10 and loss of ICC-DMP is associated with slower small bowel transit (Ward *et al.*, 2006; Kondo *et al.*, 2015). To which degree a loss of CLMP might influence ICC-DMP function and whether a dysfunction of ICC-DMP would result in a reduction of small bowel length is unclear. Preliminary experiments analysing bowel motility in neonates did not reveal differences between homozygous *Clmp* mutants and control littermates (Dr A. Friebe, personal communication; section 6.2), but at these early postnatal stages ICC-DMP differentiation is not yet completed (Ward *et al.*, 2006).

As a second approach, discrepancies between the complete knockout of *Clmp* in mice and the nature of mutations in human *CLMP* might serve as explanation for the differences in gut length. The genetic targeting of *Clmp* in mice in this study utilised the deletion of the *Clmp* start codon and thus leads to the prevention of translation of *Clmp* mRNA, resulting in a complete loss of CLMP. In contrast, the mutated transcripts of *CLMP* in CSBS patients resulting from point mutations or from larger sequence deletions might not only entail a loss of CLMP function but instead have additional negative effects on expressing cells. The mutated *Clmp* transcripts might not be completely degraded but might give rise to misfolded proteins with cytotoxic impacts as has been described for instance for amyloid deposits caused by protein misfolding (Stefani, 2008).

Finally, the contradictions in small bowel length among *CLMP*-associated CSBS patients and adult *Clmp* knockout mice might also be explained on the background of a compensatory effect of adult surviving mice. As outlined in section 6.2, CLMP-deficient animals display high postnatal lethality with only few mice surviving up to adulthood. Although the cause of the

enormous mortality rate remains to be determined, it might be hypothesised that mutant animals might survive due an unknown compensatory mechanism and therefore do not show apparent phenotypes in the gastrointestinal tract. In order to clarify this, a putative compensation has to be circumvented by using mice with conditional intestine-specific ablation of *Clmp* or by analysing earlier developmental stages in the constitutive *Clmp* knockout line. The murine intestine matures postnatally by the epithelial morphogenesis of the mucosal gut surface (Spence *et al.*, 2011; Noah *et al.*, 2011), but functional gut motility can be already observed perinatally (Burns *et al.*, 2009). Thus, for using the global *Clmp* mutant strain, it might be advised to investigate gut lengths during late embryonic and neonatal development to better conclude whether the loss of CLMP in the mouse indeed does not cause a CSBS-like reduction in small bowel length.

In CSBS patients, the short small intestine is accompanied by malrotation of the gut. It is not clear yet, whether malrotation is an independent phenotype or a secondary effect caused by the decrease in gut length, as intestinal elongation and rotation processes are connected (Martin & Shaw-Smith, 2010; Van der Werf *et al.*, 2015). In surviving juvenile or adult *Clmp*$^{-/-}$ mice, a disorganised arrangement of the intestine could be observed (FIGURE 14), although no statistical analysis about the frequency was performed. It was not determined whether this observation indeed represents intestinal malrotation, thus it might be of interest to examine this further. However, the observed disorganised bowel architecture might simply be a consequence of a displacement by the highly hydronephrotic kidneys in older mutant animals. Analysis of the dissected gastrointestinal tracts of adult *Clmp* knockout mice also revealed a dilation of the duodenum in 100 % of the preparations (FIGURE 13 and FIGURE 14). This finding was not studied further, therefore it remains to be elucidated, whether the duodenal lumen is expanded or the duodenal wall is thickened. In the literature, cases of duodenal dilations have been reported to be a result of compression of the duodenum by for instance the third lumbar vertebra or a peritoneo-mesocolic band (Summers, 1928). Likewise, it might be possible that the disorganised gut arrangement exerts pressure to one site of the duodenum which in turn leads to the dilation of duodenal regions above the compression site. Therefore, analysis of gut disorganisation in CLMP-deficient neonates, which do not display a severe degree of hydronephrosis as in adults, or in conditional *Clmp* lines will clarify whether ablation of *Clmp* leads to gut malrotation and/or a congenital duodenal dilation independent from the urinary tract phenotype.

In conclusion, the bowel pathology in CSBS patients caused by single mutations in the *CLMP* gene, including two different homozygous point mutations, one compound heterozygous condition and two different homozygous sequence deletions, could not be transferred to adult *Clmp* knockout mice used in this study. It might be likely that the CSBS-associated shortening of the small bowel is not due to a loss of CLMP function but instead to a cytotoxic effect of misfolded mutated CLMP protein. However, it is still possible that CSBS-like phenotypes might be found in early postnatal stages, but further research is required to determine this. A bowel-

specific conditional deletion of *Clmp* could reliably shed light on the question, whether CLMP is implicated in CSBS-like pathologic conditions in the mouse. Taken together, the constitutive knockout of *Clmp* in the mouse strains of this study might not be a suitable model for CSBS.

6.4 Deficiency of CLMP manifests in bilateral hydronephrosis caused by impaired ureteral peristalsis

Dissections of juvenile and adult animals uncovered a very severe malformation of the urogenital system in both genders of CLMP-deficient mice (section 5.3.3). In contrast to wild type and heterozygous littermates, 100 % of *Clmp* mutants displayed a high degree of bilateral hydronephrosis (FIGURE 15), a pathologic condition that is characterised by a distention of the renal pelvis and calyces due to consecutive urine accumulation (Woolf, 2000; Rasouly & Lu, 2013). This kidney phenotype is in line with observations in a constitutive *Clmp* knockout mouse model published in a large scale knockout screen, which discovered bilateral hydronephrosis in homozygous *Clmp*$^{-/-}$ mice by necropsy and computer tomography scans, but did not analyse this further (Tang *et al.*, 2010). In the present study, also the complete reproductive tracts in both females and male knockout animals appeared maldeveloped (FIGURE 15), which likely explains the inability of homozygous mutants to produce offspring (TABLE 4).

Because of the severity of bilateral hydronephrosis caused by the lack of CLMP in mice and its associated clinical significance, hydronephrosis was set in focus of phenotypic analyses in *Clmp* strains. Therefore, developmental defects in the reproductive system were not characterised further and instead investigations concentrated on the determination of onset and underlying mechanisms of bilateral hydronephrosis in *Clmp* mutant mice. The onset of the renal abnormality was traced back to early murine development, with symptoms of pelvic dilation detected as early as embryonic day E 18, as shown by kidney sections or intrapelvic dye injections (FIGURE 17 and FIGURE 20). This embryonic onset indicates that the hydronephrotic phenotype might develop independently and might not be a secondary effect caused by malnutrition due to abnormalities of the gastrointestinal tract, since the foetal nutrition is operated by placenta and umbilical cord, and the nutritional function of stomach and intestine becomes essential not before birth. After onset, bilateral hydronephrosis aggravated rapidly within days by extensive dilation of the pelvis and calyces, accompanied by thinning of renal parenchyma (FIGURE 16 and FIGURE 17). This thinning might indicate tissue atrophy and is consistent with the detection of elevated levels of the kidney injury marker NGAL in urine samples of *Clmp*$^{-/-}$ mice (FIGURE 19; Singer *et al.*, 2013). Though, the hydronephrotic parenchyma likely still contains enough nephrons and collecting duct systems to be functional, since urinary parameters including electrolytes, glucose, urea, protein, and pH obtained from surviving adult CLMP-deficient mice with a massive degree of bilateral hydronephrosis were not significantly different from those of wild type and heterozygous littermates (FIGURE 18). Thus, the homeostatic function was not affected in hydronephrotic kidneys, suggesting no

gross impairment in renal filtrative, reabsorptive and secretory processes. As the development of highly severe bilateral hydronephrosis in adult mutant animals did not interfere with their survival, it might be suggested that this renal phenotype is not the main cause of early postnatal lethality in *Clmp* knockout mice (FIGURE 8 and TABLE 3).

Since renal physiology appeared to be unaffected by the lack of CLMP, the question arised which mechanisms might account for the generation of hydronephrosis. The fact that hydronephrosis in CLMP-deficient mice develops to 100 % as bilateral condition and rapidly aggravates postnatally indicates a congenital defect that is likely due to failures in the development of the urinary system. In humans, foetal hydronephrosis is frequently diagnosed by prenatal ultrasonography. Information on prevalence of antenatal hydronephrosis varies widely among the studies, for instance Lee *et al*. report a frequency of 1-5 % of all pregnancies (Lee *et al.*, 2006), while Garne and colleagues specify the prevalence of prenatally diagnosed hydronephrosis with 8.4 cases out of 10,000 births among European countries (Garne *et al.*, 2009). Although many cases of diagnosed antenatal hydronephrosis occur unilaterally and spontaneously resolve after birth, persisting hydronephrosis may result in clinical significance (Lee *et al.*, 2006; Rasouly & Lu, 2013). Hydronephrosis is usually reported to be a cause of obstructed urine outflow. Sites of obstruction mainly include the junction between kidney and ureter, which is called the ureteropelvic junction (UPJ), the ureter and the connection between ureter and urinary bladder, namely the ureterovesical junction (UVJ; Becker & Baum, 2006; Chen, 2009; Rasouly & Lu, 2013). Obstructions at these sites can emerge from physical barriers by ureteral stones or due to developmental defects during kidney and ureter formation or fusion of the ureter to the urinary bladder.

In order to assess whether bilateral hydronephrosis was the outcome of physical obstruction, kidneys of $Clmp^{+/+}$, $Clmp^{+/-}$ and $Clmp^{-/-}$ animals were intrapelvically injected with ink and the ability of the dye to pass forward to the urinary bladder was monitored. Surprisingly, ink propagation was not compromised in CLMP-deficient urinary tracts, indicating no physical barriers at the UPJ, the ureter and the UVJ due to developmental malformations (FIGURE 20). Therefore, urine accumulation in the mutant renal pelvis was hypothesised to be a consequence of a functional defect. Urine is actively propelled towards the urinary bladder via the ureter and dysfunctions of ureteral contractility have been associated with hydronephrotic phenotypes. The ureter is a tube composed of an outer smooth muscle layer, an intermediate stromal cell layer and an inner epithelium, which is also known as urothelium. Smooth muscle function is crucial for ureteral contractility, whereas a contribution of ureteral stroma and urothelium to contractility have not been proven yet, although targeting of genes expressed in these stromal and urothelial layers have been reported to result in hydronephrosis (Hu *et al.*, 2000; Yu *et al.*, 2002; Chang *et al.*, 2004; Kong *et al.*, 2004; Airik *et al.*, 2006, 2010; Mahoney *et al.*, 2006; Caubit *et al.*, 2008; Cain *et al.*, 2011; Tripathi *et al.*, 2012; Yan *et al.*, 2014). In the absence of CLMP, no gross changes in ureteral smooth muscle, stromal and urothelial layer anatomy and differentiation were observed, as indicated by immunofluorescent stainings

(FIGURE 21). The majority of analysed ureters had a normal outward appearance and only some mutant ureters were dilated at the proximal end (FIGURE 21). Furthermore, lengths of ureteral explants obtained from *Clmp*$^{-/-}$ embryos were comparable to control ureters (FIGURE 22). Although ureteral anatomy looked normal, peristaltic motility was significantly altered in ureteral *Clmp* knockout explants (FIGURE 23, FIGURE 24, supplemental VIDEOS). Wild type and heterozygous ureteral explant cultures showed normal anterograde, wave-shaped peristaltic contractions, which were directed from the proximal to the distal ureter end. In between two peristaltic waves, a refractory period was observed, and during peristaltic movements, the ureteral lumen was strongly constricted up to 60 % of the relaxation state (FIGURE 23 and supplemental VIDEOS). In contrast, the CLMP-deficient ureters did not demonstrate peristaltic waves. Instead, local sites of the ureters continuously contracted in a slow and weak manner and independently from other ureteral regions (FIGURE 23B and B', supplemental VIDEO 3). These slight contractions of mutant ureters were best visualised in fast playbacks of rapid time-lapse recordings (VIDEO 4). Consistent with impaired peristaltic contractions, cultured ureteral explants of *Clmp* knockout embryos did not exhibit Ca^{2+} waves (FIGURE 24), which are necessary for proper smooth muscle function. Taken together, these data suggest that signal propagation in ureteral smooth muscle is compromised. For further analysis of the mechanisms underlying defective peristalsis in *Clmp*$^{-/-}$ mice, information about CLMP expression in the urinary system is required. Unfortunately, several attempts trying to prove CLMP protein and *Clmp* transcript expression in cell types of the urinary tract have failed (section 5.8), therefore it might only be speculated how CLMP influences peristaltic motility in the ureter. In the following sections, impact of CLMP on ureteral peristalsis is hypothesised in the context of a putative expression of CLMP in the individual ureteral cell types.

6.4.1 Influence of CLMP on ureteral peristalsis

To date, the localisation of CLMP is unclear. In this study, CLMP expression could be shown in several stages of brain development by Western blot and *in situ* hybridisation (section 5.8) and RT-PCR analyses discovered *Clmp* transcript in kidney, ureter, and urinary bladder. Unfortunately, the CLMP-expressing cell types could not be determined. Previous studies detected CLMP in epithelial cells of several organs (Raschperger *et al.*, 2004; Sze *et al.*, 2008*a*; Van der Werf *et al.*, 2012) and gene expression atlases Gene Paint (www.genepaint.org) and Allen Brian Atlas (www.brain-map.org) confirmed *Clmp* mRNA in neural tissues. In addition, *in situ* hybridisations of embryonic mouse sections in the Gene Paint database suggest expression of *Clmp* in outer layers of intestinal tissue, which might represent the smooth muscle layer of the gut. Intestinal smooth muscle executes peristaltic contractions that are similar to those of the ureter, and gut peristalsis has been shown to be controlled by interactions of pacemaker cells known as interstitial cells of Cajal (ICC) and enteric nerves (Burns *et al.*, 2009; Huizinga & Lammers, 2009).

Time-lapse recordings and calcium imaging in ureters lacking CLMP suggests that the absence of CLMP affects the contraction apparatus since mutant ureters did not exhibit Ca^{2+} waves as

compared to control ureters. Ureteral smooth muscle executes the propagation of peristaltic waves, but peristalsis is initiated and controlled by two types of pacemaker cells located within the smooth muscle layer in the renal pelvis and to a lesser extent in the proximal ureter (Di Benedetto *et al.*, 2013). Defects in pacemaker cells and/or typical smooth muscle cells therefore might account for malfunctions of peristaltic contractions (sections 6.4.1.1 and 6.4.1.2). However, other cell types have also been reported to be able to influence ureteral peristalsis, as for instance shown by genetic targeting of specific ureteral molecules (sections 6.4.1.3, 6.4.1.4, and 6.4.1.5).

Thus, a detailed understanding of ureteral cell types and molecules controlling peristalsis is required in order to hypothesise about the basis of impaired peristalsis in CLMP-depleted ureters. In order to evaluate a putative expression of CLMP in distinct ureteral cell types, a brief overview of the ureter development is given in the following. Ureter formation commences directly after E 10.5, when an epithelial diverticulum called the ureteric bud protrudes from the nephric duct, also known as Wolffian duct, into the metanephric mesenchyme. While the tip of the ureteric bud then undergoes branching processes and initiates the formation of the metanephric kidney, the ureteric bud stalk elongates, fuses to the urinary bladder at E 12.5 and from E 13.5 to E 14.5 on forms the future ureteral urothelium, whereas the surrounding ureteric mesenchyme gives rise to ureteral adventitial fibroblasts, smooth muscle and stromal cells. Epithelial-mesenchymal interactions have been found to be essential for differentiation processes (Airik & Kispert, 2007; Bohnenpoll & Kispert, 2014). Besides, the ureter is enwrapped by periureteral adipose tissue (Killian & Bund, 2012).

Although several genes have been identified to be involved in ureteral development and function, no CAM has been reported to be associated with hydronephrosis and/or ureteral peristalsis yet. CLMP was identified as closest homologue to the IgCAM CAR and is a type I transmembrane protein with an ectodomain composed of one V-type and one C2-type Ig-like domain. Intracellularly, CLMP is predicted to exhibit a PDZ domain binding motif. CLMP has been shown to possess homophilic adhesive properties, which are likely mediated via the Ig-like domains, and to localise to intercellular contacts (Raschperger *et al.*, 2004; Eguchi *et al.*, 2005). Thus, CLMP is able to interact extra- and intracellularly with other molecules and therefore might be involved in cell adhesion and/or intercellular signalling. Apart from homophilic CLMP interactions, information about other CLMP binding partners is unfortunately not available yet, and especially the inability to determine CLMP-expressing cell types in the urinary tract only allows speculation about the link between CLMP and ureteral peristalsis.

Onset of peristaltic motility in mouse ureters is after differentiation of ureteral cell layers and is synchronised with the beginning of renal urine production at E 16.5 (Airik & Kispert, 2007; Bohnenpoll & Kispert, 2014). Cultivation of isolated ureter explants obtained from E 15 embryos for five days suggests that ureteral peristalsis at this stage is independent from neural control and literature suggests that innervation of the ureter by sensory afferent nerve fibres

has only a modulatory effect on contractile waves (Weiss *et al.*, 2006). Therefore, a contribution of nervous innervations to impaired peristalsis in explant cultures of CLMP-deficient ureters was deemed unlikely and not considered further in this section, although CLMP as neural molecule shown to be expressed in the brain might be also expressed by the nerve fibres innervating the urinary system. Peristalsis in ureteral explants furthermore occurred in the absence of renal tissue, of which pacemaker cells belonging to the renal pelvis might influence peristalsis. However, based on the isolated explant cultures, expression of CLMP in ureteral pacemaker, smooth muscle, stromal, and epithelial cell types as well as periureteral adipose tissue might be possible and the consequence of a putative CLMP expression in these cell types will be discussed in the following sections.

6.4.1.1 Putative CLMP expression in ureteral smooth muscle cells?

As outlined in section 6.4, smooth muscle function is crucial for normal ureteral peristalsis. The ureteral smooth muscle layer consists of so-called typical and atypical smooth muscle cells, the former of which form a functional syncytium by gap junctions and contain contractile filaments to execute peristaltic contractions (Santicioli & Maggi, 2000). Several mutant mouse lines have been established to investigate underlying mechanisms of smooth muscle formation and a signalling pathway has been proposed in which binding of epithelial-secreted sonic hedgehog (SHH) to its receptor Patched 1 (PTCH 1) in adjacent mesenchymal cells causes upregulation of bone morphogenetic protein 4 (BMP 4), leading to subsequent stimulation of transcription factor teashirt 3 (TSHZ 3) and activation of the smooth muscle regulator myocardin in order to trigger differentiation of mesenchymal cells to smooth muscle cells by transcription of smooth muscle contractile proteins (Lye *et al.*, 2010). Failures in this signalling pathway lead to defects in ureteral smooth muscle formation and hydronephrosis, as assessed by genetic targeting in mice (Yu *et al.*, 2002; Caubit *et al.*, 2008; Cain *et al.*, 2011). Similar phenotypes were observed by ablation of the mesenchymal T-box 18 (TBX 18) transcription factor, which acts upstream of SHH and BMP 4 (Airik *et al.*, 2006). However, a number of other molecules has also been implicated in smooth muscle formation and differentiation, including epithelial-derived Wnt 7B and Wnt 9B, mesenchymal β-catenin, transcription factor SRY-box 9 (SOX 9), SIX homeobox protein 1 (SIX 1) and calcineurin B, as well as Smad 4 and discs-large homologue 1 (DLGH 1), which are both expressed by ureteric mesenchyme and epithelium (Chang *et al.*, 2004; Mahoney *et al.*, 2006; Iizuka-Kogo *et al.*, 2007; Airik *et al.*, 2010; Nie *et al.*, 2010; Tripathi *et al.*, 2012; Trowe *et al.*, 2012; Martin *et al.*, 2013; Yan *et al.*, 2014).

While almost all of the molecules stated above lead to lack or reduction of ureteric smooth muscle and subsequently to hydronephrosis, the smooth muscle layer is preserved in CLMP-deficient ureters (FIGURE 21). One interesting candidate for interaction with CLMP might be the scaffolding protein DLGH 1 due to the presence of its PDZ domain, its membrane-proximal localisation and its association with the cytoskeleton (Reuver & Garner, 1998). *Dlgh 1* knockout mice display normal immunoreactivity for α-SMA and other markers for late-stage differentiated smooth muscle. Further analysis revealed smooth muscle disorganisation, which

was accompanied by defective ureteral peristalsis (Mahoney *et al.*, 2006). A more detailed investigation is required to determine whether ureters of *Clmp* knockout mice exhibit similarly misaligned smooth muscle cells, but failures in the arrangement of smooth muscle cells might account for impaired ureteral contractility in *Clmp* mutants. However, motility abnormalities in *Dlgh 1*$^{-/-}$ ureters differ from those observed in *Clmp*$^{-/-}$ ureters and in addition, loss of DLGH 1 goes along with the complete lack of the ureteral stromal cell layer (Mahoney *et al.*, 2006), which was still present in *Clmp* mutant ureters.

Thus, among the molecules known to contribute to smooth muscle development, none exhibits similar ureteral phenotypes as the *Clmp* knockout lines presented in this study. Since ureters lacking CLMP exhibited a mature smooth muscle layer, which had been identified by immunopositivity of differentiation marker α-SMA in neonatal cryosections, and mutant ureters were able to form at least weak and incoherent contractile movements, production of contractile elements in smooth muscle cells might be unaffected. Instead, the function of the contractile apparatus and/or intramuscular signal transduction might be impaired as illustrated by the loss of Ca^{2+} waves (FIGURE 24). Thus, it might be hypothesised that transmembranous CLMP could influence the function of contractile molecules by yet unknown mechanisms or that its absence leads to disruption of the smooth muscle network. Therefore, putatively expressed CLMP in smooth muscle cells might act via intracellular signalling pathways or likely acts at intercellular contact sites by mediating intercellular adhesion in order to contribute to the formation of a functional syncytium and facilitation of signal propagation in the smooth muscle layer.

6.4.1.2 Putative CLMP expression in ureteral pacemaker cells?

Two distinct subpopulations of cells within the smooth muscle layer are responsible for the control of the ureteral peristaltic machinery by processing pacemaker activities (Lang & Klemm, 2005; Weiss *et al.*, 2006; Feeney & Rosenblum, 2014; Hammad, 2015). In contrast to normal typical smooth muscle cells, so-called atypical smooth muscle cells have fewer contractile elements, are restricted to the pelvi-calyceal region and are characterised by generation of low-frequency pacemaker waves and by the expression of hyperpolarisation-activated cyclic nucleotide-gated channel 3 (HCN 3; Klemm *et al.*, 1999; Lang & Klemm, 2005; Hurtado *et al.*, 2010). Importantly, HCN 3 function is crucial for these cells, as inhibition of HCN 3 results in impaired electrical activity and consequently to defective peristalsis, referred to as randomised, twitch-like contractions (Hurtado *et al.*, 2010), which are similar to the uncoordinated, local contractions observed in the CLMP-lacking ureters. However, UPJ-associated atypical smooth muscle cells might not be present in isolated ureter explants of the *Clmp* strains, where defective peristalsis was observed.

In addition to atypical smooth muscle cells, a second population of cells has been discovered to be required for peristaltic function. Similarly to intestinal ICC, which act as pacemakers for gut motility, this subpopulation has been reported to localise to the renal pelvis and the proximal ureter, and to generate electrical slow wave autorhythmicity in order to drive

ureteral peristalsis, and is therefore referred to as ICC-like cells (ICC-LC) (Lang & Klemm, 2005; Lang *et al.*, 2006, 2007*a*, 2007*b*). There is some controversy among the studies, since ICC-LC have mainly been detected by immunoreactivity for the receptor tyrosine kinase Kit, however differential stainings required to distinguish ICC-LC from Kit-positive mast cells have not been performed (Pezzone *et al.*, 2003; van der Aa *et al.*, 2004; David *et al.*, 2005). ICC-LC have been shown to be responsible for spontaneous peristaltic activity in isolated ureteral explants, where the kidneys had been removed, as neutralisation of Kit by specific antibodies prevented proper ureteral peristalsis. Strikingly, these isolated ureters blocked in Kit activity showed normal smooth muscle differentiation and uncoordinated and undirected fibrillation-like motility (David *et al.*, 2005), which highly resembles the ureteral phenotypes observed in CLMP-deficient mice.

Thus, these data suggest a relation between ureteral pacemaker activity and CLMP. It might be of great interest to investigate how a cell adhesion protein might be able to modulate electrical activity. CLMP, Kit and HCN 3 are all transmembrane proteins and might interact intracellularly at the plasma membrane of ICC-LC and atypical smooth muscle cells or intercellularly between these pacemaker cells and adjacent typical smooth muscle cells. Lack of CLMP might disrupt cellular intercellular networks, and thus coupling of pacemaker cells from contractility-mediating smooth muscle cells might occur, finally leading to the creation of uncoordinated ureteral contractility. Analysis of distribution and function of Kit-positive ICC-LC and HCN 3-positive atypical smooth muscle cells in CLMP-depleted urinary tracts will be indispensable and will provide substantial insight into peristaltic motility in the absence of CLMP.

Restricted expression of CLMP in ureteral pacemaker cells might not only be likely due to similar phenotypes of ureteral motility, it would also give an explanation for the unsuccessful attempts to localise CLMP in ureteral cells (section 5.8), since pacemaker cells are expressed more or less abundantly at the UPJ, but are only sparsely distributed at the proximal site of the ureter. Therefore, levels of CLMP protein and *Clmp* transcript might not be high and thus be difficult to detect in the urinary tract. In the gut, microarray analyses have uncovered *Clmp* transcripts to be differentially expressed in intestinal ICC-DMP as compared to adjacent tissues (Chen *et al.*, 2007). Intensive research will now be required to finally determine whether CLMP is also expressed in pacemakers of the urinary tract.

6.4.1.3 Putative CLMP expression in ureteral urothelium?

The ureteral urothelium consists of three different epithelial cell types, namely basal, intermediate and superficial cells. Superficial cells, also known as umbrella cells, line the ureteral lumen and apically express four types of integral uroplakins (UPK), which belong to the tetraspanin superfamily and form crystalline plaques that render impermeability to and protection from urine (Jenkins & Woolf, 2007; Wu *et al.*, 2009). Mice depleted in *Upk 3* lack urothelial umbrella cells and display impaired plaque formation, which led to loss of urine barrier function (Hu *et al.*, 2000). Similar results were observed by ablation of *Upk 2* (Kong *et*

al., 2004). In both *Upk* knockout mouse modes, vesicoureteric reflux was detected by dye injections into the urinary bladder as well as formation of hydronephrotic kidneys. Interestingly, absence of UPK 2 and UPK 3 led to hyperplasticity of urothelial tissue and obstruction of the ureteral lumen, which might explain hydronephrosis in mutant animals (Hu *et al.*, 2000; Kong *et al.*, 2004).

In this study, immunofluorescent stainings using cytokeratin 8 detected all types of urothelial cells (FIGURE 21). Stainings to assess uroplakin expressions were not carried out. However, obstructive ureteral lumens were not observed and histological examinations led to the assumption that urothelial plaques were present, suggesting that CLMP and UPK serve different functions. To date, other urothelial molecules implicated in the formation of hydronephrosis and/or defective ureteral peristalsis are not known.

Several studies have reported CLMP as epithelial molecule that co-localises with tight junction protein ZO-1 (Raschperger *et al.*, 2004; Sze *et al.*, 2008*a*; Van der Werf *et al.*, 2012). More information about putative interaction partners and involvement in the formation or function of tight junctions is not available yet. If CLMP was expressed in umbrella cell tight junctions, CLMP might help tightening the apical surface to ensure close and correct alignment of umbrella cells, which could contribute to proper formation of UPK plaques. In this case, however, it remained to be determined how this might influence ureteral peristalsis.

6.4.1.4 Putative CLMP expression in ureteral stromal cells?

To date, the function of ureteral stromal cells has not been clarified yet and only limited information about these cells is available. Ureteral stroma is the cell layer between smooth muscle and urothelium and its only known marker is the enzyme RALDH 2, which is encoded by the *Aldh1a2* gene and responsible for the production of retinoic acid. Retinoic acid is secreted and stimulates transcription via activation of retinoic acid receptors (Rochette-Egly & Germain, 2009). The global knockout of *Aldh1a2* in mice is lethal, but can be rescued by application of retinoic acid. In the urinary tract, retinoic acid signalling has mainly been explored during kidney formation but impaired retinoic acid signalling results in defective ureter insertion to the urinary bladder and thus in hydronephrosis (Batourina *et al.*, 2001, 2002, 2005; Rosselot *et al.*, 2010; Chia *et al.*, 2011).

In this study, staining of RALDH 2 as stromal marker was difficult in ureteral cryosections independent from the genotype, as the antibody detected RALDH 2 in some sections but not in adjacent ones. RALDH 2 was observed in the stromal layer of control and mutant ureters, though (not shown) and fusion of ureter and bladder was not impaired (FIGURE 20). Therefore, production of retinoic acid and thus retinoic acid signalling might not be compromised in the absence of CLMP, however further investigations are required to reliably support this hypothesis. Apart from the expression of the marker protein RALDH 2, the function of ureteral stroma remains to be elucidated, which makes it difficult to estimate a putative role of CLMP in ureteral stroma.

6.4.1.5 Putative CLMP expression in periureteral adipose tissue?

The ureter is embedded by layers of periureteral adipose tissue. A single study elucidated the influence of periureteral fat on ureteral peristalsis since vasculature-surrounding adipose tissue had been shown to inhibit vascular smooth muscle contractility (Verlohren *et al.*, 2004; Greenstein *et al.*, 2009; Lee *et al.*, 2009). Similarly, the presence of periureteral adipose tissue had anticontractile effects on the ureter *in vitro*, while removal of periureteral fat from the ureter amplified contraction magnitudes and frequencies (Killian & Bund, 2012). The underlying mechanisms have not been determined but it has been proposed that a yet unknown factor secreted from periureteral fat cells is responsible for this contractility-regulative property (Killian & Bund, 2012).

CLMP has been described to be abundantly expressed by adipose tissue (Hida *et al.*, 2000; Eguchi *et al.*, 2005), thus it might be possible that CLMP is also distributed among periureteral fat. As a soluble factor is suggested to control ureteral smooth muscle contractions, the question arises how CLMP as transmembrane and cell adhesive protein could contribute to the production and/or secretion of such a regulating factor. Due to the lack of relevant information about for instance identity and secretion period of this factor, a putative contribution of CLMP is highly speculative. Further investigation is required to associate CLMP with the anticontractile function of periureteral fat.

7 CONCLUSION AND FUTURE PERSPECTIVES

In this study, it was shown that the absence of CLMP causes a complex phenotype during mouse development. The reason for early lethality of CLMP-deficient animals could not be clarified, however it might be likely that pyloric stenosis followed by malnutrition and loss of body weight is one of the underlying mechanisms (section 6.2). Future experiments are planned to analyse a putative pyloric stenosis by assessing obstruction via dye passage through the pyloric junction, by examining the histology of the pyloric muscle and by investigating pyloric explant cultures for defects in contractility. An impact on small bowel length, as shown for human CSBS patients, could not be deduced to CLMP in mice lacking CLMP, while associated disorganisation of the intestine and a dilation of the duodenum in adult *Clmp*$^{-/-}$ animals might be secondary effects of severe dimensions of hydronephrotic kidneys (section 6.3). Monitoring gut length in neonatal pups will help clarifying a role of CLMP in CSBS, however in order to reliably determine whether these gastrointestinal phenotypes develop independently from the defects in the urinary tract and whether pyloric stenosis is the cause for mortality, a conditional ablation of *Clmp* in mice is required. Detailed information about CLMP expression in the gastrointestinal tract is essential to select appropriate *Cre* driver lines. Currently, our laboratory is generating *Clmp* mice with conditional potential by using ES cells provided by EUCOMM, the European Conditional Mouse Mutagenesis Programme. These ES cells make use of a knockout-first strategy by means of a gene trapping cassette, which can be converted into a *loxP*-flanked conditional allele. In addition, a *lacZ* cassette is included that offers the ability to detect *Clmp* expression by *lacZ*-mediated β-galactosidase staining. Thus, this conditional *Clmp* knockout line will help elucidating the expression of *Clmp* during murine development and the function of CLMP in gastrointestinal tract and survival.

Deletion of *Clmp* led to hydronephrosis caused by impaired ureteral peristalsis (section 6.4). However, due to the lack of information about CLMP expression patterns in the urinary tract, mechanisms underlying an influence of CLMP on the contractile machinery in the murine ureter remain to be determined. Although further investigation of urinary pacemaker cells is intended to elucidate whether pacemaker function is compromised by the loss of CLMP, detection of *Clmp* transcripts by β-galactosidase stainings in the conditional mouse model will greatly enhance the knowledge of subcellular localisation of CLMP in the urinary system and – dependent on the cell type expressing CLMP – thereby will indicate directions for further research.

Taken together, this study implicates CLMP as novel, essential factor for growth and survival as well as for gastrointestinal and urinary tract development in the mouse.

8 SUPPLEMENTARY INFORMATION

8.1 Contents of the CD attached to this thesis

Directory of the CD attached to this thesis

01_Dissertation
> Dissertation_Hanna_Langhorst.pdf
02_Supplementary_Information
> Targeting_vector_sequence.seq (*)
> Targeting_vector_sequence.txt (*)
> Targeting_vector_sequence.xdna (*)
> Video_1_WT_real-time.avi (**)
> Video_2_WT_10x speed.avi (**)
> Video_3_KO_real-time.avi (**)
> Video_4_KO_10x-speed.avi (**)

(*) Supplemental pVBTK-CLMP targeting vector sequence files.

Files contain the sequenced region of the pVBTK-CLMP targeting vector according to sections 4.2.2 and 5.1.2. and can be accessed via Lasergene (.seq) and Serial Cloner (.xdna) software or via common text editing programmes (.txt), respectively.

(**) Supplemental ureteral peristalsis video files.

Videos show peristalsis in ureteral explants dissected from wild type (WT) and *Clmp* knockout (KO) E 15.5 embryos after five days in culture according to section 5.6. Contractions are shown either in real-time or at 10x speed.

8.2 Data of body weight and body length analyses

The following supplemental tables contain the values of body weight and body length measurements corresponding to FIGURE 8 and to FIGURE 11 in section 5.2.

TABLE S1. Body weight analysis of pups of the *Clmp*-2043 strain (to FIGURE 8).
Data are presented ± SEM. Number of animals is indicated in brackets. WT, wild type; Het., heterozygous; Ctrl., control; KO, knockout; *t*, *t*-test; MW, Mann Whitney Rank Sum test; n.s., not significant; * indicating P ≤ 0.05, ** indicating P ≤ 0.01 and *** indicating P ≤ 0.001.

Postnatal day	*Clmp*-2043 strain: B6;129P2-*Clmp*^{tm1aFgr} body weight (g)					
P 0	WT	1.594 ± 0.065 (18)	P = 0.091	Ctrl.	1.538 ± 0.036 (42)	P = 0.222
	Het.	1.496 ± 0.038 (24)	n. s. [MW]	KO	1.442 ± 0.078 (12)	n. s. [MW]
P 1	WT	1.812 ± 0.064 (26)	P = 0.530	Ctrl.	1.768 ± 0.040 (56)	P = 0.001
	Het.	1.730 ± 0.052 (30)	n. s. [MW]	KO	1.436 ± 0.073 (11)	*** [*t*]

Postnatal day	*Clmp*-2043 strain: B6;129P2-*Clmp*^{tm1aFgr} body weight (g) *(continued)*					
P 2	WT	2.100 ± 0.063 (29)	P = 0.657	Ctrl.	2.077 ± 0.049 (61)	P < 0.001
	Het.	2.056 ± 0.073 (32)	n. s. [*t*]	KO	1.445 ± 0.084 (11)	*** [*t*]
P 3	WT	2.568 ± 0.087 (28)	P = 0.505	Ctrl.	2.522 ± 0.065 (59)	P < 0.001
	Het.	2.481 ± 0.096 (31)	n. s. [*t*]	KO	1.656 ± 0.127 (9)	*** [*t*]
P 4	WT	3.079 ± 0.110 (24)	P = 0.880	Ctrl.	3.067 ± 0.080 (49)	P < 0.001
	Het.	3.056 ± 0.118 (25)	n. s. [MW]	KO	1.920 ± 0.182 (10)	*** [MW]
P 5	WT	3.521 ± 0.118 (28)	P = 0.822	Ctrl.	3.548 ± 0.082 (61)	P < 0.001
	Het.	3.570 ± 0.115 (33)	n. s. [MW]	KO	2.156 ± 0.205 (9)	*** [MW]
P 6	WT	4.154 ± 0.121 (28)	P = 0.938	Ctrl.	4.146 ± 0.090 (61)	P < 0.001
	Het.	4.139 ± 0.133 (33)	n. s. [MW]	KO	2.486 ± 0.369 (7)	*** [*t*]
P 7	WT	4.681 ± 0.126 (31)	P = 0.939	Ctrl.	4.673 ± 0.097 (66)	P < 0.001
	Het.	4.666 ± 0.146 (35)	n. s. [*t*]	KO	2.850 ± 0.325 (8)	*** [*t*]
P 8	WT	5.274 ± 0.135 (31)	P = 0.822	Ctrl.	5.274 ± 0.108 (70)	P < 0.001
	Het.	5.274 ± 0.162 (39)	n. s. [MW]	KO	3.313 ± 0.346 (8)	*** [*t*]
P 9	WT	5.950 ± 0.151 (30)	P = 0.824	Ctrl.	5.953 ± 0.115 (68)	P < 0.001
	Het.	5.955 ± 0.170 (38)	n. s. [MW]	KO	3.625 ± 0.387 (8)	*** [*t*]
P 10	WT	6.527 ± 0.162 (30)	P = 0.591	Ctrl.	6.603 ± 0.125 (68)	P < 0.001
	Het.	6.663 ± 0.184 (38)	n. s. [*t*]	KO	4.271 ± 0.478 (7)	*** [*t*]
P 11	WT	6.972 ± 0.203 (29)	P = 0.443	Ctrl.	7.097 ± 0.140 (67)	P < 0.001
	Het.	7.192 ± 0.194 (38)	n. s. [*t*]	KO	4.614 ± 0.456 (7)	*** [*t*]
P 12	WT	7.607 ± 0.203 (29)	P = 0.891	Ctrl.	7.657 ± 0.146 (65)	P < 0.001
	Het.	7.697 ± 0.209 (36)	n. s. [*t*]	KO	5.100 ± 0.513 (7)	*** [*t*]
P 13	WT	7.762 ± 0.185 (26)	P = 0.236	Ctrl.	7.978 ± 0.159 (60)	P < 0.001
	Het.	8.144 ± 0.240 (34)	n. s. [*t*]	KO	5.620 ± 0.630 (5)	*** [*t*]
P 14	WT	8.340 ± 0.227 (30)	P = 0.498	Ctrl.	8.456 ± 0.171 (66)	P = 0.005
	Het.	8.553 ± 0.252 (36)	n. s. [*t*]	KO	6.071 ± 0.693 (7)	** [MW]
P 15	WT	8.430 ± 0.256 (27)	P = 0.360	Ctrl.	8.629 ± 0.198 (59)	P < 0.001
	Het.	8.797 ± 0.295 (32)	n. s. [*t*]	KO	6.357 ± 0.725 (7)	*** [*t*]
P 16	WT	8.659 ± 0.251 (29)	P = 0.592	Ctrl.	8.772 ± 0.189 (65)	P < 0.001
	Het.	8.864 ± 0.276 (36)	n. s. [*t*]	KO	6.657 ± 0.669 (7)	*** [*t*]
P 17	WT	8.766 ± 0.260 (29)	P = 0.506	Ctrl.	8.911 ± 0.200 (63)	P = 0.002
	Het.	9.035 ± 0.299 (34)	n. s. [*t*]	KO	6.857 ± 0.667 (7)	** [*t*]
P 18	WT	8.955 ± 0.274 (29)	P = 0.484	Ctrl.	9.109 ± 0.199 (64)	P = 0.002
	Het.	9.237 ± 0.285 (35)	n. s. [*t*]	KO	7.071 ± 0.666 (7)	** [*t*]
P 19	WT	9.392 ± 0.305 (24)	P = 0.705	Ctrl.	9.489 ± 0.217 (57)	P = 0.007
	Het.	9.561 ± 0.306 (33)	n. s. [*t*]	KO	7.300 ± 0.929 (5)	** [*t*]
P 20	WT	9.871 ± 0.291 (24)	P = 0.917	Ctrl.	9.897 ± 0.204 (58)	P < 0.001
	Het.	9.915 ± 0.285 (34)	n. s. [*t*]	KO	6.914 ± 0.635 (7)	*** [*t*]
P 21	WT	10.907 ± 0.389 (15)	P = 0.612	Ctrl.	10.636 ± 0.319 (33)	P = 0.007
	Het.	10.411 ± 0.490 (18)	n. s. [MW]	KO	7.840 ± 0.478 (5)	** [MW]
P 22	WT	11.164 ± 0.339 (11)	P = 0.504	Ctrl.	11.033 ± 0.401 (24)	---
	Het.	10.923 ± 0.698 (13)	n. s. [MW]	KO	8.100 (1)	

TABLE S2. Body weight analysis of pups of the *Clmp*-KO strain (to FIGURE 8).

Data are presented ± SEM. Number of animals is indicated in brackets. WT, wild type; Het., heterozygous; Ctrl., control; KO, knockout; *t*, *t*-test; MW, Mann Whitney Rank Sum test; n.s., not significant; * indicating P ≤ 0.05, ** indicating P ≤ 0.01 and *** indicating P ≤ 0.001.

Postnatal day	*Clmp*-KO strain: B6.129P2-*Clmp*$^{tm1a.1Fgr}$ (N1-5) Body weight (g)					
P 0	WT	1.515 ± 0.063 (13)	P = 0.441	Ctrl.	1.465 ± 0.030 (48)	P < 0.001
	Het.	1.446 ± 0.034 (35)	n. s. [MW]	KO	1.292 ± 0.026 (13)	*** [MW]
P 1	WT	1.565 ± 0.066 (17)	P = 0.395	Ctrl.	1.610 ± 0.038 (49)	P < 0.001
	Het.	1.634 ± 0.047 (32)	n. s. [*t*]	KO	1.240 ± 0.040 (10)	*** [MW]
P 2	WT	1.867 ± 0.093 (18)	P = 0.287	Ctrl.	1.955 ± 0.057 (56)	P < 0.001
	Het.	1.997 ± 0.071 (38)	n. s. [*t*]	KO	1.222 ± 0.062 (9)	*** [*t*]
P 3	WT	2.272 ± 0.114 (18)	P = 0.303	Ctrl.	2.352 ± 0.063 (56)	P < 0.001
	Het.	2.389 ± 0.075 (38)	n. s. [MW]	KO	1.425 ± 0.101 (8)	*** [MW]
P 4	WT	2.794 ± 0.135 (18)	P = 0.349	Ctrl.	2.896 ± 0.074 (56)	P < 0.001
	Het.	2.945 ± 0.089 (38)	n. s. [*t*]	KO	1.700 ± 0.155 (6)	*** [*t*]
P 5	WT	3.326 ± 0.154 (19)	P = 0.222	Ctrl.	3.483 ± 0.087 (60)	P < 0.001
	Het.	3.556 ± 0.105 (41)	n. s. [*t*]	KO	2.029 ± 0.184 (7)	*** [*t*]
P 6	WT	3.932 ± 0.189 (19)	P = 0.260	Ctrl.	4.097 ± 0.096 (63)	P < 0.001
	Het.	4.168 ± 0.110 (44)	n. s. [*t*]	KO	2.414 ± 0.238 (7)	*** [MW]
P 7	WT	4.617 ± 0.305 (18)	P = 0.522	Ctrl.	4.640 ± 0.125 (58)	P < 0.001
	Het.	4.650 ± 0.121 (40)	n. s. [MW]	KO	2.717 ± 0.336 (6)	*** [MW]
P 8	WT	5.026 ± 0.233 (19)	P = 0.527	Ctrl.	5.138 ± 0.115 (63)	P < 0.001
	Het.	5.186 ± 0.131 (44)	n. s. [*t*]	KO	3.029 ± 0.334 (7)	*** [*t*]
P 9	WT	5.553 ± 0.240 (19)	P = 0.761	Ctrl.	5.613 ± 0.128 (63)	P < 0.001
	Het.	5.639 ± 0.154 (44)	n. s. [*t*]	KO	3.300 ± 0.346 (7)	*** [*t*]
P 10	WT	6.079 ± 0.250 (19)	P = 0.882	Ctrl.	6.113 ± 0.147 (63)	P < 0.001
	Het.	6.127 ± 0.182 (44)	n. s. [*t*]	KO	3.457 ± 0.338 (7)	*** [*t*]
P 11	WT	6.716 ± 0.325 (19)	P = 0.753	Ctrl.	6.717 ± 0.187 (63)	P < 0.001
	Het.	6.718 ± 0.231 (44)	n. s. [MW]	KO	4.050 ± 0.352 (6)	*** [*t*]
P 12	WT	6.984 ± 0.290 (19)	P = 0.985	Ctrl.	6.979 ± 0.179 (63)	P < 0.001
	Het.	6.977 ± 0.226 (44)	n. s. [*t*]	KO	3.940 ± 0.474 (5)	*** [*t*]
P 13	WT	7.353 ± 0.281 (19)	P = 0.946	Ctrl.	7.333 ± 0.186 (63)	P < 0.001
	Het.	7.325 ± 0.240 (44)	n. s. [*t*]	KO	4.625 ± 0.624 (4)	*** [*t*]
P 14	WT	7.737 ± 0.294 (19)	P = 0.672	Ctrl.	7.606 ± 0.200 (63)	P < 0.001
	Het.	7.550 ± 0.258 (44)	n. s. [*t*]	KO	4.625 ± 0.839 (4)	*** [*t*]
P 15	WT	8.021 ± 0.324 (19)	P = 0.768	Ctrl.	7.927 ± 0.208 (62)	P = 0.013
	Het.	7.886 ± 0.266 (43)	n. s. [*t*]	KO	5.467 ± 0.882 (3)	* [*t*]
P 16	WT	8.232 ± 0.336 (19)	P = 0.768	Ctrl.	8.141 ± 0.204 (61)	P = 0.004
	Het.	8.100 ± 0.257 (42)	n. s. [*t*]	KO	5.333 ± 1.141 (3)	** [*t*]
P 17	WT	8.268 ± 0.342 (19)	P = 0.943	Ctrl.	8.246 ± 0.208 (61)	P = 0.076
	Het.	8.236 ± 0.262 (42)	n. s. [*t*]	KO	6.150 ± 0.550 (2)	n. s. [*t*]
P 18	WT	8.189 ± 0.339 (19)	P = 0.889	Ctrl.	8.231 ± 0.198 (61)	P = 0.072
	Het.	8.250 ± 0.247 (42)	n. s. [*t*]	KO	6.200 ± 0.800 (2)	n. s. [*t*]
P 19	WT	8.458 ± 0.346 (19)	P = 0.723	Ctrl.	8.508 ± 0.209 (61)	P = 0.076
	Het.	8.531 ± 0.263 (42)	n. s. [MW]	KO	6.400 ± 0.700 (2)	n. s. [*t*]
P 20	WT	8.684 ± 0.349 (19)	P = 0.869	Ctrl.	8.739 ± 0.221 (61)	P = 0.082
	Het.	8.764 ± 0.283 (42)	n. s. [*t*]	KO	6.550 ± 0.750 (2)	n. s. [*t*]
P 21	WT	8.600 ± 0.304 (16)	P = 0.379	Ctrl.	8.844 ± 0.183 (52)	P = 0.014
	Het.	8.953 ± 0.228 (36)	n. s. [*t*]	KO	6.450 ± 0.350 (2)	* [*t*]

Postnatal day	*Clmp*-KO strain: B6.129P2-*Clmp*$^{tm1a.1Fgr}$ (N1-5) Body weight (g) *(Continued)*					
P 22	WT	8.714 ± 0.301 (14)	P = 0.182	Ctrl.	9.136 ± 0.234 (39)	P = 0.020
	Het.	9.372 ± 0.319 (25)	n. s. [*t*]	KO	6.600 ± 0.100 (2)	* [*t*]

TABLE S3. Body weight analysis of juvenile *Clmp*-2043 animals (to FIGURE 11).

Data are presented ± SEM. Number of animals is indicated in brackets. WT, wild type; Het., heterozygous; Ctrl., control; KO, knockout; *t*, *t*-test; MW, Mann Whitney Rank Sum test; n.s., not significant; * indicating P ≤ 0.05, ** indicating P ≤ 0.01 and *** indicating P ≤ 0.001.

Postnatal day	*Clmp*-2043 strain: B6;129P2-*Clmp*^{tm1aFgr} body weight (g)					
P 35	WT	21.217 ± 1.350 (12)	P = 0.720	Ctrl.	20.897 ± 0.676 (32)	P = 0.018
	Het.	20.705 ± 0.745 (20)	n. s. [*t*]	KO	18.194 ± 0.855 (18)	* [*t*]
P 42	WT	23.458 ± 1.070 (12)	P = 0.425	Ctrl.	22.841 ± 0.588 (32)	P = 0.009
	Het.	22.470 ± 0.697 (20)	n. s. [*t*]	KO	20.189 ± 0.754 (18)	** [*t*]
P 49	WT	24.700 ± 1.067 (12)	P = 0.428	Ctrl.	24.011 ± 0.617 (35)	P = 0.018
	Het.	23.652 ± 0.762 (23)	n. s. [*t*]	KO	21.836 ± 0.606 (25)	* [*t*]
P 56	WT	25.558 ± 1.057 (12)	P = 0.721	Ctrl.	25.254 ± 0.601 (35)	P = 0.010
	Het.	25.096 ± 0.744 (23)	n. s. [*t*]	KO	22.836 ± 0.659 (25)	** [*t*]
P 63	WT	26.500 ± 1.093 (12)	P = 0.629	Ctrl.	26.081 ± 0.601 (36)	P = 0.023
	Het.	25.871 ± 0.730 (24)	n. s. [*t*]	KO	23.833 ± 0.755 (24)	* [*t*]
P 70	WT	27.192 ± 1.102 (12)	P = 0.868	Ctrl.	27.039 ± 0.637 (36)	P = 0.022
	Het.	26.963 ± 0.798 (24)	n. s. [*t*]	KO	24.637 ± 0.811 (24)	* [*t*]
P 77	WT	27.983 ± 1.166 (12)	P = 0.763	Ctrl.	27.886 ± 0.673 (36)	P = 0.045
	Het.	27.838 ± 0.841 (24)	n. s. [MW]	KO	25.646 ± 0.877 (24)	* [*t*]
P 84	WT	28.317 ± 1.087 (12)	P = 0.973	Ctrl.	28.286 ± 0.646 (36)	P = 0.064
	Het.	28.271 ± 0.818 (24)	n. s. [MW]	KO	26.317 ± 0.830 (24)	n.s. [*t*]
P 91	WT	29.325 ± 1.307 (12)	P = 0.814	Ctrl.	29.083 ± 0.639 (36)	P = 0.075
	Het.	28.962 ± 0.810 (24)	n. s. [MW]	KO	27.474 ± 0.791 (23)	n. s. [MW]
P 98	WT	29.292 ± 1.193 (12)	P = 0.725	Ctrl.	29.644 ± 0.694 (36)	P = 0.125
	Het.	29.821 ± 0.869 (24)	n. s. [*t*]	KO	27.935 ± 0.843 (23)	n. s. [*t*]
P 105	WT	31.378 ± 1.344 (9)	P = 0.653	Ctrl.	30.807 ± 0.850 (28)	P = 0.104
	Het.	30.537 ± 1.098 (19)	n. s. [*t*]	KO	28.597 ± 1.040 (19)	n. s. [*t*]

TABLE S4. Naso-anal body length analysis of juvenile *Clmp*-2043 animals (to FIGURE 11).

Data are presented ± SEM. Number of animals is indicated in brackets. WT, wild type; Het., heterozygous; Ctrl., control; KO, knockout; *t*, *t*-test; MW, Mann Whitney Rank Sum test; n.s., not significant; * indicating P ≤ 0.05, ** indicating P ≤ 0.01 and *** indicating P ≤ 0.001.

Postnatal day	*Clmp*-2043 strain: B6;129P2-*Clmp*^{tm1aFgr} naso-anal body length (cm)					
P 35	WT	8.583 ± 0.229 (12)	P = 0.183	Ctrl.	8.375 ± 0.138 (28)	P = 0.095
	Het.	8.219 ± 0.164 (16)	n. s. [MW]	KO	8.000 ± 0.154 (15)	n. s. [*t*]
P 42	WT	8.636 ± 0.244 (11)	P = 0.725	Ctrl.	8.574 ± 0.143 (27)	P = 0.204
	Het.	8.531 ± 0.180 (16)	n. s. [*t*]	KO	8.233 ± 0.161 (15)	n. s. [MW]
P 49	WT	8.833 ± 0.198 (12)	P = 0.710	Ctrl.	8.783 ± 0.126 (30)	P = 0.213
	Het.	8.750 ± 0.168 (18)	n. s. [MW]	KO	8.545 ± 0.135 (22)	n. s. [MW]
P 56	WT	9.091 ± 0.200 (11)	P = 0.150	Ctrl.	9.147 ± 0.105 (33)	P = 0.026
	Het.	8.727 ± 0.153 (22)	n. s. [MW]	KO	8.360 ± 0.151 (25)	* [MW]

Postnatal day		*Clmp*-2043 strain: B6;129P2-*Clmp*^{tm1aFgr} naso-anal body length (cm) *(continued)*				
P 63	WT	9.333 ± 0.128 (12)	P = 0.193	Ctrl.	9.147 ± 0.105 (34)	P = 0.002
	Het.	9.045 ± 0.143 (22)	n. s. [*t*]	KO	8.545 ± 0.127 (22)	** [MW]
P 70	WT	9.091 ± 0.163 (11)	P = 0.293	Ctrl.	9.25 ± 0.100 (34)	P = 0.100
	Het.	9.326 ± 0.124 (23)	n. s. [MW]	KO	8.955 ± 0.104 (22)	n. s. [MW]
P 77	WT	9.333 ± 0.128 (12)	P = 0.732	Ctrl.	9.292 ± 0.092 (36)	P = 0.004
	Het.	9.271 ± 0.124 (24)	n. s. [MW]	KO	8.727 ± 0.170 (22)	** [MW]
P 84	WT	9.500 ± 0.117 (11)	P = 0.309	Ctrl.	9.368 ± 0.093 (34)	P = 0.024
	Het.	9.304 ± 0.125 (23)	n. s. [MW]	KO	8.881 ± 0.176 (21)	* [MW]
P 91	WT	9.375 ± 0.186 (12)	P = 0.563	Ctrl.	9.264 ± 0.103 (36)	P = 0.068
	Het.	9.208 ± 0.124 (24)	n. s. [MW]	KO	8.913 ± 0.132 (23)	n. s. [MW]
P 98	WT	9.458 ± 0.130 (12)	P = 0.659	Ctrl.	9.400 ± 0.082 (35)	P = 0.076
	Het.	9.370 ± 0.105 (23)	n. s. [MW]	KO	9.065 ± 0.134 (23)	n. s. [MW]
P 105	WT	9.333 ± 0.167 (9)	P = 0.898	Ctrl.	9.357 ± 0.096 (28)	P = 0.150
	Het.	9.368 ± 0.120 (19)	n. s. [MW]	KO	9.184 ± 0.134 (19)	n. s. [MW]

9 REFERENCES

Van der Aa F, Roskams T, Blyweert W, Ost D, Bogaert G & De Ridder D (2004). Identification of kit positive cells in the human urinary tract. *J Urol* **171,** 2492–2496.

Adams DJ, Quail MA, Cox T, van der Weyden L, Gorick BD, Su Q, Chan W, Davies R, Bonfield JK, Law F, Humphray S, Plumb B, Liu P, Rogers J & Bradley A (2005). A genome-wide, end-sequenced 129Sv BAC library resource for targeting vector construction. *Genomics* **86,** 753–758.

Airik R, Bussen M, Singh MK, Petry M & Kispert A (2006). Tbx18 regulates the development of the ureteral mesenchyme. **116,** 663–674.

Airik R & Kispert A (2007). Down the tube of obstructive nephropathies: the importance of tissue interactions during ureter development. *Kidney Int* **72,** 1459–1467.

Airik R, Trowe MO, Foik A, Farin HF, Petry M, Schuster-Gossler K, Schweizer M, Scherer G, Kist R & Kispert A (2010). Hydroureternephrosis due to loss of Sox9-regulated smooth muscle cell differentiation of the ureteric mesenchyme. *Hum Mol Genet* **19,** 4918–4929.

Ansorge W (1985). Fast and sensitive detection of protein and DNA bands by treatment with potassium permanganate. *J Biochem Biophys Methods* **11,** 13–20.

Arrate MP, Rodriguez JM, Tran TM, Brock TA & Cunningham SA (2001). Cloning of Human Junctional Adhesion Molecule 3 (JAM3) and Its Identification as the JAM2 Counter-receptor. *J Biol Chem* **276,** 45826–45832.

Asher DR, Cerny AM, Weiler SR, Horner JW, Keeler ML, Neptune MA, Jones SN, Bronson RT, DePinho RA & Finberg RW (2005). Coxsackievirus and adenovirus receptor is essential for cardiomyocyte development. *Genesis* **42,** 77–85.

Aurrand-Lions M, Johnson-Leger C, Wong C, Du Pasquier L & Imhof BA (2001). Heterogeneity of endothelial junctions is reflected by differential expression and specific subcellular localization of the three JAM family members. *Blood* **98,** 3699–3707.

Barclay AN (2003). Membrane proteins with immunoglobulin-like domains - A master superfamily of interaction molecules. *Semin Immunol* **15,** 215–223.

Batourina E, Choi C, Paragas N, Bello N, Hensle T, Costantini FD, Schuchardt A, Bacallao RL & Mendelsohn CL (2002). Distal ureter morphogenesis depends on epithelial cell remodeling mediated by vitamin A and Ret. *Nat Genet* **32,** 109–115.

Batourina E, Gim S, Bello N, Shy M, Clagett-Dame M, Srinivas S, Costantini F & Mendelsohn C (2001). Vitamin A controls epithelial/mesenchymal interactions through Ret expression. *Nat Genet* **27,** 74–78.

Batourina E, Tsai S, Lambert S, Sprenkle P, Viana R, Dutta S, Hensle T, Wang F, Niederreither K, McMahon AP, Carroll TJ & Mendelsohn CL (2005). Apoptosis induced by vitamin A signaling is crucial for connecting the ureters to the bladder. *Nat Genet* **37,** 1082–1089.

Becker A & Baum M (2006). Obstructive uropathy. *Early Hum Dev* **82,** 15–22.

Di Benedetto A, Arena S, Nicotina PA, Mucciardi G, Galì A & Magno C (2013). Pacemakers in the upper urinary tract. *Neurourol Urodyn* **32,** 349–353.

Bergelson JM, Cunningham JA, Droguett G, Kurt-Jones EA, Krithivas A, Hong JS, Horwitz MS, Crowell RL & Finberg RW (1997). Isolation of a common receptor for Coxsackie B viruses and adenoviruses 2 and 5. *Science* **275,** 1320–1323.

Bergelson JM, Krithivas A, Celi L, Droguett G, Horwitz MS, Wickham T, Crowell RL & Finberg RW (1998). The murine CAR homolog is a receptor for coxsackie B viruses and adenoviruses. *J Virol* **72,** 415–419.

Bohnenpoll T & Kispert A (2014). Ureter growth and differentiation. *Semin Cell Dev Biol* **36,** 21–30.

Bork P, Holm L & Sander C (1994). The immunoglobulin fold. Structural classification, sequence patterns and common core. *J Mol Biol* **242,** 309–320.

Braissant O & Wahli W (1998). A Simplified In Situ Hybridization Protocol Using Non-radioactively Labeled Probes to Detect Abundant and Rare mRNAs on Tissue Sections. *Biochemica* **1,** 10–16.

Brümmendorf T, Kenwrick S & Rathjen FG (1998). Neural cell recognition molecule L1: from cell biology to human hereditary brain malformations. *Curr Opin Neurobiol* **8,** 87–97.

Brümmendorf T & Rathjen FG (1995). Cell adhesion molecules 1: immunoglobulin superfamily. *Protein Profile* **2,** 963–1108.

Burns AJ, Roberts RR, Bornstein JC & Young HM (2009). Development of the enteric nervous system and its role in intestinal motility during fetal and early postnatal stages. *Semin Pediatr Surg* **18,** 196–205.

Bush KT, Vaughn DA, Li X, Rosenfeld MG, Rose DW, Mendoza SA & Nigam SK (2006). Development and differentiation of the ureteric bud into the ureter in the absence of a kidney collecting system. *Dev Biol* **298,** 571–584.

Van Buul JD, Kanters E & Hordijk PL (2007). Endothelial Signaling by Ig-Like Cell Adhesion Molecules. *Arter Thromb Vasc Biol* **27,** 1870–1876.

Cain JE, Islam E, Haxho F, Blake J & Rosenblum ND (2011). GLI3 repressor controls functional development of the mouse ureter. *J Clin Invest* **121,** 1199–1206.

Carson SD, Chapman NN & Tracy SM (1997). Purification of the putative coxsackievirus B receptor from HeLa cells. *Biochem Biophys Res Commun* **233,** 325–328.

Caubit X, Lye CM, Martin E, Coré N, Long DA, Vola C, Jenkins D, Garratt AN, Skaer H, Woolf AS & Fasano L (2008). Teashirt 3 is necessary for ureteral smooth muscle differentiation downstream of SHH and BMP4. *Development* **135,** 3301–3310.

Chang C-P, McDill BW, Neilson JR, Joist HE, Epstein JA, Crabtree GR & Chen F (2004). Calcineurin is required in urinary tract mesenchyme for the development of the pyeloureteral peristaltic machinery. *J Clin Invest* **113,** 1051–1058.

Chen F (2009). Genetic and developmental basis for urinary tract obstruction. *Pediatr Nephrol* **24,** 1621–1632.

Chen H, Ordög T, Chen J, Young DL, Bardsley MR, Redelman D, Ward SM & Sanders KM (2007). Differential gene expression in functional classes of interstitial cells of Cajal in murine small intestine. *Physiol Genomics* **31,** 492–509.

Chen J-W, Ghosh R, Finberg RW & Bergelson JM (2003). Structure and chromosomal localization of the murine coxsackievirus and adenovirus receptor gene. *DNA Cell Biol* **22,** 253–259.

Chen J-W, Zhou B, Yu QC, Shin SJ, Jiao K, Schneider MD, Baldwin HS & Bergelson JM (2006). Cardiomyocyte-specific deletion of the coxsackievirus and adenovirus receptor results in hyperplasia of the embryonic left ventricle and abnormalities of sinuatrial valves. *Circ Res* **98,** 923–930.

Chia I, Grote D, Marcotte M, Batourina E, Mendelsohn C & Bouchard M (2011). Nephric duct insertion is a crucial step in urinary tract maturation that is regulated by a Gata3-Raldh2-Ret molecular network in mice. *Development* **138,** 2089–2097.

Chothia C & Jones EY (1997). The molecular structure of cell adhesion molecules. *Annu Rev Biochem* **66,** 823–862.

Chrétien I, Marcuz A, Courtet M, Katevuo K, Vainio O, Heath JK, White SJ & Du Pasquier L (1998). CTX, a Xenopus thymocyte receptor, defines a molecular family conserved throughout vertebrates. *Eur J Immunol* **28,** 4094–4104.

Clamp M, Fry B, Kamal M, Xie X, Cuff J, Lin MF, Kellis M, Lindblad-Toh K & Lander ES (2007). Distinguishing protein-coding and noncoding genes in the human genome. *Proc Natl Acad Sci U S A* **104,** 19428–19433.

Cohen CJ, Shieh JT, Pickles RJ, Okegawa T, Hsieh JT & Bergelson JM (2001). The coxsackievirus and adenovirus receptor is a transmembrane component of the tight junction. *Proc Natl Acad Sci U S A* **98,** 15191–15196.

Coyne CB, Voelker T, Pichla SL & Bergelson JM (2004). The coxsackievirus and adenovirus receptor interacts with the multi-PDZ domain protein-1 (MUPP-1) within the tight junction. *J Biol Chem* **279,** 48079–48084.

Cunningham SA, Arrate MP, Rodriguez JM, Bjercke RJ, Vanderslice P, Morris AP & Brock TA (2000). A novel protein with homology to the junctional adhesion molecule. Characterization of leukocyte interactions. *J Biol Chem* **275,** 34750–34756.

David SG, Cebrian C, Vaughan ED & Herzlinger D (2005). c-kit and ureteral peristalsis. *J Urol* **173,** 292–295.

Dijkman HBPM, Mentzel S, de Jong AS & Assmann KJM (2008). RNA in situ hybridization using DIG-labeled cRNA probes. In *DIG Application Manual for Nonradioactive In Situ Hybridization*, 4th edn., pp. 160–167. Roche Diagnostics GmbH.

Dorner AA, Wegmann F, Butz S, Wolburg-Buchholz K, Wolburg H, Mack A, Nasdala I, August B, Westermann J, Rathjen FG & Vestweber D (2005). Coxsackievirus-adenovirus receptor (CAR) is essential for early embryonic cardiac development. *J Cell Sci* **118,** 3509–3521.

Eguchi J, Wada J, Hida K, Zhang H, Matsuoka T, Baba M, Hashimoto I, Shikata K, Ogawa N & Makino H (2005). Identification of adipocyte adhesion molecule (ACAM), a novel CTX gene family, implicated in adipocyte maturation and development of obesity. *Biochem J* **387,** 343–353.

Elangbam CS, Qualls CW & Dahlgren RR (1997). Cell Adhesion Molecules--Update. *Vet Pathol* **34,** 61–73.

Excoffon KJDA, Gansemer ND, Mobily ME, Karp PH, Parekh KR & Zabner J (2010). Isoform-Specific Regulation and Localization of the Coxsackie and Adenovirus Receptor in Human Airway Epithelia. *PLoS One*; DOI: 10.1371/journal.pone.0009909.

Excoffon KJDA, Hruska-Hageman A, Klotz M, Traver GL & Zabner J (2004). A role for the PDZ-binding domain of the coxsackie B virus and adenovirus receptor (CAR) in cell adhesion and growth. *J Cell Sci* **117,** 4401–4409.

Fechner H, Haack A, Wang H, Wang X, Eizema K, Pauschinger M, Schoemaker R, Veghel R, Houtsmuller A, Schultheiss HP, Lamers J & Poller W (1999). Expression of coxsackie adenovirus receptor and alphav-integrin does not correlate with adenovector targeting in vivo indicating anatomical vector barriers. *Gene Ther* **6,** 1520–1535.

Fechner H, Noutsias M, Tschoepe C, Hinze K, Wang X, Escher F, Pauschinger M, Dekkers D, Vetter R, Paul M, Lamers J, Schultheiss HP & Poller W (2003). Induction of coxsackievirus-adenovirus-receptor expression during myocardial tissue formation and remodeling: Identification of a cell-to-cell contact-dependent regulatory mechanism. *Circulation* **107,** 876–882.

Feeney MM & Rosenblum ND (2014). Urinary tract pacemaker cells: current knowledge and insights from nonrenal pacemaker cells provide a basis for future discovery. *Pediatr Nephrol* **29,** 629–635.

Garne E, Loane M, Wellesley D, Barisic I & EUROCAT Working Group (2009). Congenital hydronephrosis: Prenatal diagnosis and epidemiology in Europe. *J Pediatr Urol* **5,** 47–52.

Gray KA, Daugherty LC, Gordon SM, Seal RL, Wright MW & Bruford EA (2013). Genenames.org: the HGNC resources in 2013. *Nucleic Acids Res* **41,** 545–552.

Greenstein AS, Khavandi K, Withers SB, Sonoyama K, Clancy O, Jeziorska M, Laing I, Yates AP, Pemberton PW, Malik RA & Heagerty AM (2009). Local Inflammation and Hypoxia Abolish

the Protective Anticontractile Properties of Perivascular Fat in Obese Patients. *Circulation* **119,** 1661–1670.

Gundry RL, Raginski K, Tarasova Y, Tchernyshyov I, Bausch-Fluck D, Elliott ST, Boheler KR, Van Eyk JE & Wollscheid B (2009). The mouse C2C12 myoblast cell surface N-linked glycoproteome: identification, glycosite occupancy, and membrane orientation. *Mol Cell Proteomics* **8,** 2555–2569.

Gye MC, Oh YS, Lee JE, Shim S, Choi KJ & Ahn HS (2011). Expression of coxsackievirus and adenovirus receptor isoforms in developing mouse bladder uroepithelium. *Urology* **77,** 9–18.

Halaby DM & Mornon JPE (1998). The immunoglobulin superfamily: An insight on its tissular, species, and functional diversity. *J Mol Evol* **46,** 389–400.

Hamilton JR, Reilly BJ & Morecki R (1969). Short small intestine associated with malrotation: a newly described congenital cause of intestinal malabsorption. *Gastroenterology* **56,** 124–136.

Hammad FT (2015). Electrical propagation in the renal pelvis, ureter and bladder. *Acta Physiol* **213,** 371–383.

Harada H, Suzu S, Hayashi Y & Okada S (2005). BT-IgSF, a novel immunoglobulin superfamily protein, functions as a cell adhesion molecule. *J Cell Physiol* **204,** 919–926.

Harpaz Y & Chothia C (1994). Many of the immunoglobulin superfamily domains in cell adhesion molecules and surface receptors belong to a new structural set which is close to that containing variable domains. *J Mol Biol* **238,** 528–539.

Hattori M et al. (2000). The DNA sequence of human chromosome 21. *Nature* **405,** 311–319.

Heath JK, White SJ, Johnstone CN, Catimel B, Simpson RJ, Moritz RL, Tu GF, Ji H, Whitehead RH, Groenen LC, Scott AM, Ritter G, Cohen L, Welt S, Old LJ, Nice EC & Burgess AW (1997). The human A33 antigen is a transmembrane glycoprotein and a novel member of the immunoglobulin superfamily. *Proc Natl Acad Sci U S A* **94,** 469–474.

Hida K, Wada J, Zhang H, Hiragushi K, Tsuchiyama Y, Shikata K & Makino H (2000). Identification of genes specifically expressed in the accumulated visceral adipose tissue of OLETF rats. *J Lipid Res* **41,** 1615–1622.

Hirabayashi S, Tajima M, Yao I, Nishimura W, Mori H & Hata Y (2003). JAM4, a Junctional Cell Adhesion Molecule Interacting with a Tight Junction Protein, MAGI-1. *Mol Cell Biol* **23,** 4267–4282.

Hirata KI, Ishida T, Penta K, Rezaee M, Yang E, Wohlgemuth J & Quertermous T (2001). Cloning of an Immunoglobulin Family Adhesion Molecule Selectively Expressed by Endothelial Cells. *J Biol Chem* **276,** 16223–16231.

Honda T, Saitoh H, Masuko M, Katagiri-Abe T, Tominaga K, Kozakai I, Kobayashi K, Kumanishi T, Watanabe YG, Odani S & Kuwano R (2000). The coxsackievirus-adenovirus receptor

protein as a cell adhesion molecule in the developing mouse brain. *Brain Res Mol Brain Res* **77,** 19–28.

Hooper M, Hardy K, Handyside A, Hunter S & Monk M (1987). HPRT-deficient (Lesch-Nyhan) mouse embryos derived from germline colonization by cultured cells. *Nature* **326,** 292–295.

Hotta Y, Honda T, Naito M & Kuwano R (2003). Developmental distribution of coxsackie virus and adenovirus receptor localized in the nervous system. *Dev Brain Res* **143,** 1–13.

Hu P, Deng FM, Liang FX, Hu CM, Auerbach AB, Shapiro E, Wu XR, Kachar B & Sun TT (2000). Ablation of uroplakin III gene results in small urothelial plaques, urothelial leakage, and vesicoureteral reflux. *J Cell Biol* **151,** 961–971.

Huizinga JD & Lammers WJEP (2009). Gut peristalsis is governed by a multitude of cooperating mechanisms. *Am J Physiol Gastrointest Liver Physiol* **296,** G1–G8.

Hurtado R, Bub G & Herzlinger D (2010). The pelvis–kidney junction contains HCN3, a hyperpolarization-activated cation channel that triggers ureter peristalsis. *Kidney Int* **77,** 500–508.

Iino S, Ward SM & Sanders KM (2004). Interstitial cells of Cajal are functionally innervated by excitatory motor neurones in the murine intestine. *J Physiol* **556,** 521–530.

Iizuka-Kogo A, Ishidao T, Akiyama T & Senda T (2007). Abnormal development of urogenital organs in Dlgh1-deficient mice. *Development* **134,** 1799–1807.

Ito M, Kodama M, Masuko M, Yamaura M, Fuse K, Uesugi Y, Hirono S, Okura Y, Kato K, Hotta Y, Honda T, Kuwano R & Aizawa Y (2000). Expression of coxsackievirus and adenovirus receptor in hearts of rats with experimental autoimmune myocarditis. *Circ Res* **86,** 275–280.

Jenkins D & Woolf AS (2007). Uroplakins: New molecular players in the biology of urinary tract malformations. *Kidney Int* **71,** 195–200.

Kanerva A & Hemminki A (2004). Modified adenoviruses for cancer gene therapy. *Int J Cancer* **110,** 475–480.

Katoh M & Katoh M (2003). IGSF11 gene, frequently up-regulated in intestinal-type gastric cancer, endoced adhesion molecule homologous to CXADR, FLJ22415 and ESAM. *Int J Oncol* **23,** 525–531.

Killian LM & Bund SJ (2012). The Inhibition of Ureteral Motility by Periureteral Adipose Tissue. *ISRN Urol* **2012,** 1–7.

Klemm MF, Exintaris B & Lang RJ (1999). Identification of the cells underlying pacemaker activity in the guinea-pig upper urinary tract. *J Physiol* **519,** 867–884.

Kondo J, Powell AE, Wang Y, Musser MA, Southard-Smith EM, Franklin JL & Coffey RJ (2015). LRIG1 Regulates Ontogeny of Smooth Muscle−Derived Subsets of Interstitial Cells of Cajal in Mice. *Gastroenterology* **149,** 407–419.e8.

Kong X-T, Deng F-M, Hu P, Liang F-X, Zhou G, Auerbach AB, Genieser N, Nelson PK, Robbins ES, Shapiro E, Kachar B & Sun T-T (2004). Roles of uroplakins in plaque formation, umbrella cell enlargement, and urinary tract diseases. *J Cell Biol* **167,** 1195–1204.

Kühn R, Rajewsky K & Müller W (1991). Generation and analysis of interleukin-4 deficient mice. *Science* **254,** 707–710.

Lang RJ, Hashitani H, Tonta MA, Parkington HC & Suzuki H (2007*a*). Spontaneous electrical and Ca 2+ signals in typical and atypical smooth muscle cells and interstitial cell of Cajal-like cells of mouse renal pelvis. *J Physiol* **583,** 1049–1068.

Lang RJ & Klemm MF (2005). Interstitial cell of Cajal-like cells in the upper urinary tract. *J Cell Mol Med* **9,** 543–556.

Lang RJ, Tonta MA, Zoltkowski BZ, Meeker WF, Wendt I & Parkington HC (2006). Pyeloureteric peristalsis: role of atypical smooth muscle cells and interstitial cells of Cajal-like cells as pacemakers. *J Physiol* **576,** 695–705.

Lang RJ, Zoltkowski BZ, Hammer JM, Meeker WF & Wendt I (2007*b*). Electrical Characterization of Interstitial Cells of Cajal-Like Cells and Smooth Muscle Cells Isolated From the Mouse Ureteropelvic Junction. *J Urol* **177,** 1573–1580.

Lee RMKW, Ding L, Lu C, Su L-Y & Gao Y-J (2009). Alteration of perivascular adipose tissue function in angiotensin II-induced hypertension. *Can J Physiol Pharmacol* **87,** 944–953.

Lee RS, Cendron M, Kinnamon DD & Nguyen HT (2006). Antenatal Hydronephrosis as a Predictor of Postnatal Outcome: A Meta-analysis. *Pediatrics* **118,** 586–593.

Li F, Miao X, Chen Y & Curry TE (2014). CXADR-like membrane protein (CLMP) in the rat ovary: stimulation by human chorionic gonadotrophin during the periovulatory period. *Reprod Fertil Dev*; DOI: 10.1071/RD14201.

Lim BK, Xiong D, Dorner A, Youn TJ, Yung A, Liu TI, Gu Y, Dalton ND, Wright AT, Evans SM, Chen J, Peterson KL, McCulloch AD, Yajima T & Knowlton KU (2008). Coxsackievirus and adenovirus receptor (CAR) mediates atrioventricular-node function and connexin 45 localization in the murine heart. *J Clin Invest* **118,** 2758–2770.

Lisewski U, Shi Y, Wrackmeyer U, Fischer R, Chen C, Schirdewan A, Jüttner R, Rathjen F, Poller W, Radke MH & Gotthardt M (2008). The tight junction protein CAR regulates cardiac conduction and cell-cell communication. *J Exp Med* **205,** 2369–2379.

Liu Y, Nusrat A, Schnell FJ, Reaves TA, Walsh S, Pochet M & Parkos CA (2000). Human junction adhesion molecule regulates tight junction resealing in epithelia. *J Cell Sci* **113,** 2363–2374.

Lucarelli G, Mancini V, Galleggiante V, Rutigliano M, Vavallo A, Battaglia M & Ditonno P (2014). Emerging Urinary Markers of Renal Injury in Obstructive Nephropathy. *Biomed Res Int*.

Luo B-H, Carman C V & Springer TA (2007). Structural basis of integrin regulation and signaling. *Annu Rev Immunol* **25,** 619–647.

Lye CM, Fasano L & Woolf AS (2010). Ureter myogenesis: putting Teashirt into context. *J Am Soc Nephrol* **21,** 24–30.

Mahoney ZX, Sammut B, Xavier RJ, Cunningham J, Go G, Brim KL, Stappenbeck TS, Miner JH & Swat W (2006). Discs-large homolog 1 regulates smooth muscle orientation in the mouse ureter. *Proc Natl Acad Sci U S A* **103,** 19872–19877.

Martin E, Caubit X, Airik R, Vola C, Fatmi A, Kispert A & Fasano L (2013). TSHZ3 and SOX9 regulate the timing of smooth muscle cell differentiation in the ureter by reducing myocardin activity. *PLoS One* **8,** e63721.

Martin V & Shaw-Smith C (2010). Review of genetic factors in intestinal malrotation. *Pediatr Surg Int* **26,** 769–781.

Martìn-Padura I, Lostaglio S, Schneemann M, Williams L, Romano M, Fruscella P, Panzeri C, Stoppacciaro A, Ruco L, Villa A, Simmons D & Dejana E (1998). Junctional adhesion molecule, a novel member of the immunoglobulin superfamily that distributes at intercellular junctions and modulates monocyte transmigration. *J Cell Biol* **142,** 117–127.

Matter K & Balda MS (2007). Epithelial tight junctions, gene expression and nucleo-junctional interplay. *J Cell Sci* **120,** 1505–1511.

McEver RP (2015). Selectins : initiators of leucocyte adhesion and signalling at the vascular wall. *Cardiovasc Res* **107,** 331–339.

Mirza M, Hreinsson J, Strand ML, Hovatta O, Söder O, Philipson L, Pettersson RF & Sollerbrant K (2006). Coxsackievirus and adenovirus receptor (CAR) is expressed in male germ cells and forms a complex with the differentiation factor JAM-C in mouse testis. *Exp Cell Res* **312,** 817–830.

Mirza M, Pang MF, Zaini MA, Haiko P, Tammela T, Alitalo K, Philipson L, Fuxe J & Sollerbrant K (2012). Essential role of the coxsackie - and adenovirus receptor (CAR) in development of the lymphatic system in mice. *PLoS One* **7,** 1–9.

Mirza M, Raschperger E, Philipson L, Pettersson RF & Sollerbrant K (2005). The cell surface protein coxsackie- and adenovirus receptor (CAR) directly associates with the Ligand-of-Numb Protein-X2 (LNX2). *Exp Cell Res* **309,** 110–120.

Moog-Lutz C (2003). JAML, a novel protein with characteristics of a junctional adhesion molecule, is induced during differentiation of myeloid leukemia cells. *Blood* **102,** 3371–3378.

Mori K & Nakao K (2007). Neutrophil gelatinase-associated lipocalin as the real-time indicator of active kidney damage. *Kidney Int* **71,** 967–970.

Nagai M, Yaoita E, Yoshida Y, Kuwano R, Nameta M, Ohshiro K, Isome M, Fujinaka H, Suzuki S, Suzuki J, Suzuki H & Yamamoto T (2003). Coxsackievirus and adenovirus receptor, a tight junction membrane protein, is expressed in glomerular podocytes in the kidney. *Lab Invest* **83,** 901–911.

Nasdala I, Wolburg-Buchholz K, Wolburg H, Kuhn A, Ebnet K, Brachtendorf G, Samulowitz U, Kuster B, Engelhardt B, Vestweber D & Butz S (2002). A transmembrane tight junction protein selectively expressed on endothelial cells and platelets. *J Biol Chem* **277,** 16294–16303.

Ng ANY, De Jong-Curtain TA, Mawdsley DJ, White SJ, Shin J, Appel B, Dong PDS, Stainier DYR & Heath JK (2005). Formation of the digestive system in zebrafish: III. Intestinal epithelium morphogenesis. *Dev Biol* **286,** 114–135.

Nie X, Sun J, Gordon RE, Cai C-L & Xu P-X (2010). SIX1 acts synergistically with TBX18 in mediating ureteral smooth muscle formation. *Development* **137,** 755–765.

Noah TK, Donahue B & Shroyer NF (2011). Intestinal development and differentiation. *Exp Cell Res* **317,** 2702–2710.

Noyan A, Parmaksiz G, Ezer SS, Anarat R & Cengiz N (2015). Urinary NGAL, KIM-1 and L-FABP concentrations in antenatal hydronephrosis. *Pediatr Urol*.

Palmeri D, Van Zante A, Huang CC, Hemmerich S & Rosen SD (2000). Vascular endothelial junction-associated molecule, a novel member of the immunoglobulin superfamily, is localized to intercellular boundaries of endothelial cells. *J Biol Chem* **275,** 19139–19145.

Patel SD, Chen CP, Bahna F, Honig B & Shapiro L (2003). Cadherin-mediated cell-cell adhesion: Sticking together as a family. *Curr Opin Struct Biol* **13,** 690–698.

Patzke C, Max KEA, Behlke J, Schreiber J, Schmidt H, Dorner AA, Kröger S, Henning M, Otto A, Heinemann U & Rathjen FG (2010). The coxsackievirus-adenovirus receptor reveals complex homophilic and heterophilic interactions on neural cells. *J Neurosci* **30,** 2897–2910.

Paxinos G & Franklin K (2012). *Paxinos and Franklin's the Mouse Brain in Stereotaxic Coordinates*, 4th edn. Academic Press.

Pazirandeh A, Sultana T, Mirza M, Rozell B, Hultenby K, Wallis K, Vennström B, Davis B, Arner A, Heuchel R, Löhr M, Philipson L & Sollerbrant K (2011). Multiple phenotypes in adult mice following inactivation of the coxsackievirus and adenovirus receptor (Car) gene. *PLoS One*; DOI: 10.1371/journal.pone.0020203.

Peeters B, Benninga MA & Hennekam RCM (2012). Infantile hypertrophic pyloric stenosis—genetics and syndromes. *Nat Rev Gastroenterol Hepatol* **9,** 646–660.

Petrella J, Cohen CJ, Gaetz J & Bergelson JM (2002). A zebrafish coxsackievirus and adenovirus receptor homologue interacts with coxsackie B virus and adenovirus. *J Virol* **76,** 10503–10506.

Pezzone MA, Watkins SC, Alber SM, King WE, de Groat WC, Chancellor MB & Fraser MO (2003). Identification of c-kit-positive cells in the mouse ureter: the interstitial cells of Cajal of the urinary tract. *Am J Physiol Renal Physiol* **284,** F925–F929.

Ranells JD, Carver JD & Kirby RS (2011). Infantile Hypertrophic Pyloric Stenosis: Epidemiology, Genetics, and Clinical Update. *Adv Pediatr* **58,** 195–206.

Raschperger E, Engstrom U, Pettersson RF & Fuxe J (2004). CLMP, a Novel Member of the CTX Family and a New Component of Epithelial Tight Junctions. *J Biol Chem* **279,** 796–804.

Raschperger E, Neve EPA, Wernerson A, Hultenby K, Pettersson RF & Majumdar A (2008). The coxsackie and adenovirus receptor (CAR) is required for renal epithelial differentiation within the zebrafish pronephros. *Dev Biol* **313,** 455–464.

Raschperger E, Thyberg J, Pettersson S, Philipson L, Fuxe J & Pettersson RF (2006). The coxsackie- and adenovirus receptor (CAR) is an in vivo marker for epithelial tight junctions, with a potential role in regulating permeability and tissue homeostasis. *Exp Cell Res* **312,** 1566–1580.

Rasouly HM & Lu W (2013). Lower urinary tract development and disease. *Wiley Interdiscip Rev Syst Biol Med* **5,** 307–342.

Reuver SM & Garner CC (1998). E-cadherin mediated cell adhesion recruits SAP97 into the cortical cytoskeleton. *J Cell Sci* **111 (Pt 8,** 1071–1080.

Richardson JS (1981). The Anatomy & Taxonomy of Protein Structure. *Adv Protein Chem* **34,** 167–339.

Rochette-Egly C & Germain P (2009). Dynamic and combinatorial control of gene expression by nuclear retinoic acid receptors (RARs). *Nucl Recept Signal* **7,** 1–18.

Rosselot C, Spraggon L, Chia I, Batourina E, Riccio P, Lu B, Niederreither K, Dolle P, Duester G, Chambon P, Costantini F, Gilbert T, Molotkov A & Mendelsohn C (2010). Non-cell-autonomous retinoid signaling is crucial for renal development. *Development* **137,** 283–292.

Rougon G & Hobert O (2003). New insights into the diversity and function of neuronal immunoglobulin superfamily molecules. *Annu Rev Neurosci* **26,** 207–238.

Sambrook J & Russell DW (2001). *Molecular Cloning - Sambrook & Russel*.

Santicioli P & Maggi CA (1998). Myogenic and neurogenic factors in the control of pyeloureteral motility and ureteral peristalsis. *Pharmacol Rev* **50,** 683–722.

Santicioli P & Maggi CA (2000). Effect of 18beta-glycyrrhetinic acid on electromechanical coupling in the guinea-pig renal pelvis and ureter. *Br J Pharmacol* **129,** 163–169.

Schreiber J, Langhorst H, Jüttner R & Rathjen FG (2014). The IgCAMs CAR, BT-IgSF, and CLMP: Structure, Function, and Diseases. In *Cell Adhesion Molecules - Implications in Neurological Diseases*, ed. Berezin V & Walmod PS, pp. 21–45. Springer.

Schwenk F, Baron U & Rajewsky K (1995). A cre-transgenic mouse strain for the ubiquitous deletion of loxP-flanked gene segments including deletion in germ cells. *Nucleic Acids Res* **23,** 5080–5081.

Serrano M, Moreno M, Bassols J, Moreno-Navarrete JM, Ortega F, Ricart W & Fernández-Real JM (2015). Coxsackie and Adenovirus Receptor Is Increased in Adipose Tissue of Obese Subjects: A Role for Adenovirus Infection? *J Clin Endocrinol Metab* **100,** 1156–1163.

Shapiro L, Love J & Colman DR (2007). Adhesion molecules in the nervous system: structural insights into function and diversity. *Annu Rev Neurosci* **30,** 451–474.

Shaw CA, Holland PC, Sinnreich M, Allen C, Sollerbrant K, Karpati G & Nalbantoglu J (2004). Isoform-specific expression of the Coxsackie and adenovirus receptor (CAR) in neuromuscular junction and cardiac intercalated discs. *BMC Cell Biol* **5,** 42.

Singer E, Markó L, Paragas N, Barasch J, Dragun D, Müller DN, Budde K & Schmidt-Ott KM (2013). Neutrophil gelatinase-associated lipocalin: pathophysiology and clinical applications. *Acta Physiol* **207,** 663–672.

Sollerbrant K, Raschperger E, Mirza M, Engström U, Philipson L, Ljungdahl PO & Pettersson RF (2003). The Coxsackievirus and adenovirus receptor (CAR) forms a complex with the PDZ domain-containing protein Ligand-of-Numb protein-X (LNX). *J Biol Chem* **278,** 7439–7444.

Spence JR, Lauf R & Shroyer NF (2011). Vertebrate intestinal endoderm development. *Dev Dyn* **240,** 501–520.

Srinivasan M & Roeske RW (2005). Immunomodulatory peptides from IgSF proteins: a review. *Curr Protein Pept Sci* **6,** 185–196.

Stefani M (2008). Protein Folding and Misfolding on Surfaces. *Int J Mol Sci* **9,** 2515–2542.

Sultana T, Hou M, Stukenborg JB, Töhönen V, Inzunza J, Chagin AS & Sollerbrant K (2014). Mice depleted of the coxsackievirus and adenovirus receptor display normal spermatogenesis and an intact blood-testis barrier. *Reproduction* **147,** 875–883.

Summers JE (1928). The dilated duodenum. *Ann Surg* **88,** 576–581.

Suzu S, Hayashi Y, Harumi T, Nomaguchi K, Yamada M, Hayasawa H & Motoyoshi K (2002). Molecular cloning of a novel immunoglobulin superfamily gene preferentially expressed by brain and testis. *Biochem Biophys Res Commun* **296,** 1215–1221.

Sze KL, Lee WM & Lui WY (2008*a*). Expression of CLMP, a novel tight junction protein, is mediated via the interaction of GATA with the Kruppel family proteins, KLF4 and Sp1, in mouse TM4 sertoli cells. *J Cell Physiol* **214,** 334–344.

Sze K-L, Lui W-Y & Lee WM (2008*b*). Post-transcriptional regulation of CLMP mRNA is controlled by tristetraprolin in response to TNFalpha via c-Jun N-terminal kinase signalling. *Biochem J* **410,** 575–583.

Tang T et al. (2010). A mouse knockout library for secreted and transmembrane proteins. *Nat Biotechnol* **28,** 749–755.

Thoelen I, Magnusson C, Tågerud S, Polacek C, Lindberg M & Van Ranst M (2001). Identification of alternative splice products encoded by the human coxsackie-adenovirus receptor gene. *Biochem Biophys Res Commun* **287,** 216–222.

Tomko RP, Johansson CB, Totrov M, Abagyan R, Frisén J & Philipson L (2000). Expression of the adenovirus receptor and its interaction with the fiber knob. *Exp Cell Res* **255,** 47–55.

Tomko RP, Xu R & Philipson L (1997). HCAR and MCAR: the human and mouse cellular receptors for subgroup C adenoviruses and group B coxsackieviruses. *Proc Natl Acad Sci U S A* **94,** 3352–3356.

Tripathi P, Wang Y, Casey AM & Chen F (2012). Absence of canonical Smad signaling in ureteral and bladder mesenchyme causes ureteropelvic junction obstruction. *J Am Soc Nephrol* **23,** 618–628.

Trowe M-O, Airik R, Weiss A-C, Farin HF, Foik AB, Bettenhausen E, Schuster-Gossler K, Taketo MM & Kispert A (2012). Canonical Wnt signaling regulates smooth muscle precursor development in the mouse ureter. *Development* **139,** 3099–3108.

Turgeon B & Meloche S (2009). Interpreting neonatal lethal phenotypes in mouse mutants: insights into gene function and human diseases. *Physiol Rev* **89,** 1–26.

Verdino P, Witherden DA, Havran WL & Wilson IA (2010). The molecular interaction of CAR and JAML recruits the central cell signal transducer PI3K. *Science* **329,** 1210–1214.

Verlohren S, Dubrovska G, Tsang S-Y, Essin K, Luft FC, Huang Y & Gollasch M (2004). Visceral Periadventitial Adipose Tissue Regulates Arterial Tone of Mesenteric Arteries. *Hypertension* **44,** 271–276.

Wang X & Bergelson JM (1999). Coxsackievirus and adenovirus receptor cytoplasmic and transmembrane domains are not essential for coxsackievirus and adenovirus infection. *J Virol* **73,** 2559–2562.

Wang X-Y, Ward SM, Gerthoffer WT & Sanders KM (2003). PKC-epsilon translocation in enteric neurons and interstitial cells of Cajal in response to muscarinic stimulation. *Am J Physiol Gastrointest Liver Physiol* **285,** G593–G601.

Ward SM, McLaren GJ & Sanders KM (2006). Interstitial cells of Cajal in the deep muscular plexus mediate enteric motor neurotransmission in the mouse small intestine. *J Physiol* **573,** 147–159.

Weiss RM, Tamarkin FJ & Wheeler MA (2006). Pacemaker activity in the upper urinary tract. *J Smooth Muscle Res* **42,** 103–115.

Van der Werf CS et al. (2012). CLMP is required for intestinal development, and loss-of-function mutations cause congenital short-bowel syndrome. *Gastroenterology* **142,** 453–462.

Van der Werf CS, Halim D, Verheij JBGM, Alves MM & Hofstra RMW (2015). Congenital Short Bowel Syndrome: from clinical and genetic diagnosis to the molecular mechanisms involved in intestinal elongation. *Biochim Biophys Acta - Mol Basis Dis* **1852,** 2352–2361.

Van der Werf CS, Hsiao NH, Conroy S, Paredes J, Ribeiro AS, Sribudiani Y, Seruca R, Hofstra RMW, Westers H & van IJzendoorn SCD (2013*a*). CLMP Is Essential for Intestinal Development, but Does Not Play a Key Role in Cellular Processes Involved in Intestinal Epithelial Development. *PLoS One* **8,** 4–9.

Van der Werf CS, Sribudiani Y, Verheij JBGM, Carroll M, O'Loughlin E, Chen C-H, Brooks AS, Liszewski MK, Atkinson JP & Hofstra RMW (2013*b*). Congenital short bowel syndrome as the presenting symptom in male patients with FLNA mutations. *Genet Med* **15,** 310–313.

Williams AF & Barclay AN (1988). The Immunoglobulin Superfamily-- Domains For Cell Surface Recognition. *Ann Rev Immunol* **6,** 381–405.

Witherden DA, Verdino P, Rieder SE, Garijo O, Robyn E, Teyton L, Fischer WH, Wilson IA & Havran WL (2010). The adhesion molecule JAML is a costimulatory receptor for epithelial gammadelta T cell activation. *Science* **329,** 1205–1210.

Woolf AS (2000). A molecular and genetic view of human renal and urinary tract malformations. *Kidney Int* **58,** 500–512.

Wu X-R, Kong X-P, Pellicer A, Kreibich G & Sun T-T (2009). Uroplakins in urothelial biology, function, and disease. *Kidney Int* **75,** 1153–1165.

Xu Z & Jin B (2010). A novel interface consisting of homologous immunoglobulin superfamily members with multiple functions. *Cell Mol Immunol* **7,** 11–19.

Yan J, Zhang L, Xu J, Sultana N, Hu J, Cai X, Li J, Xu P-X & Cai C-L (2014). Smad4 Regulates Ureteral Smooth Muscle Cell Differentiation during Mouse Embryogenesis. *PLoS One* **9,** e104503.

Yu J, Carroll TJ & McMahon AP (2002). Sonic hedgehog regulates proliferation and differentiation of mesenchymal cells in the mouse metanephric kidney. **5312,** 5301–5312.

Zen K, Liu Y, McCall IC, Wu T, Lee W, Babbin BA, Nusrat A & Parkos CA (2005). Neutrophil migration across tight junctions is mediated by adhesive interactions between epithelial coxsackie and adenovirus receptor and a junctional adhesion molecule-like protein on neutrophils. *Mol Biol Cell* **16,** 2694–2703.

ACKNOWLEDGEMENTS

This thesis was prepared at the Department for Developmental Neurobiology at the Max Delbrück Centre for Molecular Medicine in Berlin-Buch. Throughout the years of my study, I received numerous support, motivation and invaluable advice on experimental subjects. It has been a pleasure but also a challenging time for me, and I would like to acknowledge the persons who facilitated completing this thesis.

I wish to express my sincere gratitude to Professor Dr Fritz G. Rathjen for the supervision of this thesis, and I greatly acknowledge his faith and confidence in my research as well as his promotion and challenge of my skills in scientific working and thinking.

I appreciate Professor Dr Kai M. Schmidt-Ott for his expertise and advice on interpreting the urinary tract phenotype of my knockout animals and for providing me with several antibodies and chemicals. I am also very grateful for the review of my thesis.

For financial support during the first three years of this project I would like to thank the International Helmholtz Research School "Molecular Neurobiology". Furthermore, I am grateful for funding during the thesis completion by the Sonnenfeld-Stiftung.

I am thankful to Andrea Leschke from the MDC Transgenic Core Facility for guidance during ES cell culture, to Karola Bach for support in mice breedings and to Dr Zoltan Cseresnyes from the MDC Microscope Core Facility for assistance in the development of automated analysis of ureteral peristalsis. I want to thank Katharina, Yesim, Janett, and Emilia from the Schmidt-Ott laboratory for help with my project.

A great thanks to all the present and past members of the Rathjen laboratory for the pleasant atmosphere, fruitful scientific discussions and support in all respects. Especially I would like to thank Dr René Jüttner for collaborative analysis of ureteral peristalsis. My PhD fellows Florian, Gohar, Claudia, Alexandre, Philip and Vincent I am particularly grateful for endless encouragement and making me enjoy and treasure the time in the laboratory.

I deeply appreciate my family and my friends for their loving support.

My heartfelt gratitude to Thomas Schmitz for infinite patience and faith in me in periods of doubt and struggle.

CURRICULUM VITAE

For privacy reasons, the curriculum vitae is not included in the online version of this dissertation.

EIDESSTATTLICHE ERKLÄRUNG

Hiermit erkläre ich, Hanna Langhorst, dass die von mir vorgelegte Dissertation von mir selbstständig angefertigt wurde. Verwendete Hilfsmittel und Hilfen wurden vollständig angegeben.
Diese Dissertation wurde noch keiner anderen Fakultät oder Universität zur Prüfung vorgelegt. Die diesem Promotionsverfahren zugrunde liegende Promotionsordnung habe ich zur Kenntnis genommen.

_____

Hanna Langhorst